12-1970

An Investigation of Broadband Current Preamplification for Obtaining Simultaneous High-Resolution Energy and Time Information from Nuclear Radiation Detectors

Joe Kenneth Millard

Recommended Citation

Millard, Joe Kenneth, "An Investigation of Broadband Current Preamplification for Obtaining Simultaneous High-Resolution Energy and Time Information from Nuclear Radiation Detectors. " PhD diss., University of Tennessee, 1970.
https://trace.tennessee.edu/utk_graddiss/938

To the Graduate Council:

I am submitting herewith a dissertation written by Joe Kenneth Millard entitled "An Investigation of Broadband Current Preamplification for Obtaining Simultaneous High-Resolution Energy and Time Information from Nuclear Radiation Detectors." I have examined the final electronic copy of this dissertation for form and content and recommend that it be accepted in partial fulfillment of the requirements for the degree of Doctor of Philosophy, with a major in Electrical Engineering.

T. V. Blalock, Major Professor

We have read this dissertation and recommend its acceptance:

J. F. Piercee, J. M. Googe, Robert E. Boclenheuier, W. D. Eavly

Accepted for the Council:
Carolyn R. Hodges

Vice Provost and Dean of the Graduate School

(Original signatures are on file with official student records.)

November 23, 1970

To the Graduate Council:

I am submitting herewith a dissertation written by Joe Kenneth Millard, entitled "An Investigation of Broadband Current Preamplification for Obtaining Simultaneous High-Resolution Energy and Time Information from Nuclear Radiation Detectors." I recommend that it be accepted in partial fulfillment of the requirements for the degree of Doctor of Philosophy, with a major in Electrical Engineering.

T. V. Blalock
Major Professor

We have read this dissertation
and recommend its acceptance:

J. F. Pierce
J. M. Googe
Robert E. Bodenheimer
Edgar D. Eaves

Accepted for the Council:

Hilton A. Smith
Vice Chancellor for
Graduate Studies and Research

AN INVESTIGATION OF BROADBAND CURRENT PREAMPLIFICATION FOR OBTAINING SIMULTANEOUS HIGH-RESOLUTION ENERGY AND TIME INFORMATION FROM NUCLEAR RADIATION DETECTORS

A Dissertation
Presented to
the Graduate Council of
The University of Tennessee

In Partial Fulfillment
of the Requirements for the Degree
Doctor of Philosophy

by
Joe Kenneth Millard
December 1970

ACKNOWLEDGMENT

This research was performed at the Oak Ridge National Laboratory under the sponsorship of the U.S. Atomic Energy Commission under contract with the Union Carbide Corporation.

The author is especially grateful to T. V. Blalock for his continued assistance and encouragement throughout the course of this work.

Special appreciation is extended to N. W. Hill for his invaluable assistance and cooperation in collecting the experimental data presented in this thesis, and to C. H. Nowlin for several stimulating discussions on time variant filters.

The author gratefully acknowledges the expressed interest and cooperation of C. J. Borkowski, Director of the Instrumentation and Controls Division of the Oak Ridge National Laboratory and to F. W. Manning and H. N. Wilson for their continued support and interest in this work.

The author sincerely appreciates the patience of his wife and the cooperation of Mrs. Georgia Card who skillfully typed the rough and final drafts.

ABSTRACT

In beginning the investigation of low noise current preamplification, noise-performance limitations of existing broadband current-amplifying stages are considered. Dominant noise sources of the general, shunt-feedback amplifier stage having both bipolar and field-effect transistor input devices are discussed. This discussion includes the reasons why optimum noise performance from this amplifier stage requires unavoidable signal integration. The integrating shunt-feedback configuration is commonly known as the charge-sensitive preamplifier. Criteria are developed for differentiating the output voltage pulse of the charge-sensitive preamplifier without degrading the signal-to-noise ratio. Subsequently, a new broadband, shunt-feedback amplifier is described having a current gain equal to the ratio of an RC feedback impedance to an RC load impedance. The value of the feedback resistance and capacitance can be made equal to that of conventional charge-sensitive preamplifiers. Basically, the configuration is similar to that of a charge-sensitive preamplifier, since a charge-proportional signal is present within the feedback network. However, differentiation is performed by the feedback network to allow a broadband current transfer function. The stage has a large bandwidth capability with linearity and noise performance comparable to that of the conventional charge-sensitive configuration. Equations predicting the bandwidth, input and output impedances, and noise-performance are derived. Also criteria are established for achieving the desired linearity and for cascading stages to achieve large current gains.

To facilitate experiments involving linear gating of the amplified detector current pulse, a review of related technology is presented and a simple RLC filter for use in a gated system is discussed.

A three-stage preamplifier having a current gain of 8000 was constructed to experimentally verify the predicted preamplifier performance characteristics. Energy resolution experiments performed with a Ge(Li) semiconductor detector yielded noise line widths as low as 2.35 kev FWHM for the integrated current output shaped by a 1.6 microsecond time constant RC-RC filter. The noise line width measured for the gated current pulse shaped by the RLC filter was 2.70 kev FWHM compared to 2.76 kev FWHM obtained, without gating, from a 0.4 microsecond RC-RC filter having the same center frequency as the RLC filter. The preamplifier was not optimized for minimum noise line width.

Leading edge timing experiments were performed with a ^{60}Co gamma-ray source using Naton 136 as the detector for the standard timing channel. With the test channel consisting of the three-stage preamplifier coupled to a 1.7 cc. planar diode, a timing uncertainty of 1.6×10^{-9} seconds FWHM for a 13.3 to 1 dynamic energy range was measured. With a 34.1 cc true coacial Ge(Li) detector in the test channel, the timing uncertainty was 3.3×10^{-9} seconds FWHM for a 7.8 to 1 dynamic energy range. Rise times as low as 7×10^{-9} seconds were measured with the 9×10^{-12} farad planar detector connected to the preamplifier.

TABLE OF CONTENTS

LIST OF FIGURES

CHAPTER I

INTRODUCTION

I. BACKGROUND

Since the inception of nuclear spectroscopy, voltage-sensitive and charge-sensitive preamplifiers have been predominantly used with low-level radiation detectors having a capacitive terminal impedance. A vast amount of literature has been published over the last decade dealing with the theoretical and experimental noise performance of these two types of preamplifiers. Insight into the performance of these preamplifiers with references to specific designs may be found in survey papers such as those by Goulding[1] and by Elad.[2]

Both the voltage-sensitive and charge-sensitive configurations illustrated in Fig. 1 give an output voltage that is proportional to the charge liberated in the detector by a radiation event. In the case of the charge-sensitive preamplifier, most of the detector current produced by a radiation event flows through the feedback capacitor C_f provided the effective input capacitance C_{in}, which is equivalent to the feedback capacitance multiplied by the open-loop gain of the forward amplification path, is much larger than the sum of the detector terminal capacitance C_D and the open-loop input capacitance of the preamplifier. After collection the charge leaks off through the shunting feedback resistor R_f, having a typical value of 10^9 ohms, with a typical time constant of several hundred microseconds. The peak value of the output voltage pulse is the integral of the detector current pulse, a quantity equal to the charge

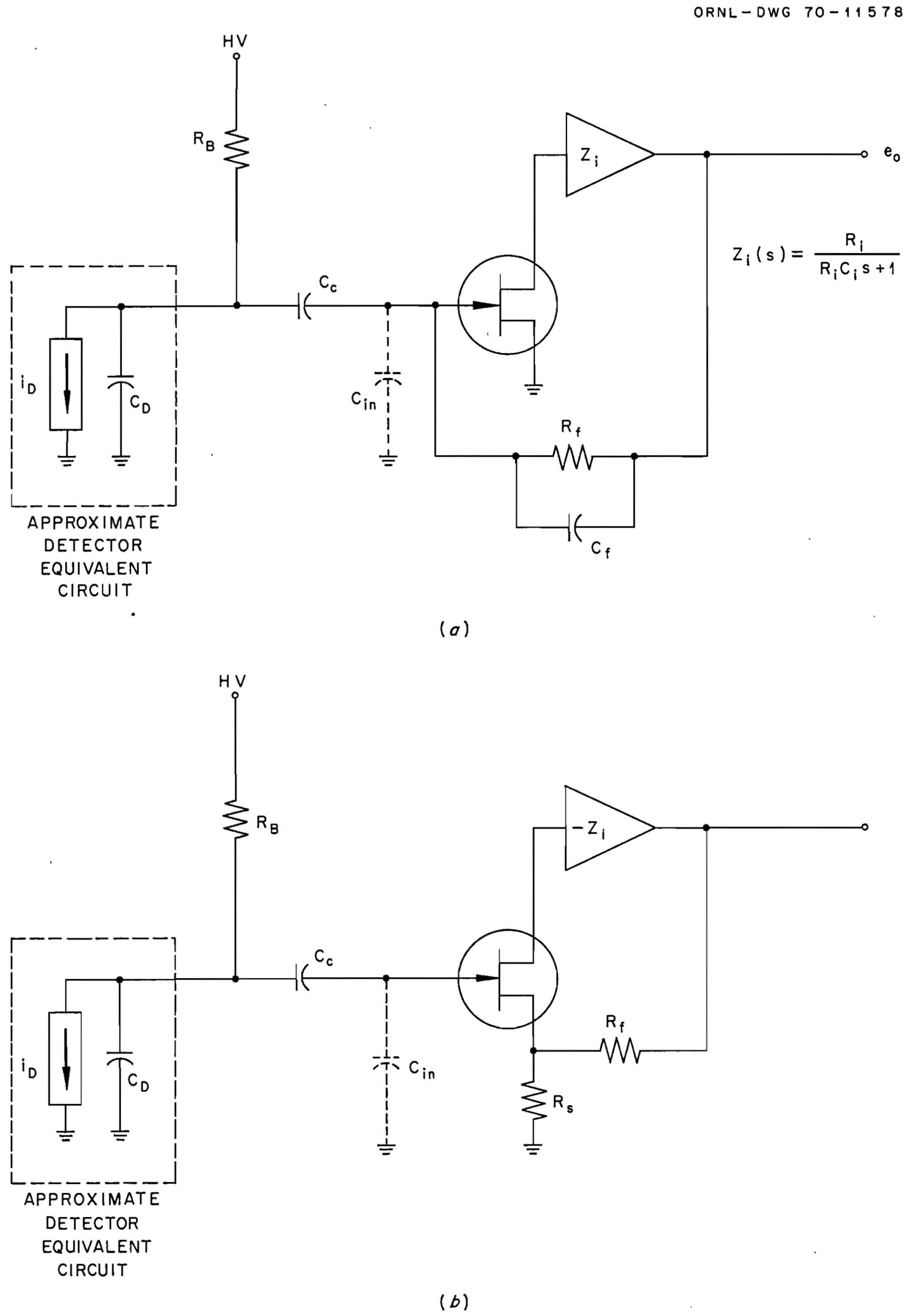

Figure 1. General configurations of (a) the charge-sensitive and (b) the voltage-sensitive preamplifiers.

liberated in the detector by the radiation event. The liberated charge is related to the energy of the causal radiation by a constant depending upon the type of detector. The voltage-sensitive preamplifier configuration of Fig. 1b also generates an output voltage pulse having a peak value proportional to the integral of the detector current pulse. Current integration for this configuration is accomplished by the input capacitance C_{in} of the preamplifier. The charge collected on both the coupling capacitor C_c and the input capacitance C_{in} leaks off through the input bias resistor R_B having also a typical value in the range of 10^9 ohms. Because of the inherent integration in the voltage-sensitive and charge-sensitive preamplifiers, the detector current signal is not readily available at the preamplifier output terminal.

II. APPLICATIONS FOR LINEAR, LOW-NOISE CURRENT PREAMPLIFICATION

For several experimental applications, low-noise preamplification of the detector current signal prior to integration is desirable. One application arises when low-energy spectral analysis is required in the presence of radiation having a much higher energy but occurring at a much lower count rate. In this case linear gating of the fast current pulse may avoid long dead times due to critical overloading of the amplifier system upon detection of the high-energy radiation. As another example the resolution of high-energy analyzing systems (particle energies in the Mev range) can be made significantly worse when a high-count-rate background of much lower energy particles is encountered. Such a situation occurs in fission-fragment experiments where a high-count-rate, α-particle background is present. For this situation resolution improvement may be achieved by linear gating of the amplified detector current pulse prior to integration. This technique has been demonstrated in experiments at the Oak Ridge National Laboratory.[3] Another application for linear gating of the detector current pulse has been reported by Blalock and Nowlin.[4] These and other authors have shown that due to the time-variant nature of gated noise, an improvement in the system signal-to-noise ratio for certain types of noise spectra and filters can be realized.

Another important need for the amplified detector current pulse is the determination of the exact time a radiation event takes place within a detector. Precise event occurrence times can be ascertained from the front edge of the fast current pulse from several detector types, especially if constant-fraction-of-pulse-height discrimination is employed.[5] Since the broadband noise constrains the minimum discrimination level, the dynamic energy range over which events may be timed is a function of the broadband noise of the current preamplifier. Thus, low noise performance is essential.

Other applications for current preamplification concern the shape of current pulses formed within the detector. Radiation particle identification, position of event occurrence and general pulse shape studies associated with detector research are areas of need that could profit by having available the amplified detector current signal without excessively large noise contribution from the preamplifier.

There are several reasons why current preamplification has not heretofore been more widely adopted. The basic reason concerns the poor noise performance of conventional types of broadband current amplifiers. The reasons for this inadequate noise performance will be detail in the next chapter. A factor which has discouraged the use of current preamplification in systems where linear gating is required is the inadequate performance of available gates with regard to linearity, speed of operation, pedestal stability, gating-transient suppression, and signal-to-noise degradation. The development of a preamplifier to linearly amplify the detector current pulse to a usable level without significant pulse-shape distortion and with a signal-to-noise ratio comparable to that of a charge-sensitive preamplifier would consitute a significant achievement. The development of a suitable linear gate would greatly enhance the value of such a preamplifier.

III. PRESENT METHODS OF CURRENT PREAMPLIFICATION

To the present date several techniques have been applied to current preamplification where linear gating is required. The basic method of generating a low-noise current preamplifier is to produce a junction FET input operational amplifier with the largest possible gain-bandwidth product and to use, for minimum noise contribution, a feedback resistor of the largest value to allow an adequate bandwidth. Because of base-current shot noise, bipolar input transistors are not competitive with junction FET's with regard to low, low-frequency noise performance from small-capacitance detectors. A preamplifier of this type was reported by Millard and Blalock.[6] The largest feedback resistance used was 50,000 ohms. It was found that the thermal noise from this resistance resulted in an energy resolution that was not closely competitive with that obtainable from a charge-sensitive preamplifier even though, because of the type of noise spectra produced, significant improvement was observed after gating.

Another technique that has been employed for detector current amplification is to electronically differentiate the output voltage of a charge-sensitive preamplifier. This preamplifier system, to be referred to as the differentiated charge-sensitive configuration, was used by Blalock and Nowlin[4] in connection with linear gating. Its success hinges on a charge-sensitive preamplifier having a large bandwidth and a differentiating technique, also of adequately large bandwidth, that will not degrade the signal-to-noise ratio from the charge-sensitive preamplifier.

The requirements on current preamplification for fast front-edge timing are not quite as stringent as those governing energy spectroscopy. For timing applications linearity is not of primary importance. However, for wide dynamic-range timing, the broadband noise spectrum of the preamplifier is an essential consideration.

Several techniques have been used to obtain fast timing signals proportional to the detector current pulse other than the methods described above in connection with linear gating. One such technique involves operating two preamplifiers from a single detector. A charge-sensitive preamplifier serving for energy analysis is operated from one detector terminal and a broadband voltage or current amplifier is operated from the other detector terminal. For this application both sides of the detector must be available. This requirement places a constraint on versatility. This and other methods of parallel fast and slow preamplifier operation to simultaneously obtain time and energy information are well summarized in a survey paper by Quaranta et al.[7] which specifically concerns applications to semiconductor detectors.

Another technique which has been reported by Sherman and Roddick[8] consists of extracting an error signal near the input of a charge-sensitive preamplifier. If the charge-sensitive preamplifier has adequate bandwidth, the transient channel current of the input FET is proportional to the detector current pulse. Good timing over small dynamic ranges has been reported.

IV. OBJECTIVES OF THE THESIS

The primary objective of this thesis is to develop a current preamplifier having sufficient bandwidth, linearity and low-noise performance to amplify, with minimum shape and amplitude distortion, the fast current pulses generated in nuclear radiation detectors. Although the application of this work is oriented toward semiconductor detectors, it could be extended to other types of radiation detectors having a capacitive terminal impedance. The characteristics of the preamplifier sought are to satisfy the requirements of nuclear spectroscopy in which both high energy resolution with or without linear gating and large dynamic range timing is desired. Thus, these characteristics include a noise performance, gain linearity and stability comparable to present charge-sensitive and voltage-sensitive preamplifiers, a large bandwidth capability, and tolerance to high counting rates without severe energy-resolution degradation.

To develop insight into the problems associated with fast current preamplification, an initial investigation will be made concerning the limitations of present current-preamplification techniques described above. Attention will then be focused on the selection of a general preamplifier configuration which exhibits the most promise in meeting the desired performance. The following work will include the circuit development required in realizing the chosen configuration, and the concluding chapter will deal with experimental investigation of the resulting preamplifier.

CHAPTER II

LIMITATIONS OF PRESENT CURRENT-AMPLIFYING TECHNIQUES

A more detailed understanding of the limitations of the current-amplifying methods described in Chapter I is necessary before development of a superior technique or configuration can begin. In this chapter a qualitative analysis of the dominant noise sources in present configurations will be made to allow a general comparison. Although noise performance is of primary interest, other limitations in regard to linearity and high-count-rate operation will be discussed.

I. CURRENT-SENSITIVE CONFIGURATIONS

Bipolar-Transistor Input Configuration

Low-input-impedance preamplifiers using currently available high-frequency bipolar transistors can easily be made to yield bandwidths in excess of 100 megahertz, even with several stages cascaded to allow appreciable gains. Many designs employing shunt or series feedback or a combination of both have been used as fast preamplifiers for radiation detectors. A few of the more common configurations are indicated in Fig. 2.

All of these designs and many more, without exception, yield extremely poor energy resolution when compared to charge-sensitive types. The poor mid-frequency noise performance is largely due to the fact that relatively low-value feedback resistors (labeled R_f in Fig. 2) are necessary to obtain the large bandwidths (the same limitation applies to R_L in Fig. 2e). These feedback resistance values ranging typically from

ORNL-DWG 70-11579

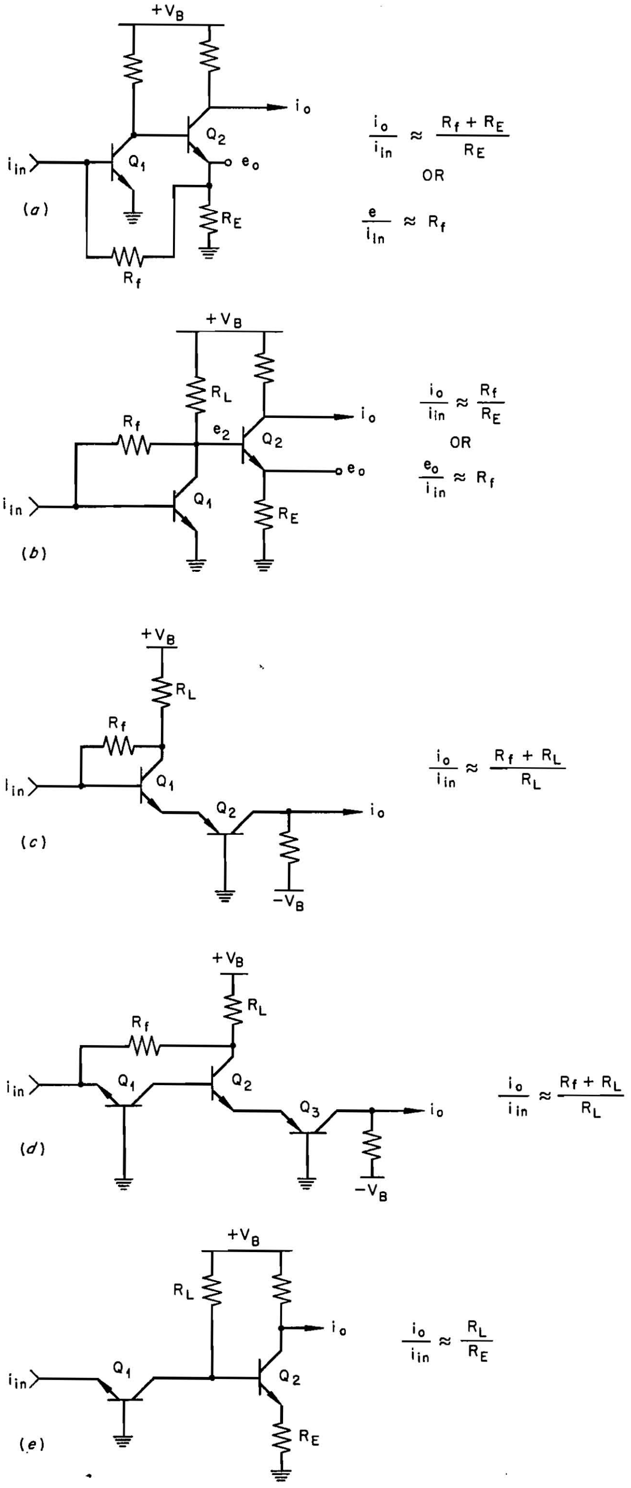

Figure 2. Current amplifying stages with approximate current gains indicated.

100 to 1000 ohms inherently generate large thermal-noise currents.

Another limitation is due to the fact that the open-loop gain of the stages indicated in Fig. 2 is relatively low over the entire bandwidth, resulting in poor gain linearity and stability. As a result most high-frequency amplifier designs consisting of local or two-transistor feedback configurations are characterized not only by poor noise performance but also by inadequate linearity when compared to charge-sensitive types. Bandwidths in excess of 100 meghaertz, however, allow good reproduction of fast-rise-time detector current pulses, provided the amplifier does not have excessive overshoot and ringing. Thus, good leading-edge timing for a small dynamic range of radiation energies can be achieved. Use of broadband, current-sensitive amplifiers consisting of several cascaded stages similar to those illustrated in Fig. 2 is limited to some form of parallel operation described in Chapter I if both energy and timing data are required.

A general form of a shunt-feedback amplifier stage having a bipolar input transistor is shown in Fig. 3a. In order to significantly improve the noise performance of this type of amplifier stage, the value of feedback resistance R_f must be made as large as possible. This is due to the fact that the thermal noise current generated in R_f, given by

$$\overline{i_n^2} = 4kT/R_f \quad \text{amps}^2/\text{Hz}, \tag{1}$$

is injected directly into the input node. The quantities k and T are respectively Boltzman's constant (1.38×10^{-23} joules/°K) and temperature in Kelvin degrees (300°K for 27°C ambient temperature). If the value of this resistor becomes large enough to allow the input-device noise to dominate the total equivalent noise current, further improvement requires

ORNL-DWG 70-11580

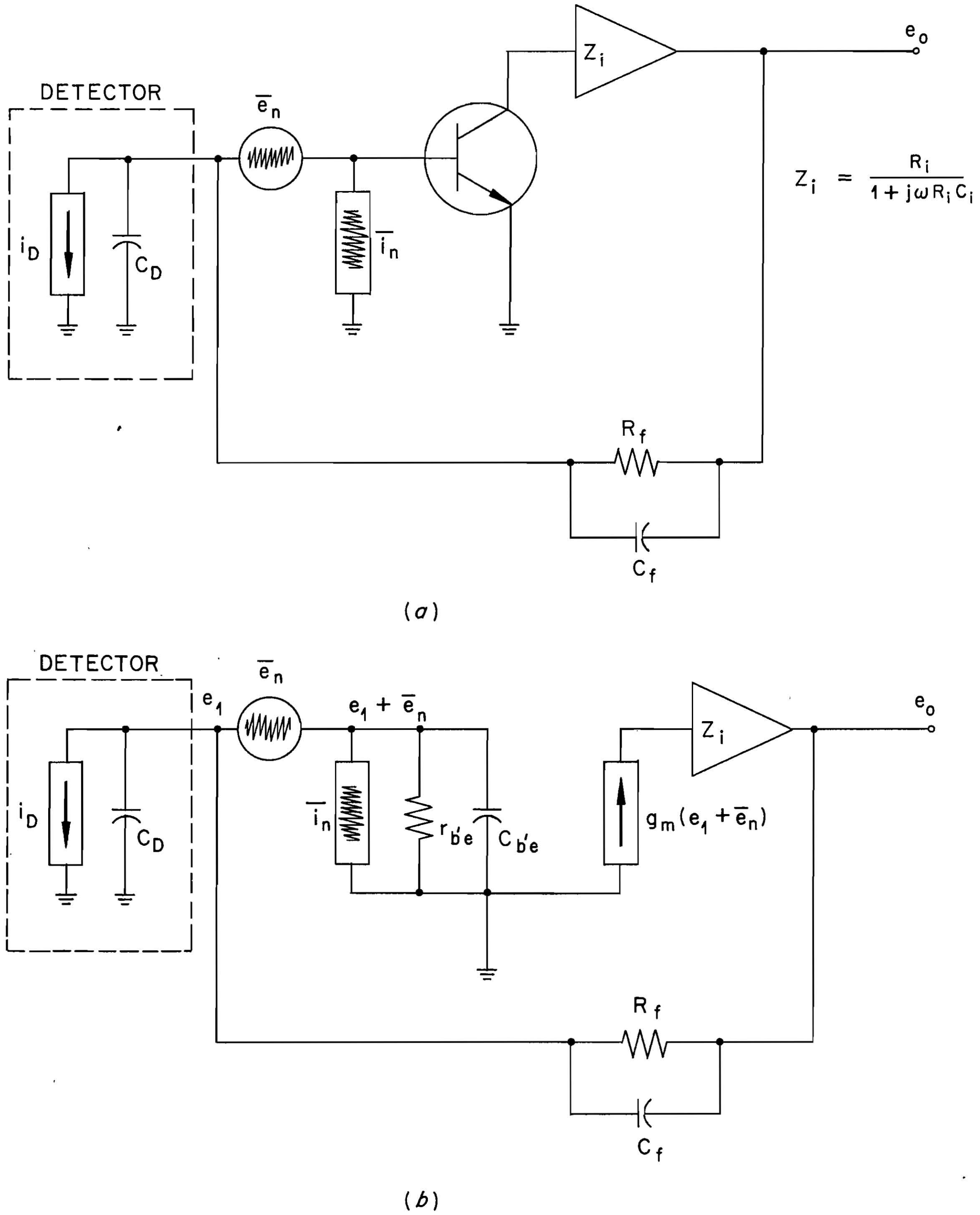

Figure 3. Generalized shunt-feedback configuration (a) and approximate equivalent circuit (b).

consideration of the input device. It is not always possible, however, to make the value of feedback resistance large enough to allow the input device to control the noise. The capacitance between the end-caps of resistors having a practical physical size (typically 0.1 to 0.2 pf for 1/4 W carbon composition types) places a limit on its resistance-capacitance product which may control the bandwidth. Also, a larger value of feedback resistance requires a larger amplifier gain-bandwidth product to achieve the desired closed-loop bandwidth. Therefore, for a given amplifier gain-bandwidth product, a maximum value of R_f exists for a desired bandwidth.

The largest feedback resistance that has been used in this type of broadband configuration was 50,000 ohms.[6] The reported bandwidth was about 50 x 10^6 Hertz. From Eq. (1) a 50,000 ohm resistor generates a noise current of about 0.58 x 10^{-12} amps/$\sqrt{\text{Hz}}$.

The mid-frequency noise contributed by the input transistor may be represented by the series mid-frequency, equivalent-noise-voltage generator and the parallel mid-frequency, equivalent-noise-current generator. Expressions for the magnitudes of these two generators as a function of the transistor parameters has been derived from the hybrid-π noise model by Kennedy.[9] The mid-frequency, equivalent-noise-voltage generator is described by

$$\overline{e_n} = \sqrt{4kT}\left\{r_{b'} + \frac{r_e}{2}\left[\alpha^2 + \left(1 + \frac{r_{b'}}{r_e}\right)^2 \left(\frac{1}{h_{FE}} + \frac{I_{CBO}}{\alpha^2 I_E}\right)\right]\right\}^{1/2}, \qquad (2)$$

and the expression for the mid-frequency, equivalent-noise-current generator is

$$\overline{i_n} = \left[2e\left(\frac{I_E}{h_{FE}}\right) + 2e\ I_{CBO}\left(\frac{1}{\alpha^2}\right)\right]^{1/2} . \qquad (3)$$

The transistor parameters indicated in these expressions are fairly well standardized among transistor texts. The quantity e is the charge of an electron (1.9 x 10^{-19} coulombs). The noise-current generator injects current into the input node as does the feedback resistor; thus, its value squared is directly additive to the square of the noise current generated in the feedback resistor. For most silicon transistors the collector-base leakage current I_{CBO} is much smaller than the quiescent, base-bias current. Thus, the mid-frequency, equivalent-noise-current generator of the input transistor, expressed in Eq. (3), is primarily due to the base-current shot noise. From this equation the base current necessary to generate a noise current at least equivalent to 0.58 x 10^{-12} amps/$\sqrt{\text{Hz}}$ found for a 50,000 ohm feedback resistor is about one microampere. This base current corresponds to a collector current of one milliampere if the transistor current gain is 1000. This is about a lower limit of collector bias current if a satisfactory gain-bandwidth product is achieved; and the device current gain of 1000 is about an upper limit for present discrete bipolar transistors.

The contribution of the mid-frequency, equivalent-noise voltage generator is not quite so apparent as that of the mid-frequency, equivalent noise-current generator. Replacing the input transistor of Fig. 3a, page 12, with its approximate hybrid-π equivalent circuit yields the simple network of Fig. 3b. The voltage gain from the noise voltage generator to the output can be found as

$$\frac{e_o}{\overline{e}_n}(j\omega) =$$

$$- \frac{g_m\, R_i(R_f + r_{b'e})(j\omega R_p C_1 + 1)}{(R_f+r_{b'e})\; R_p C_1 R_i C_i \omega^2 + (R_i C_i + R_p C_1)(R_f + r_{b'e})\; j\omega + r_{b'e} g_m R_i + (R_f + r_{b'e})}, \tag{4}$$

where $R_p = R_f r_{b'e}/(R_f + r_{b'e})$ and $C_1 = C_{b'e} + C_D + C_f$.

For low frequencies this expression reduces to $(R_f + r_{b'e})/r_{b'e}$ if $r_{b'e} g_m R_i >> R_f + r_{b'e}$. At an angular frequency of $1/R_p C_1$ radians per second, the transfer function begins a six-decibel-per-octave increase which continues to the second-order increase of the denominator occurring at a much higher frequency. Where the output noise voltage due to the mid-frequency, equivalent-noise-voltage generator equals the output noise voltage due to the mid-frequency, noise-current sources (feedback resistor and transistor equivalent-noise-current generator), a noise corner occurs, above which frequency, the total output noise voltage increases directly as ω. For a 50,000 ohm feedback resistor and an $r_{b'e}$ value of 26,000 ohms (corresponding to h_{FE} of 1000 and an emitter current of one milliampere), the magnitude of the low-frequency voltage gain from the equivalent-noise-voltage generator to the output is about 2.9 [Eq. (4)]. A typical mid-frequency, equivalent noise voltage for a silicon transistor operating at a one milliampere collector current and having a large value of h_{FE} and a low value of base spreading resistance $r_{b'}$, is about 10^{-9} volts/$\sqrt{Hz}$. The low-frequency, output noise voltage due to this source is thus 2.9×10^{-9} volts/$\sqrt{Hz}$. The total low-frequency equivalent noise current contributed by the 50,000 ohm feedback resistor and the transistor is about 0.82×10^{-12} amps/$\sqrt{\mathrm{Hz}}$. Multiplying this value by the feedback resistance of 50,000 ohms gives an output noise voltage due to these noise current sources of about 41×10^{-9} volts/$\sqrt{\mathrm{Hz}}$. The noise corner as defined above is found by solving

$$2.9 \times 10^{-9} \left|(1 + j\omega\, R_p C_1)\right| = 41 \times 10^{-9} \tag{5}$$

for frequency. The resulting value is about 2.63×10^{6} Hertz for a total input capacitance C_1 of 50×10^{-12} farads. The results are illustrated in Fig. 4 where the output noise voltage has been referred to the input as equivalent noise current by dividing by the feedback resistor value 50,000 ohms.

FET Input Configuration

If the input bipolar transistor of Fig. 3a, page 12, is replaced by a junction FET, the low-frequency noise contribution due to the input device may be decreased. For the purpose of comparing the noise performance of bipolar and field-effect transistors in this configuration, it is adequate at this point to consider only the dominant noise-generating mechanism of the junction FET. The primary noise source of this device is due to thermal noise generated in the channel. At the FET drain the noise current is described by

$$\overline{i_n} = \sqrt{4kT(0.7\, g_m)} \quad \text{amps}/\sqrt{\mathrm{Hz}}. \tag{6}$$

When operated as the input device for a shunt-feedback amplifier configuration, the effective FET current gain is equal to $g_m Z_g$ where g_m is the transconductance and Z_g is the open-loop impedance from the gate to ground, including the feedback resistance and capacitance. Thus the

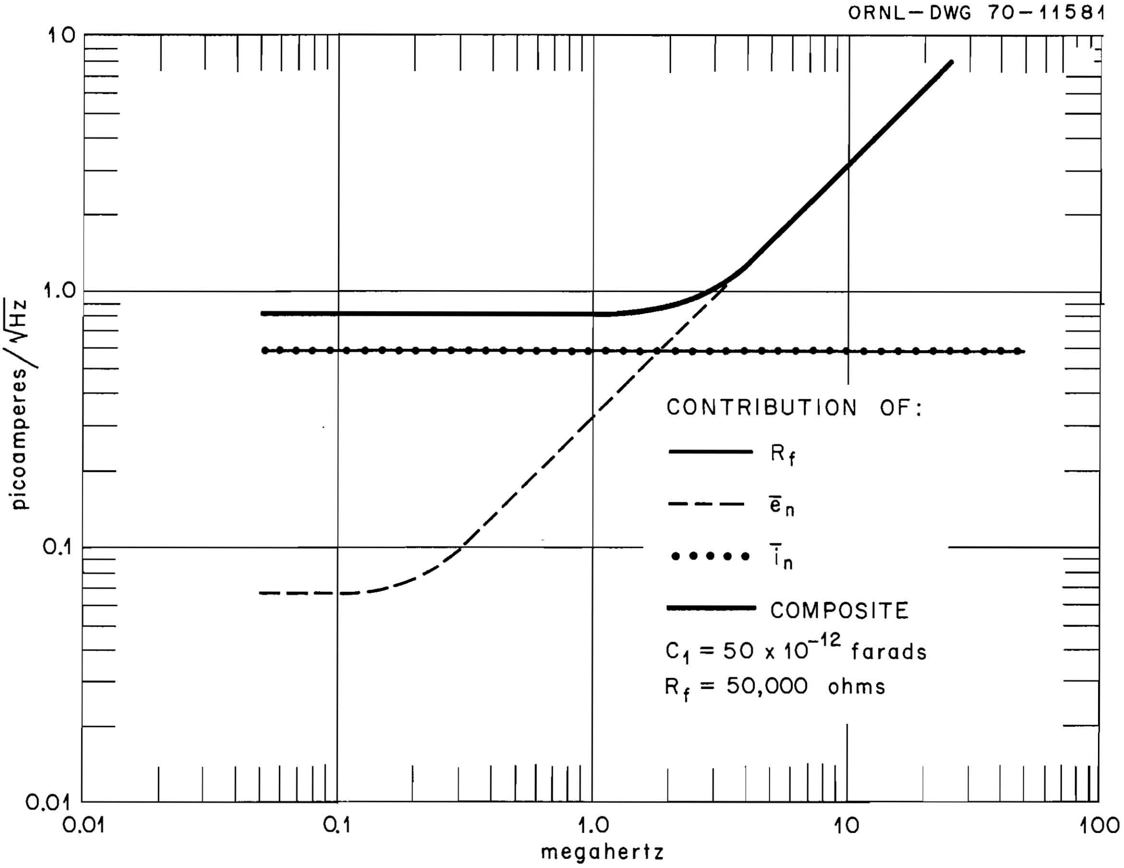

Figure 4. Equivalent-noise-current components of the bipolar-transistor input, shunt-feedback configuration.

equivalent noise current contributed by the input FET is found by dividing Eq. (6) by $g_m Z_g$. The open-loop input impedance is generally a parallel RC network with the resistance being equal to R_f (if the detector bias resistor $R_B >> R_f$). This network is simply given by

$$Z_g(j\omega) = \frac{R_f}{1 + j\omega R_f C_1} \quad , \tag{7}$$

where C_1 is the total capacitance from the gate to ground. Dividing Eq. (6) by $g_m Z_g$ gives

$$\overline{i_{eq}} = \sqrt{4kT\ (0.7\ g_m)}\ \left[(1 + j\omega R_f C_1)/g_m R_f\right] \quad . \tag{8}$$

This equation indicates an increase of the FET equivalent noise current beginning at an angular frequency of $1/R_f C_1$ radians per second. The increase in equivalent noise current occurs because of a decrease in the input capacitive reactance with increasing frequency, resulting in a diminishing FET effective current gain. From Eq. (8) the low-frequency equivalent noise current is

$$\overline{i_{eq}} = \sqrt{4kT\ (0.7\ g_m)}\ /g_m R_f \quad . \tag{9}$$

If the bipolar transistor input device of Fig. 3a, page 12, is replaced by a junction FET having a transconductance of 20 millimhos, the FET low-frequency, equivalent noise current with R_f equal to 50,000 ohms becomes about 0.015×10^{-12} amps/$\sqrt{\text{Hz}}$. Thus the total equivalent noise current of the amplifier in this frequency region is dominated by the 0.58×10^{-12} amps/$\sqrt{\text{Hz}}$ contributed by the 50,000 ohm feedback resistor. For a total input capacitance of 50×10^{-12} farads, the equivalent noise current contributed by the FET begins a six decibel per octave increase at a frequency of about 64 kilohertz. That frequency at which the equivalent noise current of the FET is equal to the noise current of the feedback resistor is the noise-corner frequency of the preamplifier. Setting the frequency dependent portion of Eq. (8) equal to the feedback resistor noise current gives

$$0.015 \times 10^{-12} (\omega R_f C_1) = 0.58 \times 10^{-12} . \tag{10}$$

The resulting noise-corner frequency is about 2.5×10^6 Hertz. The output noise voltage begins decreasing with frequency as the second-order, high-frequency response of the preamplifier becomes dominant. The equivalent-noise-current components of the FET input configuration along with the total equivalent noise current of the bipolar-transistor input configuration for comparison is shown in Fig. 5. From this figure it is evident that the FET input configuration gives a slight noise advantage for a 50,000 ohm feedback resistor and for equal total input capacitance.

Linearity and Count-Rate Performance

The linearity and gain stability of a broadband preamplifier is of primary importance only in regard to peak measurement of the integrated output signal. Variation in the gain-bandwidth product will produce corresponding variations in the output pulse rise-time. For integrating time constants several orders of magnitude longer than the fast current pulse, rise-time variations and other pulse-shape deformations are generally insignificant. A more quantitative description of the effects of such variations will appear in Chapter III. The preamplifier loop transmission in the 100 kilohertz to one megahertz frequency range can be

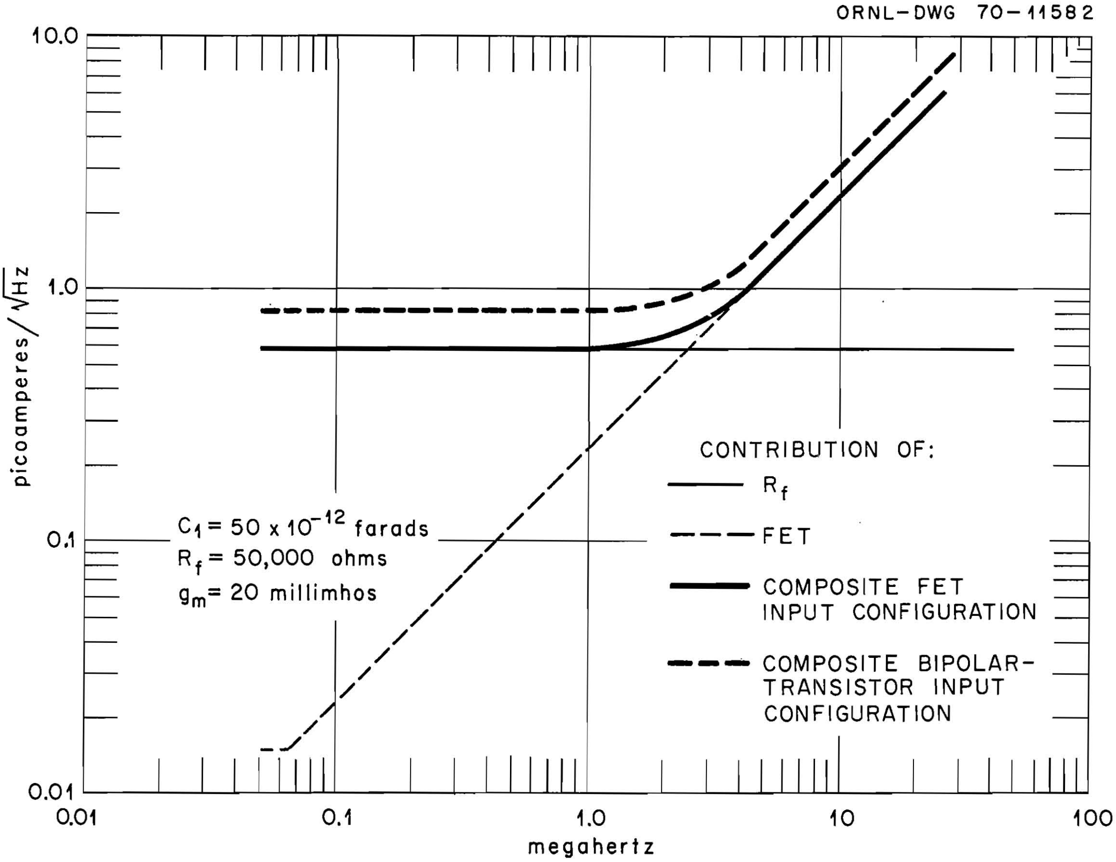

Figure 5. Equivalent-noise current components for the FET input, shunt-feedback configuration with the composite equivalent noise current of the bipolar-transistor input configuration shown for comparison.

made large enough to allow the desired gain stability and linearity for microsecond pulse shaping.

The broadband, shunt-feedback amplifier performs well under high-count-rate conditions since no long RC time constants are present in linear operation. Thus, resolution degradation due to high count rates does not become apparent until after integration. Since the circuit position of the integrating capacitor now allows it to be conveniently discharged without degrading the signal-to-noise ratio, this method of radiation energy analysis is advantageous for high counting rates.

II. DIFFERENTIATED CHARGE-SENSITIVE CONFIGURATION

A quantitative description of the noise performance of FET input charge-sensitive preamplifiers has been presented in a doctoral dissertation by Blalock.[10] A more general approach, such as that used above for the current-sensitive configuration, can be applied to allow a noise comparison of preamplifier types. As was the case for the preceding noise analysis, only the dominant noise sources, the FET channel thermal noise and the feedback resistor noise, will be included. Shot-noise components due to leakage currents will be considered negligibly small.

As the feedback resistor of the broadband, shunt-feedback stage of Fig. 3a, page 12, (with the bipolar transistor replaced by a junction FET) is increased, the impedance transfer function Z_{21} increases and the bandwidth of this transfer function decreases. As the R_fC_f time constant becomes much larger than the input pulse width, the amplifier stage performs as a current integrator. Variation of the output pulse response as a function of increasing R_f is shown in Fig. 6. With the R_fC_f time

ORNL-DWG 70-12378

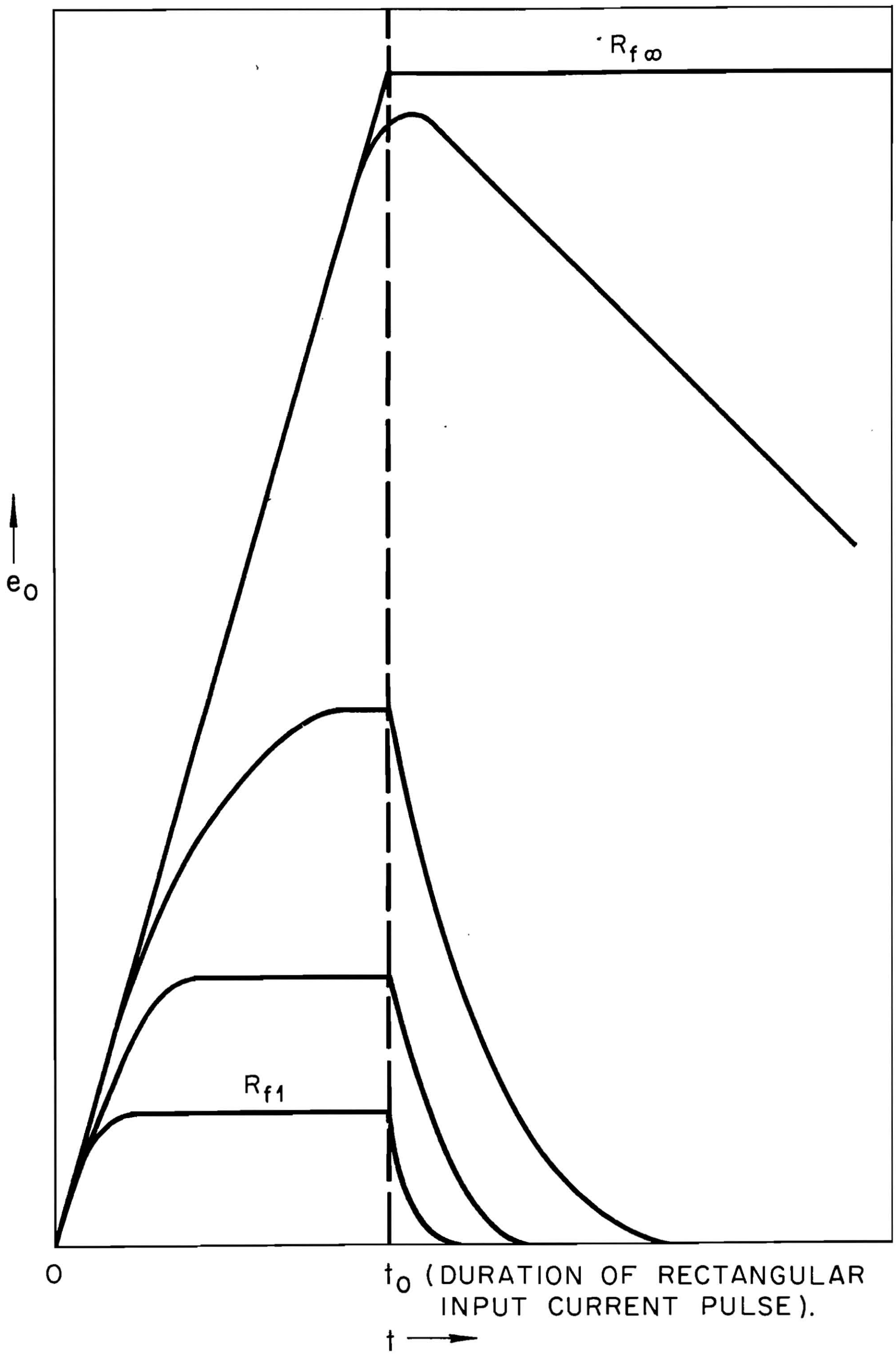

Figure 6. Output response of the general shunt-feedback configuration as the feedback resistance is increased from a value R_{f1} that allows adequate broadband performance to an infinite value $R_{f\infty}$.

constant very large, the stage is recognized as a charge-sensitive preamplifier which produces an output voltage proportional to the integral of the detector current impulse.

The equivalent noise current can be described as before. The component due to the FFT is expressed by Eq. (8) and the component due to the feedback resistor is expressed by Eq. (1). The composite equivalent noise current due to these two sources is shown in Fig. 7 as a function of R_f for a range of values of 50,000 ohms to 100 megohms. The curve for a 50,000 ohm resistor is the same as that of Fig. 5, page 20, for the FET input configuration. Feedback resistor values used in most charge-sensitive preamplifiers range from 100 megohms to 2000 megohms.

Because the charge-sensitive preamplifier has a linearily decreasing transfer function Z_{21} over a very large frequency range (typically several hundred Hertz to above 10 megahertz), the output noise spectrum is constant where the equivalent noise current is increasing with frequency and is varying as $1/\omega$ where the equivalent noise current is constant. After differentiating through a sufficiently small-time-constant RC network; however, the resulting noise spectrum again has the frequency behavior of the equivalent noise current (Fig. 7). Therefore, the differentiated charge-sensitive preamplifier has superior noise performance in the 100 kilohertz range where the band-pass of typical nuclear pulse-shaping networks occurs.

An important disadvantage to the use of charge-sensitive preamplifiers is the long time constant associated with the discharge of the feedback capacitor (typically one millisecond). If the radiation counting rate is large, the capacitor does not have time to discharge between

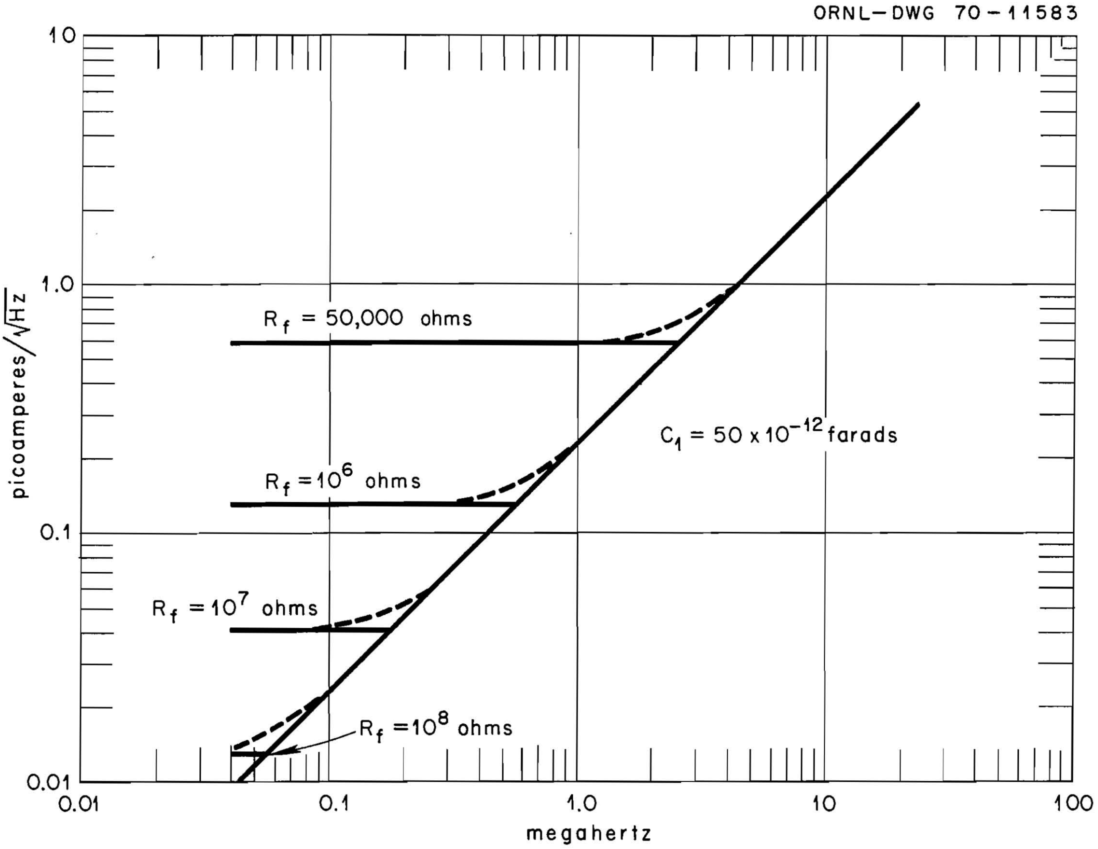

Figure 7. Equivalent noise current variation of the FET input, shunt-feedback amplifier stage showing the contribution of a range of feedback resistance values.

events; thus, a pulse pile-up condition occurs. This condition can lead to nonlinear amplifier operation, resulting in a degradation of the radiation energy resolution. Techniques have been devised to relieve this condition without degrading the noise performance.[11,12] Although effective, such techniques cause appreciable complication to the analyzing system.

III. ERROR-SIGNAL EXTRACTION FROM THE CHARGE-SENSITIVE CONFIGURATION

The transient channel current of the input FET of a charge-sensitive preamplifier is proportional to the waveform of the detector current pulse. This condition may be easily investigated from the general charge-sensitive preamplifier configuration of Fig. 1a, page 2, by applying feedback control-system theory. The configuration may be represented as the general feedback system of Fig. 8. If the output is taken immediately following the FET, the current gain to this point from the input terminal (i_o/i_D) is simply the open-loop transfer function from the input to the point at which the output is taken divided by one plus the loop transmission. Stated mathematically the expression is

$$\frac{i_o}{i_D}(j\omega) = \frac{g_m Z_g(j\omega)}{1 + g_m Z_g(j\omega) Z_i(j\omega)/Z_f(j\omega)} \; . \tag{11}$$

For frequencies up to that at which the loop transmission equals one, Eq. (11) may be simplified to

$$\frac{i_o}{i_D}(j\omega) = \frac{g_m Z_g(j\omega)}{g_m Z_g(j\omega)\, Z_i(j\omega)/Z_f(j\omega)} \; . \tag{12}$$

ORNL-DWG 70-11584

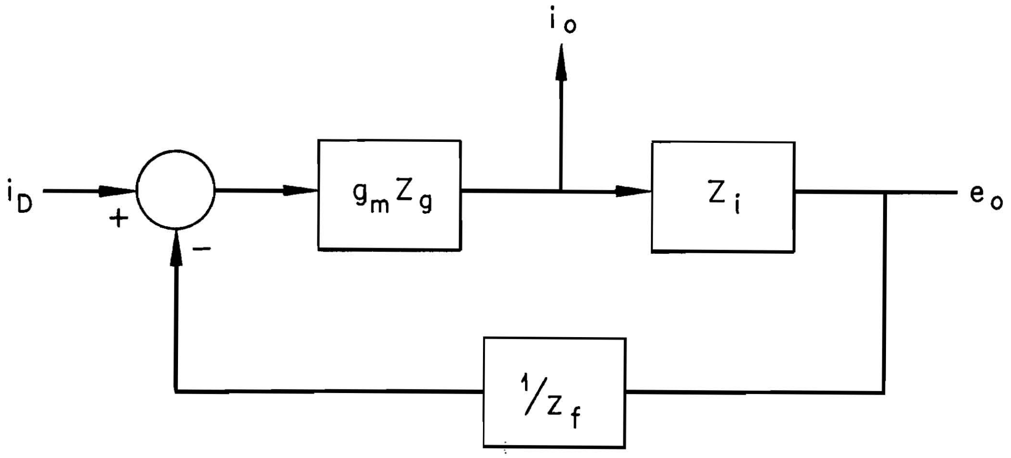

$$Z_g(j\omega) = \frac{R_g}{1 + j\omega R_g C_T}$$

WHERE $R_g = \frac{R_f R_B}{R_f + R_B}$

AND C_1 IS THE TOTAL INPUT CAPACITANCE

$$Z_i(j\omega) = \frac{R_i}{1 + j\omega R_i C_i}$$

$$Z_f(j\omega) = \frac{R_f}{1 + j\omega R_f C_f}$$

Figure 8. Block diagram of the general charge-sensitive preamplifier of Fig. 1a, page 2.

This equation further simplifies to

$$\frac{i_o}{i_D}(j\omega) = \frac{Z_f(j\omega)}{Z_i(j\omega)} \quad . \tag{13}$$

Substituting expressions for Z_f and Z_i yields the equation

$$\frac{i_o}{i_D}(j\omega) = \left(\frac{R_f}{R_i}\right)\frac{(1 + j\omega\, R_i\, C_i)}{(1 + j\omega\, R_f\, C_f)} \quad . \tag{14}$$

If R_i and R_f are very large, which is normally the case, the frequency dependent terms of the numerator and denominator control the gain over a large frequency range; thus, the current gain within this frequency range becomes

$$\frac{i_o}{i_D} = \frac{C_i}{C_f} \quad . \tag{15}$$

This ratio is typically low enough to require considerable additional amplification.

A large portion of the capacitance C_i normally is attributable to active device capacitance. Thus, its value changes with bias conditions and temperature. Stabilizing the percentage changes by adding fixed shunt capacitance lowers the bandwidth. Other nonlinearities present in the actual realization of the Z_i section also appear in the current gain i_o/i_D. Consequently, from gain stability and linearity considerations this technique of obtaining linear, low-noise current amplification is probably inadequate. Although for simultaneous radiation event timing and conventional energy analysis from the available charge proportional output, the configuration offers good performance.

The equivalent noise current is the same as discussed in the preceding section for the charge-sensitive preamplifier since the dominant noise source and the transfer function from the input node to this noise source are the same. Thus, the noise spectrum from the FET drain should be proportionally the same as from the differentiated charge-sensitive preamplifier. However, the means of boosting the drain signal to a usable level must not contribute significant noise. Because of the low-noise level, the amplified current signal from the drain or source should offer good wide-dynamic-range, leading-edge timing if the gain-bandwidth product of the feedback loop is sufficiently large.

CHAPTER III

DEVELOPMENT OF A BROADBAND PREAMPLIFIER CONFIGURATION FOR LOW-NOISE CURRENT PREAMPLIFICATION

From the investigation of Chapter II, the equivalent noise current of FET input, shunt-feedback preamplifier configurations having large, open-loop input impedances was found to be considerably smaller at low frequencies than similar bipolar-transistor types. As indicated in Fig. 7, page 24, the value of the low-frequency, equivalent noise current of the FET input, shunt-feedback configuration has a lower limit determined by the feedback-resistor thermal noise, where leakage-current shot noise is insignificant. However, as indicated in Fig. 6, page 22, the increase in the feedback resistance above a given value decreases the transfer-function bandwidth to a value that requires signal reshaping to reclaim the detector current pulse. Thus, signal integration by the feedback impedance is inherent if the maximum signal-to-noise ratio is to be realized. This condition is true only for the case of RC shunt feedback and does not include broadband, opto-electronic feedback. At the present time the linearity of the latter method in addition to other unresolved problems prevents its use for linear broadband feedback.

This chapter will include an initial investigation concerning the impulse response rise-time capability of a generalized charge-sensitive preamplifier and the appropriate way of differentiating the output voltage to obtain a signal proportional to the detector current pulse. Following this investigation will be the introduction of a new current-amplifying configuration, also with high-impedance feedback, which has several advantages over the normal charge-sensitive configuration. The analysis of this new configuration will include considerations of bandwidth, input and output impedances, and noise characteristics.

I. DESIGN CONSIDERATIONS FOR A BROADBAND, DIFFERENTIATED CHARGE-SENSITIVE PREAMPLIFIER SYSTEM

Preamplifier Bandwidth

In order to allow an adequate reproduction of the detector-current-pulse leading edge, the composite bandwidth due to the preamplifier, differentiator and any additional amplification stages should generally be at least 50 megahertz although smaller or larger values may be desired for specific applications. Before turning attention to the bandwidth degradation due to differentiation, it is essential to predict the limits imposed by the charge-sensitive preamplifier.

The fact that most charge-sensitive preamplifier designs can be reduced to the general form of Fig. 1a, page 2, allows the dominant parameters controlling the impulse response to be easily determined. The block diagram form of this feedback configuration is shown in Fig. 8, page 26. From the block diagram the impulse response of the closed-loop transfer function can be written from inspection as

$$Z_T(s) = \frac{E_o}{I_D}(s) = \frac{g_m Z_g(s)\, Z_i(s)}{1 + g_m Z_g(s) Z_i(s)/Z_f(s)} \quad . \qquad (16)$$

For transient analysis the Laplace variable s has been substituted for $j\omega$.

Replacing the impedance functions by their respective expressions and simplifying results in the equation,

$$Z_T(s) = \frac{g_m R_g R_i}{R_g C_1 R_i C_i s^2 + (R_i C_i + R_g C_1 + g_m R_g R_i C_f)s + g_m R_g R_i / R_f} . \qquad (17)$$

If the approximations $R_g C_1 \geq R_i C_i$ and $g_m R_i C_f >> C_1$ hold, Eq. (17) can be simplified to

$$Z_T(s) \approx \frac{R_f}{(R_f C_1 C_i / g_m) s^2 + R_f C_f s + 1} . \qquad (18)$$

The denominator has two poles on the negative real axis of the s-plane. Because the poles are separated by several orders of magnitude, Eq. (18) can be written in an approximate factored form with minimal error. This form is

$$Z_T(s) \approx \frac{R_f}{(R_f C_f s + 1) \left[(C_i C_1 / g_m C_f) s + 1\right]} . \qquad (19)$$

The pole at $s = -g_m C_f / C_i C_1$ determines the output risetime for an impulse input. The pole at $R_f C_f$ is the long-duration, feedback-network time constant. The C_f / C_1 portion of the high-frequency pole is the feedback attenuation due to the voltage division between the feedback capacitor C_f and the total input capacitance C_1. If this attenuation is large, a broadband current gain section may be required in the forward path (normally between the FET drain and the impedance transfer section Z_i) to boost the effective FET transconductance. With this addition the high-frequency pole is located at $s = -g_m A_i C_f / C_i C_1$, provided the pole controlling the bandwidth of the inserted current-gain section A_i has a magnitude appreciably larger than this. The impulse response given by

Eq. (19) now becomes

$$Z_T(s) = \frac{R_f}{(R_f C_f s + 1) \left[(C_i C_1 / g_m A_i C_f) s + 1\right]} \quad . \tag{20}$$

Differentiation Network

In order to adequately reporduce the detector current pulse, the pole at $s = -1/R_f C_f$ must be removed by the proper differentiating network. The differentiating network indicated in Fig. 9a is frequently used in nuclear pulse amplifiers for this purpose.[13] Since the differentiating capacitor C_D is usually much greater than the input capacitance to the following amplifier stage, the latter value is usually not considered. The zero of the network transfer function cancels the preamplifier transfer function pole due to the feedback network [Eq. (20)]; thus, the combined transfer function of the preamplifier and the differentiating network is

$$\frac{E_2}{I_D}(s) = Z_T'(s) = \frac{R_f}{R_s} \left\{ \frac{R_D}{(R_D C_D s + 1) \left[(C_i C_g / g_m A_i C_f) s + 1\right]} \right\} . \tag{21}$$

The $R_D C_D$ time constant should be as small as possible.

The choice of values in the differentiating network is based on two considerations. First, with reference to Fig. 9a, the noise voltage due to the resistor R_D plus the equivalent noise resistance R_{eq} of the following broadband amplifier stage should be much smaller than the noise current due to the feedback resistor R_f multiplied by the midband transfer function [Eq. (21) evaluated at $s = 0$] from the input to R_D. This condition is expressed by the inequality,

$$\frac{4kT}{R_f} \left(\frac{R_f \, R_D}{R_s} \right)^2 \gg 4kT \, (R_D + R_{eq}) \quad . \tag{22}$$

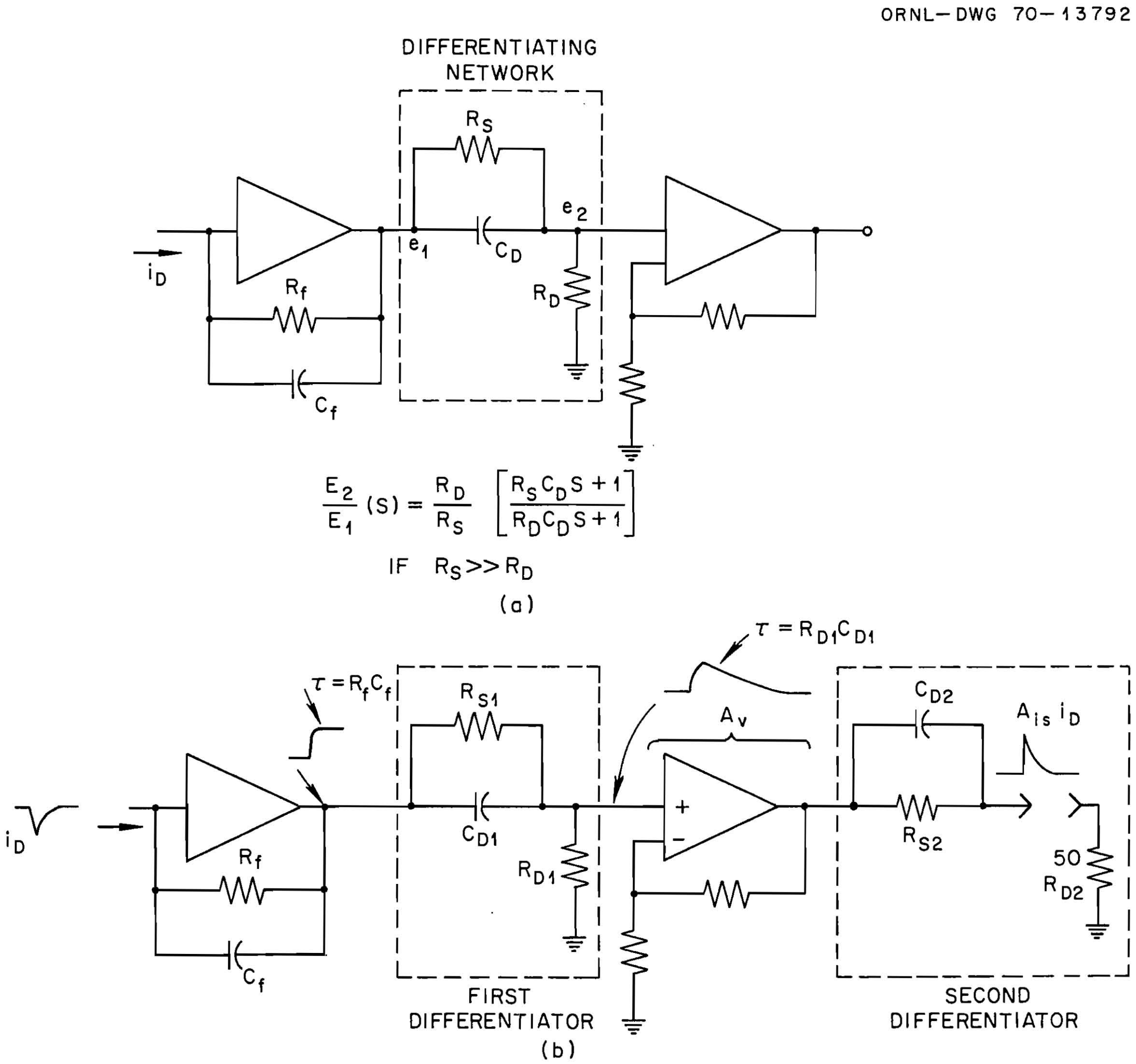

Figure 9. Illustration of a differentiation technique for recovering the detector-current waveform from a charge-sensitive preamplifier.

Both sides of this inequality have been squared and the noise voltage and current replaced by the corresponding resistance values. This first consideration prevents the differentiator from contributing to the low-frequency noise of the preamplifier and consequently increasing the noise-corner frequency. The second consideration is that the zero at $s = -1/R_sC_D$ cancel the preamplifier pole at $s = -1/R_fC_f$, requiring

$$R_sC_D = R_fC_f. \tag{23}$$

These two considerations, in effect, limit the differentiating time constant R_DC_D or τ_D. Solving Eq. (22) for R_s yields

$$R_s \ll R_D\left(\frac{R_f}{R_D + R_{eq}}\right)^{1/2} , \tag{24}$$

and solving Eq. (23) for C_D gives the expression,

$$C_D = \frac{R_fC_f}{R_s} . \tag{25}$$

The differentiating time constant τ_D may now be written as

$$\tau_D = R_DC_D = \frac{R_D}{R_s}(R_fC_f) . \tag{26}$$

Replacing R_s by Eq. (24) gives the limitation on τ_D as

$$\tau_D \gg C_f\left[(R_D + R_{eq})\, R_f\right]^{1/2} . \tag{27}$$

Thus, for any chosen value of R_D, τ_D should be at least an order of magnitude greater than the right side of the inequality. This requirement fixes C_D and subsequently R_s [Eq. (23)] . As an example, suppose $C_f = 10^{-12}$ farads, $R_{eq} = 1000$ ohms, $R_f = 10^9$ ohms, and R_D is chosen as 100 ohms. From Eq. (27) τ_D should be at least 10.5×10^{-6} seconds. As a result of this differentiation, the preamplifier transfer-function pole associated with the R_fC_f time constant (1000 x 10^{-6} seconds for this example) can only be reduced to about 10.5 x 10^{-6} seconds. Consequently, the broadband gain following the differentiator has to be large enough to allow another differentiation having an acceptable time constant (typically less than 10^{-8} sec). The transmission zero of the second differentiator should cancel the transmission pole of the first differentiator. Although the first differentiating network is not completely necessary, it prevents the following broadband amplifiers from passing the long-tail pulse from the preamplifier. For high count rates it is desirable to reduce the pulse from the preamplifier to as short a value as possible before further amplification.

The composite amplifier system response now has poles from the preamplifier, the broadband amplifier section (of one or more stages) following the first differentiating network and from the second differentiating network. The complete amplifier system is shown in Fig. 9b, page 33. The mid-frequency current A_{is} of the system to the 50 ohm load resistor R_{D2} is

$$A_{is} = \frac{R_f R_D A_v}{R_{s1} R_{s2}} \quad . \tag{28}$$

II. NEW SHUNT-FEEDBACK CONFIGURATION FOR LOW-NOISE CURRENT PREAMPLIFICATION

Conceptual Design

A shunt-feedback amplifier stage can be produced from either of two basic designs. The first design that was discussed in Chapter II consists of a low-output-impedance, broadband, operational amplifier having a feedback resistor and shunting capacitor between the input and output terminals. The product of the feedback resistor and capacitor values determines whether the closed-loop amplifier exhibits a broadband or integrating (charge-sensitive) transfer characteristic. The input impedance is low and also largely reactive depending again on the relative values of feedback capacitance and resistance. The second design of a shunt-feedback amplifier consists of a high-output-impedance, broadband operational amplifier with the output current split between a load network and a feedback network. The most basic form of this feedback configuration is found in the single-transistor stage of Fig. 2c, page 10. The common-base stage Q_2 merely serves as a means of taking the output current signal from the shunt-feedback transistor. Replacing the transistor Q_1 with a more complex gain section having an FET input allows much improvement in linearity. For low-noise performance the feedback resistor value can be made as large as that used in charge-sensitive preamplifiers so long as the ratio of the feedback resistor to load resistor equals the ratio of the load capacitor to the feedback capacitor. The general configuration is shown in Fig. 10. In this figure a secondary current output i_o' is indicated having a one to one correspondence to the primary current output i_o. The closed-loop current gain, as determined by the reciprocal of the feedback ratio, is

$$A_{CL} = \frac{i_o}{i_D} = \frac{Z_f + Z_o}{Z_o} \quad , \tag{29}$$

assuming the amplifier output impedance is insignificantly large. Substituting the impedance expressions into Eq. (29) and simplifying yields

ORNL-DWG 70-13794

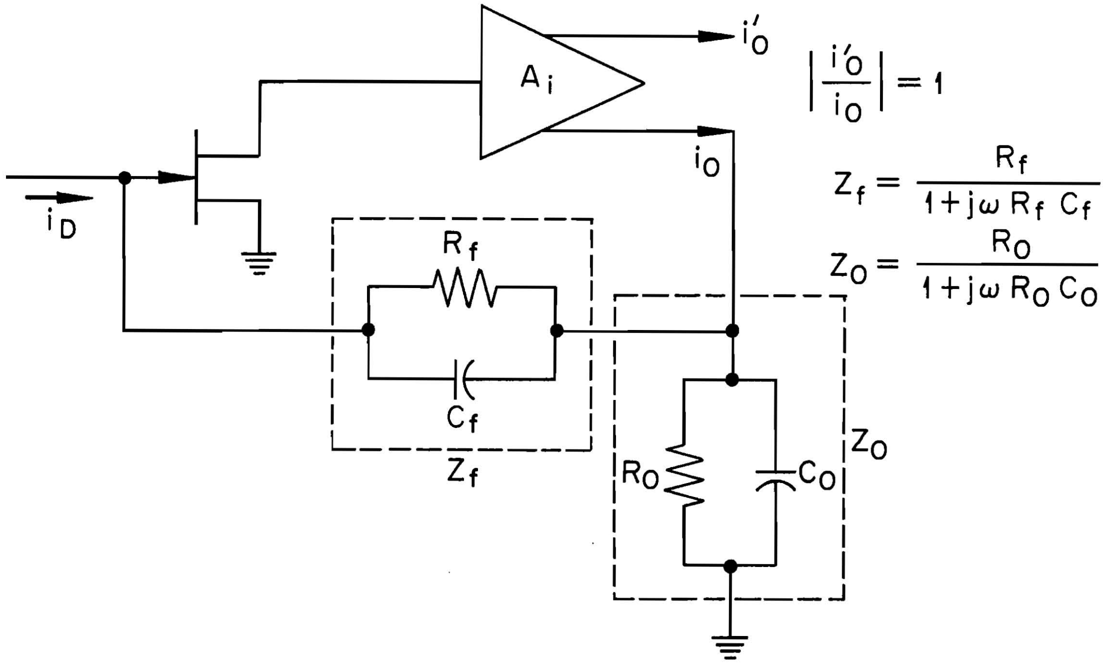

Figure 10. A basic configuration of a broadband, low-noise current preamplifier.

$$A_{CL}(s) = \frac{R_o + R_f}{R_o}\left[\frac{\left[R_f R_o/(R_f + R_o)\right](C_o + C_f)s + 1}{R_f C_f\ s + 1}\right]. \tag{30}$$

If $R_f = KR_o$ and $C_o = KC_f$ this equation reduces to

$$A_{CL} = K + 1\ . \tag{31}$$

For very large resistor values, the mid- and high-frequency closed-loop current gain is controlled essentially by the ratio of load capacitance C_o to feedback capacitance C_f. Because a large value of feedback resistance is necessary for low noise performance, the feedback time constant and subsequently the load time constant is very large compared to the widths of typical detector current pulses. The signal voltage produced at the output node is therefore the integral of the detector current pulse, even though the current gain i_o'/i_D is independent of frequency within the bandwidth of the preamplifier.

This configuration is basically a charge-sensitive preamplifier with differentiation performed by the feedback network to allow the realization of a constant current gain over the preamplifier's bandwidth. With a low input impedance and a high output impedance, this configuration can be classified as a current preamplifier, even though a charge-proportional signal is present within the feedback loop. In order to delineate the advantages of this configuration, a more detailed investigation is necessary.

Configuration Refinement and Bandwidth Analysis

The configuration of Fig. 10 has two disadvantages. First a finite amplifier output impedance parallels the load impedance Z_o. If this output impedance changes for any reason, the closed-loop current gain given by Eq. (29) changes by an amount determined by the relative value of the output impedance to the load impedance.

The other disadvantage is the difficulty of obtaining an output signal current i_o' without degrading the linearity or signal-to-noise ratio that is characteristic of the normal current output i_o. Both of these disadvantages may be excluded by taking the current signal from the grounded end of the load network. This modification is shown in Fig. 11a. The signal voltage e_o is the product of the input current i_D and the feedback impedance Z_f; and the output current is the signal voltage e_o divided by the load impedance Z_o; thus, the signal current gain is

$$\frac{i_L}{i_D} = A_{CL} = \frac{Z_f}{Z_o} . \tag{32}$$

If $Z_f = KZ_o$ then the closed loop gain A_{CL} is a constant K; whereas, for the configuration of Fig. 10, the gain was found to be (K + 1) [Eq. (31)]. With this modification the output signal current is not as dependent on that part of i_o that flows through the amplifier output impedance; however, this impedance does have a lower limit.

The output-impedance limitations and bandwidth capabilities may be derived from the equivalent circuit of Fig. 11b. The gain section A_i is assumed to have a low input impedance, a gain that is constant to frequencies well in excess of the closed-loop bandwidth of the preamplifier, and a large output impedance indicated as the resistor R_s in parallel with the capacitor C_s. The total input capacitance C_1 includes contributions from the detector, the FET and strays. The nodal equations in matrix form are

ORNL-DWG 70-13795

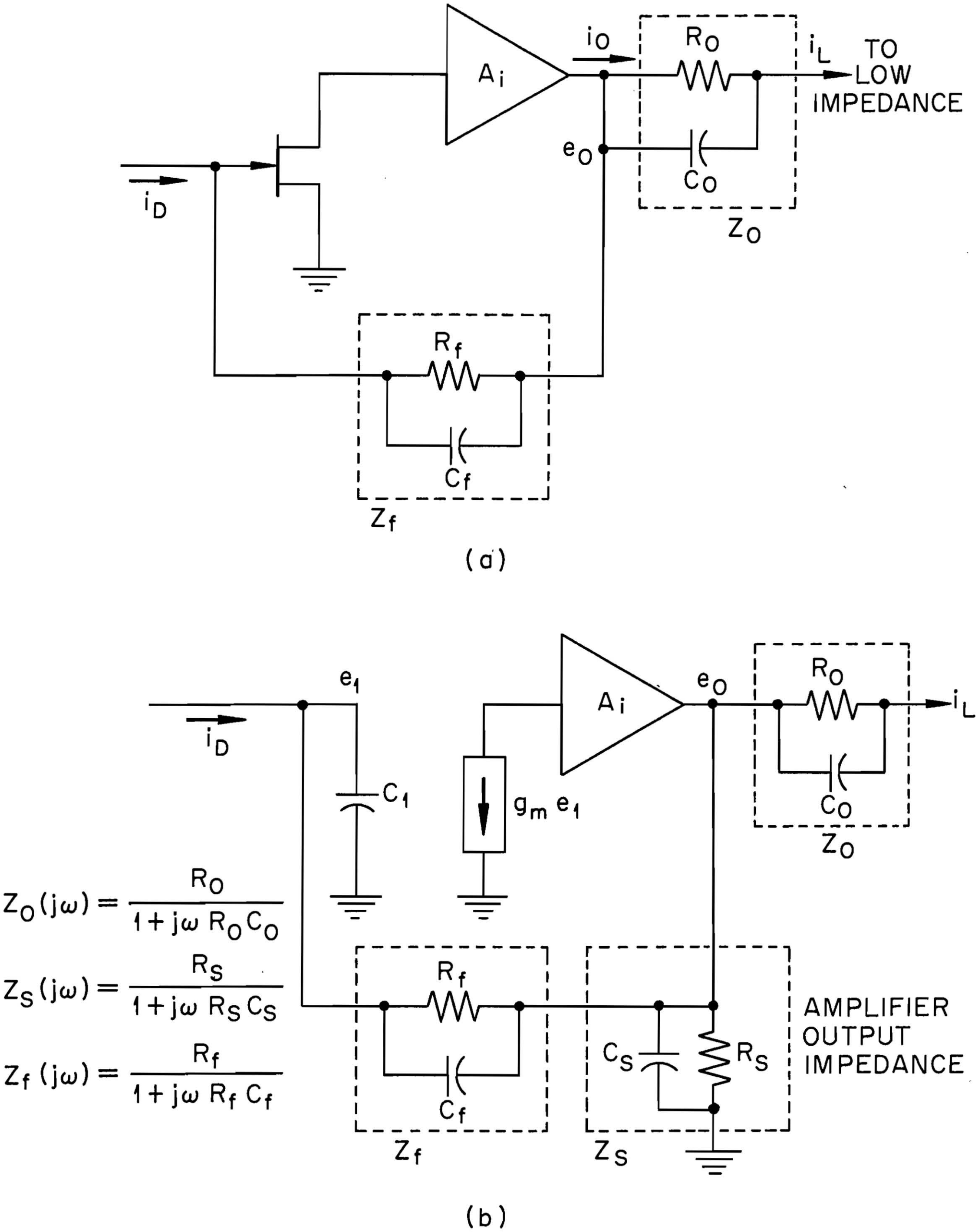

$$Z_O(j\omega) = \frac{R_O}{1 + j\omega R_O C_O}$$

$$Z_S(j\omega) = \frac{R_S}{1 + j\omega R_S C_S}$$

$$Z_f(j\omega) = \frac{R_f}{1 + j\omega R_f C_f}$$

Figure 11. (a) Modification of the preamplifier stage of Fig. 10, page 37, with (b) the equivalent circuit.

$$\begin{bmatrix} (1/Z_f + j\omega C_1) & -1/Z_f \\ (g_m A_i - 1/Z_f) & (1/Z_o + 1/Z_s + 1/Z_f) \end{bmatrix} \begin{bmatrix} e_1 \\ e_o \end{bmatrix} = \begin{bmatrix} i_D \\ 0 \end{bmatrix} . \tag{33}$$

All impedances are frequency-dependent functions. The resulting impedance transfer function is approximately

$$\frac{e_o}{i_D}(j\omega) \approx - \frac{g_m A_i Z_f Z_o Z_s}{j\omega C_1 Z_f (Z_s + Z_o) + Z_o + Z_s + g_m A_i Z_s Z_o} . \tag{34}$$

The assumptions required for this result are $g_m A_i >> |1/Z_f|$ (typically true except at very high frequencies) and $|Z_f| >> |Z_o|$ (true for closed-loop gains above about ten). At low frequencies the impedance functions reduce to their respective resistance values reducing Eq. (34) to

$$\frac{e_o}{i_D} \approx - \frac{g_m A_i R_f R_o R_s}{R_o + R_s + g_m A_i R_s R_o} . \tag{35}$$

This impedance transfer function reduces to the expected value of R_f if

$$g_m A_i R_s R_o >> R_o + R_s . \tag{36}$$

If this inequality is satisfied, the closed-loop, low-frequency current gain A_{CL} becomes

$$A_{CL} = \frac{i_L}{i_D} = - \frac{e_o}{i_D R_o} = - \frac{R_f}{R_o} . \tag{37}$$

For mid- and high-frequency performance Eq. (34) must be further simplified. Dividing the numerator and denominator of this equation by the quantity $(Z_o + Z_s)$ gives the form,

$$\frac{e_o}{i_D}(j\omega) \approx - \frac{g_m A_i Z_f Z_{po}}{1 + g_m A_i Z_{po} + j\omega C_1 Z_f} , \tag{38}$$

where

$$Z_{po} = \frac{R_{po}}{1 + j\omega R_{po} C_{To}} \quad . \tag{39}$$

The capacitance C_{To} is the sum of C_s and C_o and the resistance R_{po} is the parallel combination of R_o and R_s. Expanding and rationalizing Eq. (38) with the impedance expressions inserted yields

$$\frac{e_o}{i_D}(j\omega) \approx - \frac{R_f}{-\omega^2 (C_1 C_{To} R_f / g_m A_i) + j\omega R_f C_f + 1} \quad . \tag{40}$$

The primary assumption required for this result was that

$$g_m A_i R_{po} >> C_1 / C_f \quad . \tag{41}$$

The denominator contains two real roots separated by several orders of magnitude; thus, Eq. (40) can be represented in approximate factored form as

$$\frac{e_o}{i_D}(j\omega) \approx - \frac{R_f}{\left[j\omega(C_{To} C_1 / C_f g_m A_i) + 1\right] (j\omega R_f C_f + 1)} \quad . \tag{42}$$

The resulting current transfer function is

$$A_{CL}(j\omega) = \frac{i_L}{i_D}(j\omega) = \frac{e_o}{i_D}(j\omega) \left[1/Z_o(j\omega)\right] \quad . \tag{43}$$

Substituting Eq. (42) and the expression for $Z_o(j\omega)$ (Fig. 11b, page 40) into Eq. (43) gives

$$A_{CL}(j\omega) \approx - \frac{R_f}{R_o \left[1 + j\omega(C_{To} C_1 / C_f g_m A_i)\right]} \quad . \tag{44}$$

The frequency at which the log magnitude of the current gain has decreased by three decibels is

$$f_{-3} \approx \frac{g_m A_i C_f}{2\pi \, C_1 C_{To}} \quad , \tag{45}$$

provided the bandwidth of the broadband gain section A_i is several times greater than this value. If the gain A_i equals the feedback attenuation C_f/C_{To} (or C_f/C_o if $C_o \gg C_s$), the bandwidth expressed by Eq. (45) simplifies to

$$f_{-3} \approx \frac{g_m}{2\pi \, C_1} \quad , \tag{46}$$

which is essentially the gain-bandwidth product of the input device degraded by the detector capacitance. With the proper choice of an input device, bandwidths above 50 megahertz are possible for a wide range of detector capacitance values.

Input and Output Impedance Evaluation

The input impedance of the configuration of Fig. 11a, page 40, may be evaluated from Eq. (33) by solving for the node voltage e_1. In terms of the impedance components

$$Z_{in}(j\omega) = \frac{e_1}{i_D}(j\omega) \approx \frac{Z_{po} + Z_f}{1 + g_m A_i Z_{po} + j\omega C_1 Z_f} \quad , \tag{47}$$

where Z_{po} was defined by Eq. (39). The denominator is the same as that of the transfer impedance [Eq. (38)]. After substituting the impedance expressions into Eq. (47), the resulting equation can be simplified to

$$Z_{in}(j\omega) \approx \frac{R_f + R_{po}}{g_m A_i R_{po}} \left[\frac{1 + j\omega\, R_{po} C_{To}}{-\omega^2 C_1 C_{To} R_f / g_m A_i + j\omega R_f C_f + 1} \right] \quad , \tag{48}$$

using the same assumption that was applied to Eq. (40). By the same reasoning used to obtain Eq. (42) from Eq. (40), the denominator may be written in approximate factored form. The resulting equation is

$$Z_{in}(j\omega) \approx \frac{R_f + R_{po}}{g_m A_i R_{po}} \left\{ \frac{j\omega R_{po} C_{To} + 1}{\left[j\omega (C_{To} C_1 / C_f g_m A_i) + 1 \right] (j\omega R_f C_f + 1)} \right\} . \qquad (49)$$

If the output impedance time constant $R_s C_s$ does not appreciably affect the load impedance time constant $R_o C_o$, this time constant is approximately equal to $R_{po} C_{To}$; consequently, for $R_o C_o$ equal to $R_f C_f$, the numerator cancels the denominator factor containing $R_f C_f$. For this condition Eq.(49) reduces to

$$Z_{in}(j\omega) \approx \frac{R_f + R_{po}}{g_m A_i R_{po}} \left[\frac{1}{(1 + j\omega C_{To} C_1 / C_f g_m A_i)} \right] . \qquad (50)$$

For $R_f / R_{po} \approx C_{To} / C_f \approx A_i \gg 1$, this equation becomes

$$Z_{in}(j\omega) \approx \frac{1}{g_m (1 + j\omega C_1 / g_m)} . \qquad (51)$$

Because the gain section A_i was chosen constant over the preamplifier bandwidth, the input impedance, unlike that of the charge-sensitive preamplifier, is a constant low value over the preamplifier bandwidth. This result is important when cascading stages.

The impedance existing at the output end of the load network (Fig. 11a, page 40) consists of the impedance at the amplifier output node, indicated by the voltage e_o, plus the load impedance Z_o. The impedance at the amplifier output node is round from Eq. (33) by shifting the current drive from the input to this point. This procedure amounts to replacing the zero in the column matrix on the right side of Eq. (33) by a forcing function i_{out} and setting the upper element i_D equal to zero. Solving for the node voltage e_o and dividing both sides by the current i_{out} yields

$$Z_{out}(j\omega) = \frac{e_o}{i_{out}} \approx \frac{(1/Z_f + j\omega C_1)\, Z_f Z_{po}}{1 + g_m A_i Z_{po} + j\omega C_1 Z_f} . \qquad (52)$$

Replacing the impedance functions with the appropriate expressions and simplifying in the same manner that was described for the input impedance gives

$$Z_{out}(j\omega) \approx \frac{1}{g_m A_i} \left\{ \frac{(1 + j\omega\, R_f C_1)}{\left[j\omega(C_{To} C_1 / C_f g_m A_i) + 1 \right] (j\omega R_f C_f + 1)} \right\} . \tag{53}$$

At frequencies above $1/R_f C_f$ radians per second the behavior of Z_{out} can best be described as that of a parallel resistor and capacitor having respective values of $C_1/C_f g_m A_i$ and C_{To}. Thus, the impedance that would be measured at the output end of the load network is the sum of the impedance Z_{out} and the load network impedance Z_o. Because of the relatively small typical value of $C_1/C_f g_m A_i$, the impedance at the output end of the load network is essentially determined by the capacitor C_o. The output impedance is an important consideration when cascading stages, a topic to be considered later in this chapter.

Linearity Considerations

Of primary importance in the amplification of fast, radiation-detector current pulses is the accuracy with which the total charge in the pulse (area of the current pulse) can be measured. In considering the capability of the preamplifier to preserve area linearity two aspects must be investigated. First, instabilities or nonlinearities in the preamplifier's mid-frequency gain may cause error in the magnitude of that portion of the current pulse following the rise time. Second, variations in the preamplifier's gain-bandwidth product due to changes in g_m, A_i or C_1 (Fig. 11b, page 40) will cause a change in the rise time. Rise-time changes due to the preamplifier, however, are indistinguishable from detector rise-time changes due to various modes of pulse formation.

Regardless of the source, rise-time variation produces very small area change, if the peak measurement of the integrated output pulse is made after a sufficient time elapse from the beginning of the pulse. To visualize this fact consider an amplified detector current pulse rising on a time constant τ_r, determined by the preamplifier, and decaying exponentially on a time constant τ_d where τ_d is much greater than τ_r. After passing through an integrating network having a time constant of τ_i, the pulse may be expressed in terms of the Laplace variable s as

$$E_o(s) = \frac{A_o i_D R_i (1/\tau_r)(1/\tau_d)(1/\tau_i)}{(s + 1/\tau_r)(s + 1/\tau_d)(s + 1/\tau_i)} \quad , \tag{54}$$

where A_o is the total current gain, i_D is the peak detector current and R_i is the transfer impedance of the integrator at low frequencies. The time response may be found from the residue theorem of complex variables as

$$e(t) = A_o\, i_D R_i \left[\frac{\tau_r}{(\tau_r - \tau_d)(\tau_r - \tau_i)} e^{-t/\tau_r} + \frac{\tau_d}{(\tau_d - \tau_r)(\tau_d - \tau_i)} e^{-t/\tau_d} + \frac{\tau_i}{(\tau_i - \tau_r)(\tau_i - \tau_d)} e^{-t/\tau_i} \right] . \tag{55}$$

If the peak measurement of the output pulse is made after an adequate time elapse from t(0), the beginning of the current pulse, the first two exponential terms of Eq. (55) are essentially zero. The third term containing the pulse height information at the time of measurement requires τ_i much greater than τ_r for negligible change with changes in τ_r. Since the signal from the integrator passes through a differentiator before its amplitude is measured, the practical criteria is that the time constant of the final differentiator (normally several microseconds) be much greater than τ_r. For a broadband preamplifier this criteria can be satisfied, resulting in negligible output pulse amplitude change with variations in amplifier rise time. Due to the wide dispersion of pulse shapes from certain detectors, the integration time constant should actually be much longer than the detector collection time and the pulse-height measurement should accordingly be made after an appropriate time elapse.

The most important criteria required for mid-frequency gain stability and linearity is stated by the inequality of Eq. (41). The extent to which this inequality is satisfied determines the tolerance of the mid-frequency gain to changes in g_m, A_i, C_1, and R_s.

Noise Performance

Noise-generating mechanisms of the junction field-effect transistor have been studied in great detail. Several classic papers appearing in the early 1960's[14,15] quantitatively describe the noise characteristics of this device. Also numerous texts are now available which treat this subject; consequently, only a qualitative description of the FET noise model is necessary before calculating output noise power spectra for the preamplifier configuration of Fig. 11a, page 40.

By adding two lumped noise-current generators to the equivalent circuit of Fig. 11b, the output noise due to the major noise-generating sources of the FET and other circuit components can be described. These noise-current generators are placed at the gate and drain of the FET (illustrated in Fig. 12).

The gate-noise generator includes four major components. The noise-current $\overline{i_{go}^2}$ is due to shot noise of the gate electron reverse current I_{re}

ORNL-DWG 70-13796

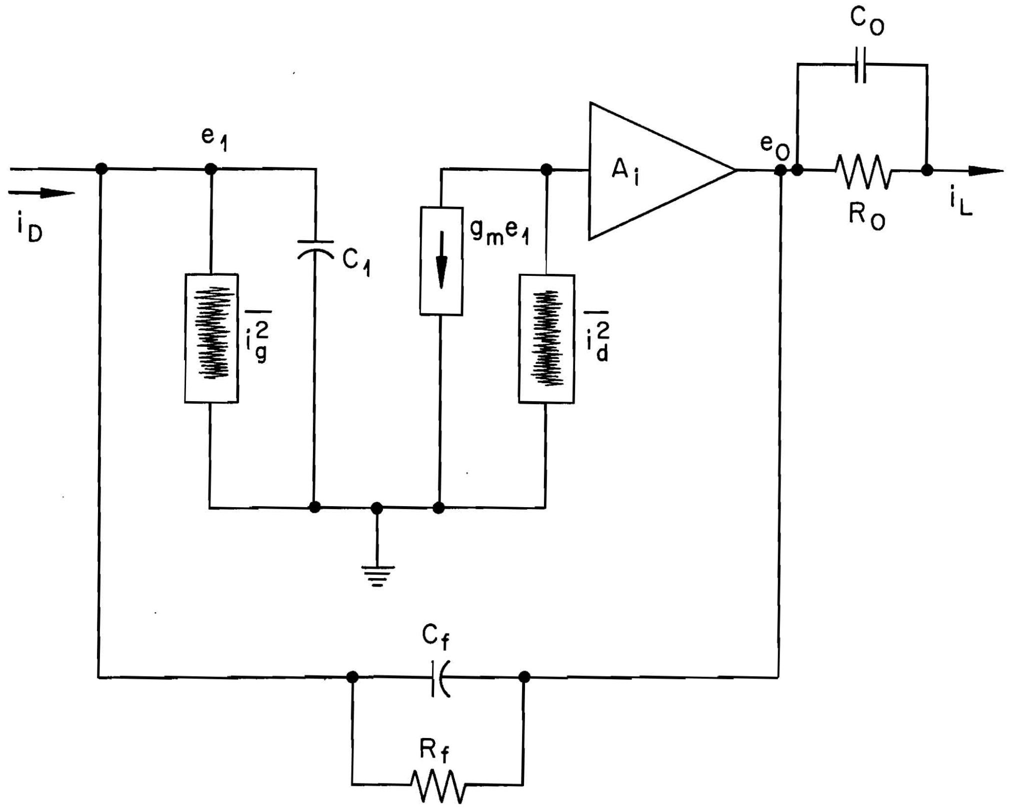

$$\overline{i_g^2} = \overline{i_{go}^2} + \overline{i_{gh}^2} + \overline{i_R^2} + \overline{i_{do}^2}$$

$$\overline{i_d^2} = \overline{i_{tn}^2} + \overline{i_f^2} + \overline{i_{eq}^2}$$

$\overline{i_{go}^2}$	GATE LEAKAGE-CURRENT SHOT NOISE	$\overline{i_{do}^2}$	DETECTOR LEAKAGE-CURRENT SHOT NOISE
$\overline{i_{gh}^2}$	HIGH-FREQUENCY GATE NOISE	$\overline{i_{th}^2}$	THERMAL NOISE OF THE FET CHANNEL
$\overline{i_R^2}$	THERMAL NOISE CURRENT DUE TO FEEDBACK AND DETECTOR BIAS RESISTORS	$\overline{i_f^2}$	FLICKER NOISE
		$\overline{i_{eq}^2}$	EQUIVALENT NOISE CURRENT OF THE CURRENT GAIN SECTION A_i

Figure 12. The equivalent circuit of Fig. 11b, page 40, with noise sources added.

and to shot noise of the hole reverse current I_{rh}. This noise-current is given by

$$\overline{i_{go}^2} = 2e\ I_g\ \Delta f, \tag{56}$$

where

$$I_g = I_{re} + I_{rh}.$$

The noise-current component $\overline{i_{gh}^2}$ is normally referred to as high-frequency gate noise and arises from the fact that, at high frequencies, a portion of the channel thermal noise is coupled by capacitance to the gate circuit. Consequently, this noise-current component has a small degree of correlation to the channel noise causing the output noise due to this source to typically be 10 to 20 percent lower than that predicted by ignoring the correlation. The output noise due to this generator increases linearily with frequency from relatively low frequencies to near g_m/C_{gs} (gate to source capacitance); however, near and above this frequency, the noise current has been shown to increase quadradically.[16] This second order effect will be ignored. The noise current generator $\overline{i_{gh}^2}$ as derived by Van der Ziel is

$$\overline{i_{gh}^2} = a \left[0.7\ (4kT\ \Delta f)/g_m\right] \omega^2\ C_{gs}^2\ , \tag{57}$$

where a is typically 1/3 for junction FET's. The two remaining gate-noise current components $\overline{i_R^2}$, the thermal-noise current due to the feedback and detector bias resistors and $\overline{i_{do}^2}$, the shot noise due to the detector leakage current, can be described by previously stated equations. The thermal noise current of resistance is described by Eq. (1), page 11, and the shot noise current of the detector may be found from Eq. (56) by substituting appropriate values.

The noise current generator in the drain of the FET consists of three basic components. The $\overline{i_{tn}^2}$ noise current is due to thermal noise in the channel and is given approximately by

$$\overline{i_{tn}^2} = 0.7\ (4\ kT\ g_m\ \Delta f). \tag{58}$$

The $\overline{i_f^2}$ component represents flicker noise arising from carrier density fluctuations. Several authors[17,18] have treated this subject in detail. The noise current represented by this generator is

$$\overline{i_f^2} = A\ g_m^2 \left(\frac{\tau}{1 + \tau^2\omega^2} \right) , \tag{59}$$

where A is a constant depending on the particular device, and τ is a fluctuation decay time constant depending on the trapping mechanisms present. The noise current component $\overline{i_{eq}^2}$ is the equivalent noise current of the broadband, current-gain section A_i to be treated in the next chapter.

The equivalent circuit of Fig. 12 can be more generally represented as the feedback system of Fig. 13. The detector bias resistor is excluded; however, its effect on the noise performance can be included by decreasing the value of R_f to the value that would be obtained after paralleling it by the bias resistor. The closed-loop gain from the $\overline{i_d^2}$ noise generator to the output can be written from inspection as

$$A_{do}\ (j\omega) = \frac{A_i}{1 + g_m Z_g\ A_i \beta} \quad . \tag{60}$$

ORNL-DWG 70-13798

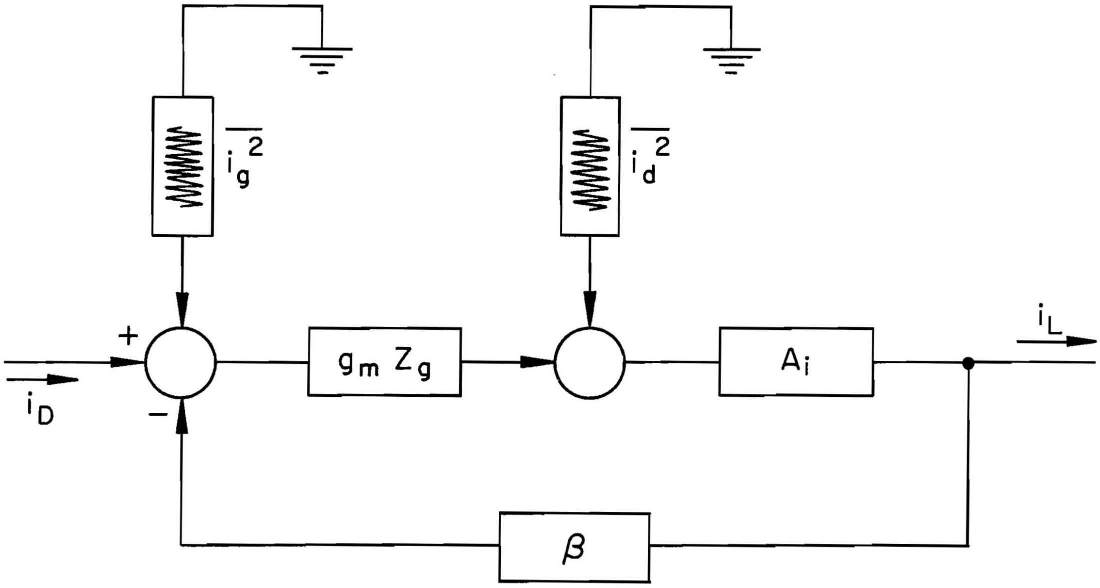

$$Z_g(j\omega) = \frac{R_f}{1 + j\omega R_f C_1} \qquad \beta = \frac{C_f}{C_O + C_f}$$

C_1 = TOTAL INPUT CAPACITANCE

Figure 13. Feedback system form of the preamplifier configuration of Fig. 11a, page 40, with the noise sources of Fig. 12, page 48, included.

Substituting indicated functions for $Z_g(j\omega)$ and β yields

$$A_{do}(j\omega) = \frac{A_i}{1 + \dfrac{g_m A_i R_f C_f}{(1 + j\omega R_f C_1)(C_o + C_f)}} \quad . \tag{60a}$$

for $g_m A_i R_f C_f/(C_o + C_f) \gg 1$,

$$A_{do}(j\omega) \approx \frac{(C_o + C_f)(1 + j\omega\, R_f C_1)}{C_f g_m R_f \left[1 + \dfrac{j\omega C_1 (C_o + C_f)}{g_m A_i C_f}\right]} \quad . \tag{61}$$

The complete output power spectral density due to the $\overline{i_d^2}$ generator (Fig. 12, page 48) can be represented generally as

$$\overline{i_1^2} = \overline{i_d^2} A_{do}(j\omega)\ A_{do}(-j\omega) \quad . \tag{62}$$

Applying Eq. (61) to this expression gives

$$\overline{i_1^2} = \overline{i_d^2} \left\{ \frac{(C_o + C_f)^2\ (1 + \omega^2 R_f^2 C_1^2)}{C_f^2\ g_m^2\ R_f^2 \left[1 + \dfrac{\omega^2 C_1^2 (C_o + C_f)^2}{g_m^2\ A_i^2(\omega)\ C_f^2}\right]} \right\} \quad . \tag{63}$$

The frequency dependency of A_i is indicated to allow for very high-frequency poles, typically in the 200 to 400 megahertz range. The effect of these poles is to diminish the output-power spectral density at very high frequencies. The frequency behavior of Eq. (63) is the same as was predicted by the simplified analysis of Chapter II dealing with the generalized, shunt-feedback amplifier stage.

The output power-spectral density due to the $\overline{i_g^2}$ noise-current generator of Fig. 12, page 48, is easily obtained since this noise-current generator is in the same circuit position as the signal source. Using the preamplifier current-transfer function i_L/i_D expressed by Eq. (44), the output-power spectral density due to the $\overline{i_g^2}$ noise current becomes

$$\overline{i_2^2} = \overline{i_g^2} \left(\frac{R_f}{R_o} \right)^2 \left[\frac{1}{1 + \omega^2 (C_{To}^2 C_1^2 / C_f^2 g_m^2 A_i^2)} \right] . \tag{64}$$

The capacitance C_{To}, defined on page 42, reduces to C_o if the output capacitance of the gain section A_i is sufficiently small.

The total mean-squared, output noise spectral density becomes

$$\overline{i_L^2} = \overline{i_1^2} + \overline{i_2^2} \quad . \tag{65}$$

Substituting Eqs. (63) and (64) into Eq. (65), inserting expressions for the components of $\overline{i_d^2}$ and $\overline{i_g^2}$ and simplifying gives

$$\begin{aligned} \overline{i_L^2} = |A_{CL}|^2 \Bigg\{ & \left[\frac{A\tau}{(1 + \tau^2 \omega^2)} \right] \left[\frac{(1 + \omega^2 R_f^2 C_1^2)}{R_f^2} \right] \\ & + \left[\frac{0.7(4kT)}{g_m} \right] \left[\omega^2 (C_1^2 + C_{gs}^2/3) \right] \\ & + \left[\overline{i_{eq}^2} (\omega^2 C_1^2 / g_m^2) \right] + \left[4kT/R_T + 2e(I_{go} + I_{do}) \right] \Bigg\} , \end{aligned} \tag{66}$$

where $|A_{CL}| = R_f/R_o = C_o/C_f \approx (C_o + C_f)/C_f$. The resistance R_T is the feedback resistance R_f in parallel with any detector bias resistors. This expression is based on a one-Hertz noise bandwidth and is arranged to show important noise contributions in the low- and mid-frequency range. The first term describes the low-frequency output noise-power contributed by FET flicker noise; the second term describes the mid-frequency contribution due to the FET; the third term describes the mid-frequency contribution due to the gain section A_i; and the last term gives the white noise components due to resistor thermal noise and leakage-current shot noise. The various components of Eq. (66) are illustrated in Fig. 14.

ORNL-DWG 70-13797

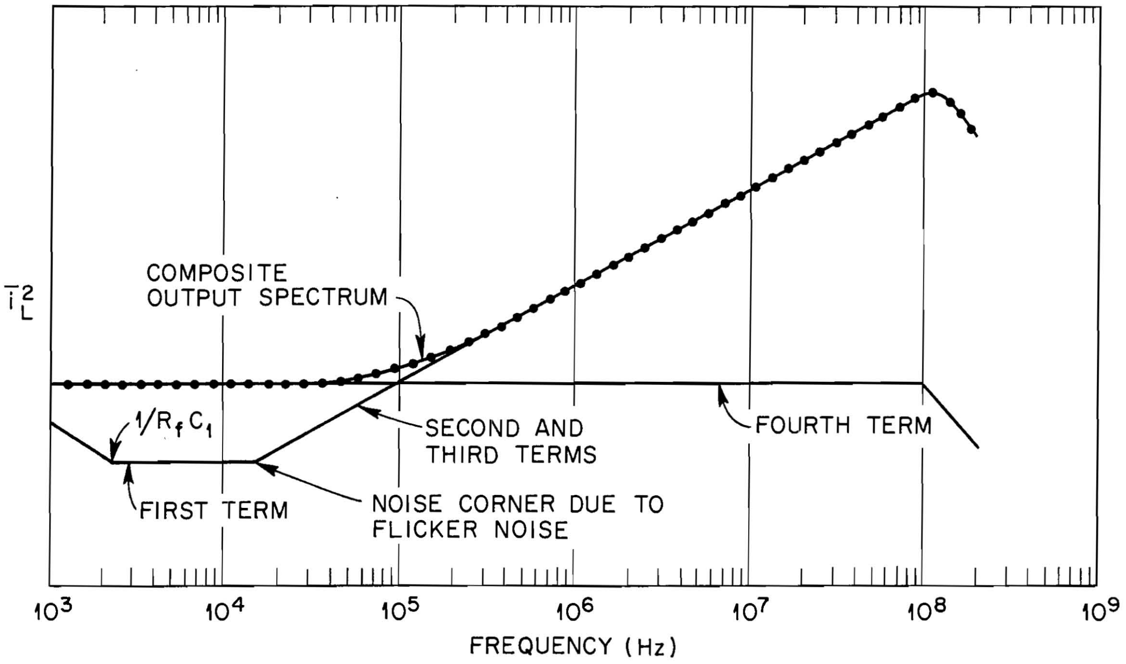

Figure 14. Illustration of a typical output noise power spectrum described by Eq. (66).

Criteria for Cascading Stages

The current gain of the preamplifier configuration of Fig. 11a, page 40, has an upper limitation imposed by the desired bandwidth [Eq. (45)]. More specifically, for a given detector capacitance, input device, and desired bandwidth, the current gain is limited by the maximum practical value of A_i. Limitations on the gain section denoted A_i will be discussed in the next chapter. For most applications it is necessary to cascade several stages to boost the signal to a usable level.

Several factors must be considered when cascading stages. First, the succeeding stages should not degrade the signal-to-noise ratio established by the input stage. However, to minimize the dc level at the load end of the feedback resistors caused by unipolar current pulses, these resistance values should be as small as noise criteria will permit. Thus, higher count rates can be tolerated without saturation. Second, the matching between stages should have a minimum effect on the high-frequency response.

In order that the total low-frequency output noise current $\overline{i}_{nL}$ of the two cascaded stages of Fig. 15 be controlled by the feedback resistor of the input stage, the mean value of the output noise-current squared due to R_{f1} must be much greater than that due to R_{f2}. (The noise current due to the detector bias resistor and input leakage currents is neglected.) Stated mathematically the expression is

$$(A_1A_2)^2\ (4\ kT/R_{f1}) >> A_2^2\ (4\ kT/R_{f2}) \quad . \tag{67}$$

This inequality may be simplified to the requirement that

$$R_{f2} >> R_{f1}/A_1^2 \quad . \tag{68}$$

ORNL-DWG 70-13793

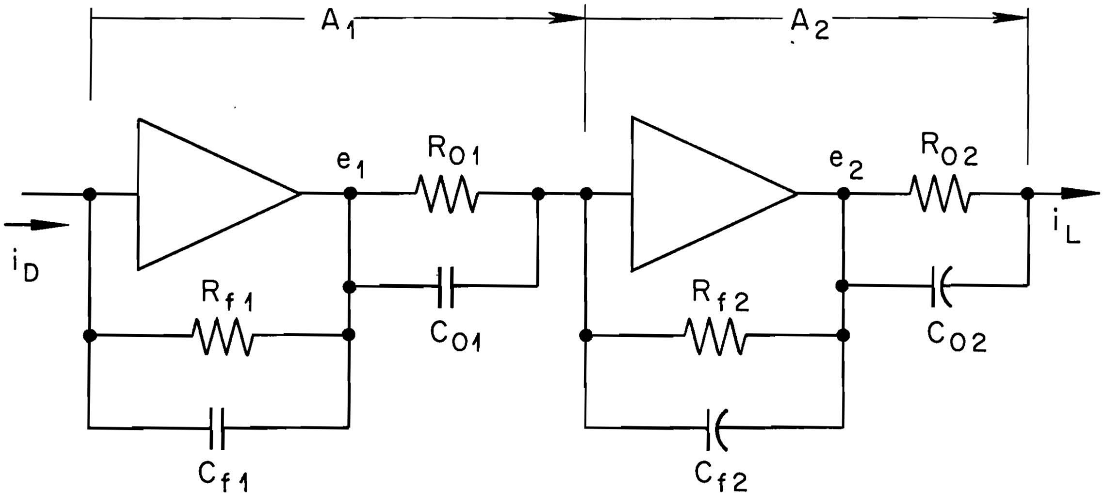

$$A_1 = \frac{C_{O1}}{C_{f1}} = \frac{R_{f1}}{R_{O1}}$$

$$A_2 = \frac{C_{O2}}{C_{f2}} = \frac{R_{f2}}{R_{O2}}$$

Figure 15. Cascaded stages of the configuration shown in Fig. 11a, page 40.

In a similar manner the constraint on the mid-frequency noise contributed by the input FET of the second stage may be found. With regard to the established output impedance of the configuration, the load capacitance of the first stage (C_{o1} in Fig. 15) is now a capacitance in parallel with the input of the second stage. Thus, the mid-frequency output noise due to the second stage input FET is found from the second term of Eq. (66) as approximately

$$\overline{i_{nL}^2}\Big|_{FET2} \approx \alpha\, \omega^2\, A_2^2\, C_2^2/g_{m2} \ , \tag{69}$$

where α is a constant and C_2 is the total input capacitance (including C_{o1}) to the second stage. Similarly, the mid-frequency output noise due to the first stage input FET is approximately

$$\overline{i_{nL}^2}\Big|_{FET1} \approx \alpha\, \omega^2\, A_1^2\, A_2^2\, C_1^2/g_{m1} \ . \tag{70}$$

For the condition that the mean-squared, mid-frequency, output noise current due to the input FET of the first stage be much greater than the mean-squared, mid-frequency, output noise current due to the input FET of the second stage, the following condition on the transconductance of the second stage input FET is required.

$$g_{m2} \gg g_{m1}\ (C_2/A_1C_1)^2 \ . \tag{71}$$

The degree of inequality expressed by Eqs. (68) and (71) determines the fraction of the output noise contributed by the second stage. If a third stage is cascaded its contribution can be computed in the same manner.

With the lower value of second-stage feedback resistance R_{f2} limited by noise requirements, the next decision concerns the choice of feedback capacitance. Ideally, it would be desirable to make C_{f2} as small as possible. For a given second-stage current gain, the value of load capacitance C_{o2} is determined by the product of the feedback capacitance C_{f2} and the current gain. To minimize the total input capacitance of an added third stage, a low value of C_{o2}, and thus C_{f2}, is desired. The feedback capacitor C_{f2}, however, has a lower limit. Assuming no pulse pile-up, the node voltage e_2 may have a peak value given by

$$e_{2\ max} = Q_d\ A_1/C_{f2}\ , \tag{72}$$

where Q_d is the charge liberated in the detector for the highest energy present of a significant count rate. Solving Eq. (72) for C_{f2} gives

$$C_{f2} \geq Q_d\ A_1/e_{2\ max}\ . \tag{73}$$

The inequality arises because of the limited dynamic range of the node voltage e_2. Thus, for this equation $e_{2\ max}$ may be interpreted as the maximum output voltage without saturation.

In regard to the high-frequency performance of cascaded stages, the influence of each stage on the other must be considered. The dominant influence of the first stage on the second is the capacitive loading of C_{o1} on the input FET of the second stage. The second-stage bandwidth computed from Eq. (45) is degraded by this added input capacitance. The influence of the second stage on the first is not so apparent. If a small resistor r_o, rather than the second stage, were placed at the output end of C_{o1}, a zero would exist in the loop transmission (a function of the Laplace variable s) of the first stage. This zero, given by

$$s = -1/r_o\ C_{o1} \tag{74}$$

is similar to the zero created in the loop transmission of a conventional shunt-feedback stage by a small capacitor placed around the feedback resistor. In Fig. 15, page 56, the input impedance to the second stage [Eq. (50)] appears as a small resistance R_{in} shunted by a capacitance C_{in}; thus, a higher frequency pole as well as a zero is created in the loop transmission of the first stage. The zero is located at

$$s = -1/R_{in}(C_2' + C_{o1}) \quad , \tag{75}$$

and the pole at approximately

$$s \approx -1/R_{in}\, C_2' \quad . \tag{76}$$

The capacitance C_2' is the input capacitance of the second stage. The difference in the magnitudes of the pole and zero depends on the relative values of C_2' and C_{o1}. To prevent first-stage bandwidth degradation, the zero given by Eq. (75) should not have a magnitude less than the dominant closed-loop pole of the first stage. However, if the second stage bandwidth, computed for an input capacitance including C_{o1}, is at least as great as that of the first stage, the condition is automatically satisfied. This fact illustrates the advantage of having a single-pole response from the configuration of Fig. 11a, page 40. If the A_i gain section has a significantly low-magnitude pole, the input impedance is a more complex function, likely resulting in undesirable interaction when cascading stages.

In summary, the arbitrary degree of inequality chosen for Eqs. (68) and (71) imposes limits on R_{f2} and g_{m2}. For a given second-stage current gain, the capacitor C_{f2} should be chosen as small as practical to insure that C_{o2}, which loads the input to possibly a third stage, will be minimum. The lower limit of C_{f2}, however, is given by Eq. (73) which is based on available dynamic range. Finally, the desired second stage bandwidth must be computed from Eq. (45) with the total input capacitance C_2 $\left[C_1\right.$ in Eq. (45)$\left.\right]$ including C_{o1}.

Advantages

The basic preamplifier configuration introduced in this chapter (Fig. 11a, page 40) is a simple design having excellent potential for large bandwidths, and linear operation. The noise performance is theoretically the same as that of a conventional charge-sensitive preamplifier. Although a charge-proportional voltage pulse having a long RC decay time is present at the load end of the feedback resistor (output node), the preamplifier stage is primarily designed for current amplification. Thus, the output-voltage driving section that is present in conventional charge-sensitive preamplifier designs to produce a low output impedance is unnecessary. With the output node driven from a current source, a large dynamic voltage range at this node can easily be realized, thus relieving the condition of output saturation at high counting rates. Because this preamplifier stage has a low-resistive input impedance over its entire bandwidth [Eq. (51)], direct cascading of several stages is possible. Consequently, large current gains having large bandwidths can be easily achieved provided proper circuit lay-out and fabrication procedure is observed. Compared to the conventionally differentiated charge-sensitive preamplifier, this configuration allows a more practical realization of a large current gain, broadband preamplifier.

CHAPTER IV

CIRCUIT REALIZATION OF THE BASIC CONFIGURATION

The general configuration of a new low-noise current preamplifier was introduced in Chapter III. Equations were derived indicating the influence of the input device on the bandwidth and output noise power spectrum. In deriving the bandwidth equations, requirements were placed on the gain and bandwidth of the interstage current gain section denoted A_i. In this chapter the choice of an input device based on desired bandwidth and noise performance will be discussed, followed by the development of an appropriate broadband current-gain section.

I. CHOICE OF INPUT DEVICE

As established in Chapter III, the dominant pole of the introduced preamplifier configuration, shown in Fig. 11a, page 40, is located at the input node. Consequently, as indicated by Eq. (45), page 43, the closed-loop bandwidth varies directly as the ratio of g_m/C_1 where g_m is the FET transconductance and C_1 is the total capacitance at the input node. Also, the second term of Eq. (66), page 53, indicates that the magnitude of the ω^2 region of the output noise power spectral density varies directly with C_1^2/g_m if $C_1 \gg C_{gs}/3$. Thus, minimum output noise occurs when the C_1^2/g_m ratio is minimized. For a given detector capacitance, the proper choice of an input FET is crucial in obtaining maximum bandwidth and signal-to-noise ratio.

The preamplifier bandwidth calculated for a given FET, detector capacitance, and interstage current gain A_i is a straightforward application of Eq. (45). For large capacitance detectors a high-transconductance input FET will allow larger bandwidths without requiring large values of A_i. Even though the input capacitance of the high transconductance devices is larger, the detector capacitance, being a smaller percentage of the total preamplifier input capacitance, causes less bandwidth degradation.

In the field of nuclear spectroscopy, the noise performance of a preamplifier is stated in terms referring to the broadening of analyzed radiation energy peaks due to the preamplifier noise. The most common terminology used to specify the broadening is noise line width, meaning the width of an analyzed energy peak usually at the half-maximum of the peak count.

The noise line width produced for a given value of g_m and C_1 cannot be directly computed since it depends also on the low-frequency noise corner of the preamplifier, the choice of filters in the main amplifier, and several other factors which may or may not make significant contribution. After passing through a low-pass network (integrator), the output power spectral density of the new preamplifier configuration has the same frequency behavior as that of the charge-sensitive preamplifier. More specifically, if the integrating capacitor divided by the current gain equals the feedback capacitance of the charge-sensitive preamplifier, the charge gains of both configurations are equal; consequently, the output power spectral densities have the same magnitudes.

The RC-RC filter has been widely adopted as a pulse shaping network for nuclear spectroscopy. Using this filter as a standard, the resolution of other filters may be found by comparing their cusp factor to that of the RC-RC filter.[21] The equivalent noise voltage of the RC-RC filter, defined as the ratio of the rms output noise voltage to the gain for a unit step input, is

$$\mathrm{ENV} = \frac{\overline{e}_{no}}{A_{step}} = \epsilon\ \overline{e}_{no} \ , \tag{77}$$

where ϵ is the natural log base. For an input noise power spectrum consisting of a white plus a $1/\omega^2$, low-frequency component such as that obtained from a charge-sensitive preamplifier (also from the integrated output of the new current preamplifier), the filter's equivalent noise voltage indicated by Blalock[10] is

$$\mathrm{ENV} = \left[\frac{\epsilon^2\ kT\ R_{no}}{2}\left(1/\tau + \omega_n^2 \tau\right)\right]^{1/2} \ , \tag{78}$$

where R_{no} is an equivalent noise resistance due primarily to the FET, τ is the RC time constant of the filter and ω_n is the preamplifier noise-corner frequency. The maximum output signal-to-noise ratio occurs if the filter time constant equals the reciprocal of the noise-corner frequency (radians per second) of the preamplifier. For this condition the noise power contributed by the $1/\omega^2$ portion of the noise spectrum equals the noise power contributed by the white portion of the spectrum and Eq.(78) may be written as

$$\mathrm{ENV} = \left[\frac{\epsilon^2\ kT\ R_{no}}{2}\left(\frac{2}{\tau}\right)\right]^{1/2} \ . \tag{79}$$

The dominant contribution of the noise resistance R_{no} is 0.7 $(C_1^2/g_m C_f^2)$. Substituting this quantity into Eq. (79) gives, at the filter input,

$$\mathrm{ENV} \approx \left[\frac{0.7\ \epsilon^2\ kT\ C_1^2}{g_m\ C_f^2\ \tau} \right]^{1/2} \quad . \tag{80}$$

For a charge-sensitive preamplifier the equivalent noise charge referred to the preamplifier input is found by multiplying the equivalent noise voltage of Eq. (80) by the feedback capacitor C_f. For the new current preamplifier the equivalent noise charge is found by multiplying the equivalent noise voltage of Eq. (80) by the ratio of the integrating capacitor to the current gain. If this ratio equals the feedback capacitance of the charge-sensitive preamplifier, the equivalent noise charge for either preamplifier is

$$\mathrm{ENC} \approx \left[\frac{0.7\ \epsilon^2\ kT\ C_1^2}{\tau\ g_m} \right]^{1/2} \quad . \tag{81}$$

The equivalent noise charge may be related to noise line width in thousands of electron volts (kev) for full width at half maximum (FWHM) by an appropriate constant that is characteristic of the particular detector. For a silicon semiconductor detector the noise line width (NLW) is

$$\mathrm{NLW}\ (\mathrm{kev\ FWHM}\ s_i) = 5.3 \times 10^{16}\ \mathrm{ENC}\ , \tag{82}$$

based on a conversion factor of 3.6 electron volts per ion pair. Substituting Eq. (81) into Eq. (82) and replacing τ with $1/2\pi f_n$ gives

$$\mathrm{NLW}\ (\mathrm{kev\ FWHM}\ s_i) \approx 5.3 \times 10^{16} \left[(1.4\pi\ \epsilon^2\ kT\ C_1^2\ f_n)\ /g_m \right]^{1/2} \quad . \tag{83}$$

The noise-corner frequency is found approximately by equating the second and fourth terms of Eq. (66), page 53. Considering only that portion of the fourth term due to the parallel combination R_T of the feedback and detector bias resistor gives the approximate noise-corner frequency as

$$f_n \approx \frac{1}{1.4\,\pi\, C_1} \sqrt{\frac{g_m}{R_T}} \quad . \tag{84}$$

An example of the variation of bandwidth [Eq. (46), page 43] and noise line width [Eq. (83)] as a function of g_m and C_1 is indicated in Fig. 16. As required for Eq. (46) the interstage gain A_i equals the reciprocal of the feedback ratio (C_f/C_o).

II. DEVELOPMENT OF THE BROADBAND GAIN SECTION A_i

Preliminary Considerations

As indicated in Chapter III, the basic requirement for the gain section denoted A_i in Fig. 11a, page 40, was that the bandwidth of this section be several times greater than the closed-loop bandwidth [Eq. (45), page 43] of the complete preamplifier stage. Since, for a desired bandwidth and a given FET transconductance, the preamplifier closed-loop current gain is limited by the magnitude of broadband current gain available from A_i, it is desirable, for versatility, to be able to choose this value as large as possible. As this statement implies, a large gain-bandwidth product is required. Also, a short signal propagation time is essential since time delay constitutes a phase shift variable with frequency. The use of local or two-transistor feedback configurations such as those of Fig. 2, page 10, allows a means of effectively utilizing large gain-bandwidth products available from present-day bipolar transistors and also provides good control of the phase characteristics of this section. In addition the use of local feedback provides a degree of gain

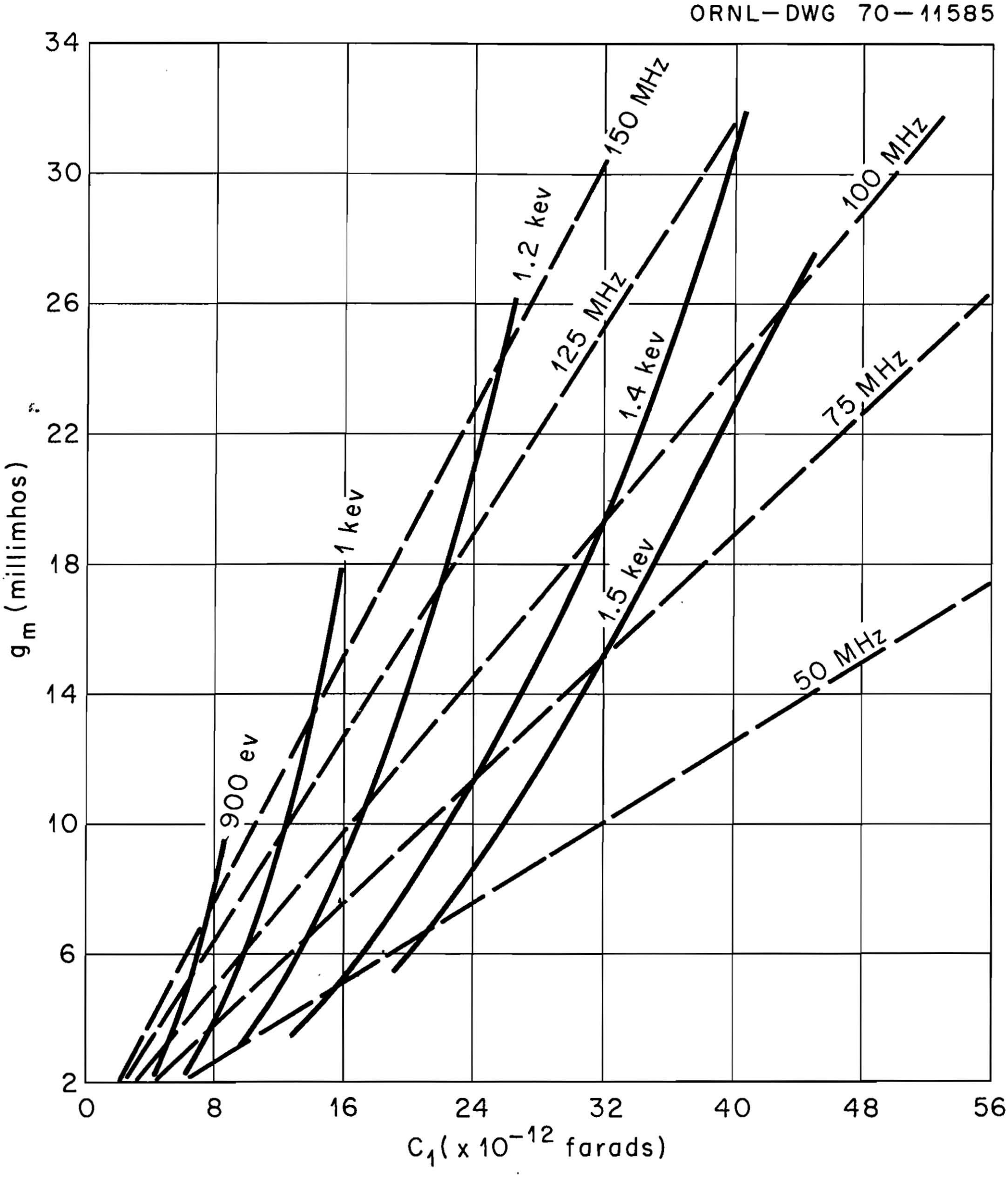

Figure 16. Calculated contours of constant bandwidth and noise line width (referred to a silicon detector) as a function of g_m and C_1.

stability for A_i; consequently, better preamplifier rise-time stability is obtained.

Phase-Shift Requirements

In choosing a high-frequency amplifier stage for operation inside of a broadband, negative-feedback loop, a very important consideration is the high-frequency phase characteristics of the stage. If a negative feedback amplifier is designed to have a bandwidth of 100 megahertz, it is desirable that the phase shift of the loop transmission not exceed about −125 degrees at 100 megahertz if excessive overshoot cannot be tolerated (see Appendix A). Since −90 degrees of phase shift is contributed by the dominant pole, only −35 additional degrees may come from other sources within the feedback loop.

A normally neglected source of phase shift, which may be significant, results from the signal propagation time around the physical length of the feedback loop. If the mean signal propagation velocity is ρc, where ρ is a fractional part of unity and c is the velocity of light in meters per second, the phase shift can be expressed as

$$\phi_d = f\ (3.05 \times 10^{-8}/\rho)\ l_c \text{ degrees.} \tag{85}$$

The quantity l_c is the physical length of the feedback loop in inches and the quantity f is frequency in Hertz. A reasonable estimate for ρ is one-half, although this value varies considerably within the same circuit because of various impedance levels. For a three-inch circuit path, ϕ_d is about eighteen degrees at 100 megahertz. If this is the desired preamplifier bandwidth, the phase shift due to signal delay and the dominant pole is about 108 degrees leaving only about seventeen degrees allowable from other sources within the loop.

Another source which may add a small contribution to the total phase shift of the loop transmission is due to a right-half-plane zero occurring in the Laplace transformed transfer function of the input device. Because of its small contribution, this zero was excluded from the approximate analysis appearing in Chapter III. The equivalent circuit of the input device with the components of input capacitance separated and placed in their proper position is shown in Fig. 17. With the drain connected to a very small impedance, the output current is

$$I_{out}(s) = E_1(s)\, C_{gd}\, s - g_m\, E_1(s) \quad . \tag{86}$$

But $E_1(s)$ is given by

$$E_1(s) = \left[\frac{R}{R(C_{gd} + C_{gs} + C_D)\, s + 1}\right] I_{in}(s) \quad . \tag{87}$$

Substituting Eq. (87) into Eq. (86) gives

$$\frac{I_{out}(s)}{I_{in}(s)} = -\frac{g_m\, R\left[1 - (C_{gd}/g_m)\right] s}{1 + R(C_{gd} + C_{gs} + C_s)\, s} \quad . \tag{88}$$

The right-half-plane zero at $s = g_m/C_{gd}$ will cause a lagging phase shift. For a good FET this zero may correspond to a frequency near 1000 megahertz. The resulting phase shift at 100 megahertz is about minus six degrees.

Considering this source of phase shift in addition to the 108 degrees attributed to the dominant pole and the propagation delay allows only about a minus eleven degree phase shift at 100 megahertz for the gain section A_1 if excessive overshoot cannot be tolerated. Although a 100 megahertz bandwidth may not be necessary, this example points out the limitations to be considered in achieving large unpeaked bandwidths for

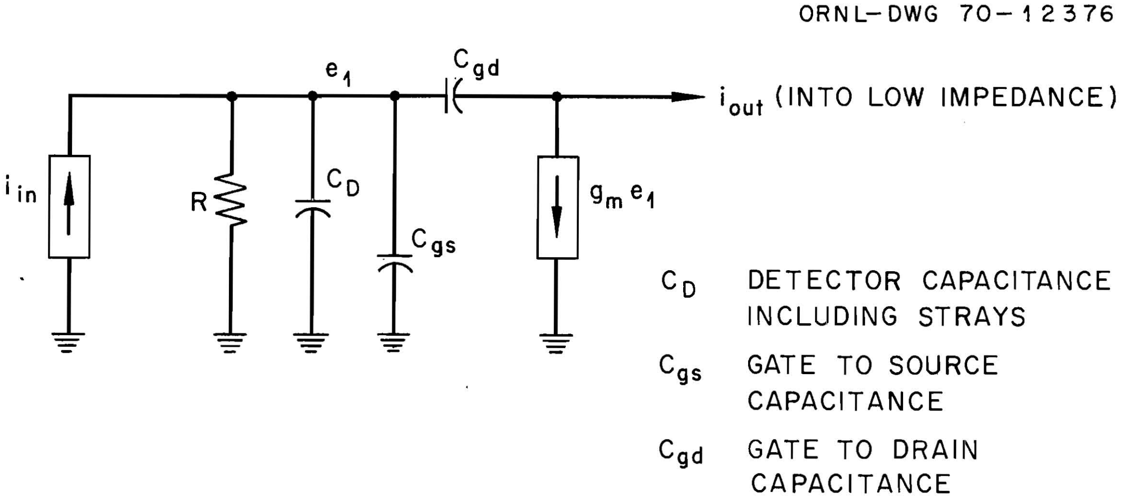

Figure 17. Equivalent circuit of the input FET.

the complete preamplifier stage and the importance of keeping the circuit lay-out geometry as small as possible to minimize propagation time.

Investigation of Available High-Frequency Stages

In choosing a broadband current-amplifier stage similar to one of those shown in Fig. 2, page 10, a primary consideration, as indicated above, is its high-frequency phase characteristics. Various broadband amplifier configurations having the same bandwidth may have significantly different phase characteristics; thus, it is important to choose the one having the minimum phase shift near that frequency at which the loop transmission of the overall preamplifier equals one. In order to compare stages, their phase shift contributions at 100 megahertz will be qualitatively evaluated.

The single-transistor, shunt-feedback configuration of Fig. 2c, page 10, has had considerable usage as a high-frequency amplifier stage. The single-pole approximate analysis of this stage yields a bandwidth of

$$f_{-3} \approx f_T/A_o \quad , \tag{89}$$

where A_o is the mid-frequency current gain i_o/i_{in} given approximately by R_f/R_L and f_T is the gain-bandwidth product of the transistor used for Q_1. The current gain A_o approaches unity near the frequency of f_T; thus, the approximate transfer function is

$$A_o\ (\omega) \approx \frac{(1 + j\omega/\omega_T)}{(1 + j\omega A_o/\omega_T)} \quad . \tag{90}$$

The phase shift resulting from this transfer function has a maximum negative value. However, since the three-decibel break frequencies associated with the numerator and denominator are separated by a factor of A_o, the phase shift contributed by the numerator at frequencies near f_{-3} [Eq. (89)] is small if A_o is near ten. For example, if a transistor having a gain-bandwidth product of 2000 megahertz is used, and a current gain of ten is desired, the resulting bandwidth is approximately 200 megahertz. At 100 megahertz the denominator of Eq. (90) contributes about −26.5 degrees and the numerator contributes about +1.1 degrees for a net phase shift of −25.4 degrees. This result, of course, is only approximate and is likely pessimistic since peaking of the frequency response around 200 megahertz can reduce the phase shift at 100 megahertz. For current gains below ten, this configuration is a good choice for the interstage gain section A_i (Fig. 11a, page 40). For larger current gains the high-frequency performance may become marginal; and, the open-loop current gain, determined by h_{fe} of Q_1, may not be adequate to establish the desired closed-loop, mid-frequency gain of R_f/R_L. The current gain h_{fe} of most high-frequency transistors is typically below 100. Although good mid-frequency gain stability is not required, a certain degree of stability is desired for reproducible performance from various transistors of the same or similar types. Blalock first described the use of this stage within the feedback loop of a charge-sensitive preamplifier.[20] A more detailed description of its performance can be found in his paper.

The stage of Fig. 2d, page 10, was introduced in 1964 by Rush.[21] The advantage of this stage over the single-transistor, shunt-feedback configuration considered above is a lower input impedance. The bandwidth and phase characteristics of the current transfer function i_o/i_{in} are essentially the same if f_α of the first transistor Q_1, connected in the common-base configuration, is at least an order of magnitude greater than the current transfer function bandwidth. Also, the stage has the same open-loop current gain as the single-transistor, shunt-feedback stage; consequently, the same error in mid-frequency current gain exists if a low h_{fe} transistor is used for Q_2.

The shunt-series gain stage introduced in 1963 by Cherry and Hooper[22] is shown in Fig. 2b, page 10. The first transistor gives an impedance transfer e_2/i_{in} and the second transistor gives an admittance transfer i_o/e_2. Thus, with the two stages cascaded, a current gain i_o/i_{in} is realized. A modified version of the shunt-series stage shown in Fig. 18 was introduced in 1967.[23] This stage has essentially the same transfer function as the original shunt-series connection except the Miller effect produced by the collector-base capacitance of Q_1 is reduced by the insertion of Q_2, which forms a cascode connection. Since the collector-base capacitance of Q_1 in Fig. 2b, page 10, essentially shunts the feedback resistor R_f, its degrading effect on the bandwidth is primarily important for feedback-resistor values greater than about 1000 ohms. The transfer functions of both the original and modified shunt-series gain stages are representative of a second-order system, because the open-loop transfer functions of the shunt-feedback stages of both configurations have two dominant poles for large values of load resistance (R_L in Fig. 2b, page 10): one at the input node having a value of $-\omega_{\beta 1}$ (roll-off frequency of the common-emitter current gain) and one at the output node (labeled e_2) having a value of $-1/C_o R_f$ where C_o is the total capacitance at this node. The bandwidth of the stage of Fig. 18 was found to be approximately

$$f_{-3} \approx f_T / \left[A_o + \omega_T R_f C_o \right]^{1/2} , \tag{91}$$

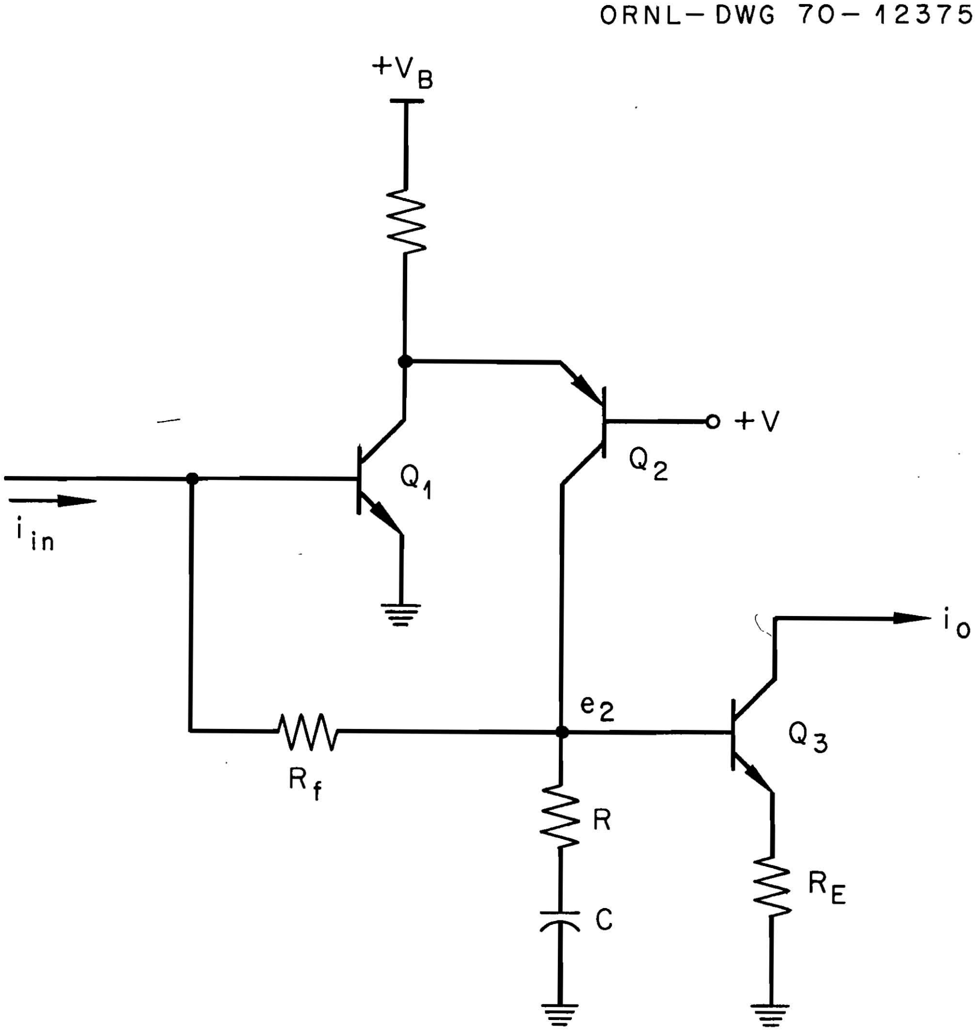

Figure 18. Modified configuration of the shunt-series, high frequency amplifier stage.

where $A_o = R_f/R_E$ and C_o consists of the collector-base capacitance of both Q_2 and Q_3, the feedback capacitance shunting R_f, and stray capacitance. A C_o value as low as 4×10^{-12} farads may be achieved. For a feedback resistance of 1000 ohms, a transistor gain-bandwidth product of 2000 megahertz, and an A_o of 10, the corresponding bandwidth is near 240 megahertz. The phase and magnitude response of a second-order system as a function of the damping ratio ξ can be found in many servo texts. For a ξ of 0.5, which is about a minimum without excessive, high-frequency gain peaking, the phase shift at 100 megahertz is about −24 degrees. This number could be improved by using lower values of feedback resistance. However, 1000 ohms is about a lower limit if the thermal noise of R_f is to be small compared to the thermal noise generated in an input FET having a typical g_m of 5000 μmhos. The approximate 100 megahertz phase shift of this stage is near the value quoted for the single-transistor, shunt-feedback stage even though the bandwidth is somewhat greater. Because of the added difficulty in compensating its second-order, high-frequency response, the shunt-series configuration probably does not offer enough advantage over the single-transistor, shunt-feedback stage to justify its use.

High-Performance Shunt-Feedback Stage

The high-frequency performance of the single-transistor shunt-feedback stage of Fig. 2c, page 10, may be significantly improved by placing an emitter-follower within the loop ahead of Q_1. This modification is indicated in Fig. 19a. The dominant pole is shifted from the base of Q_2, where it is located in the single-transistor, shunt-feedback stage, to the base of Q_1. The diffusion capacitance of Q_1 becomes very small due to its relatively large emitter impedance (equal to the input

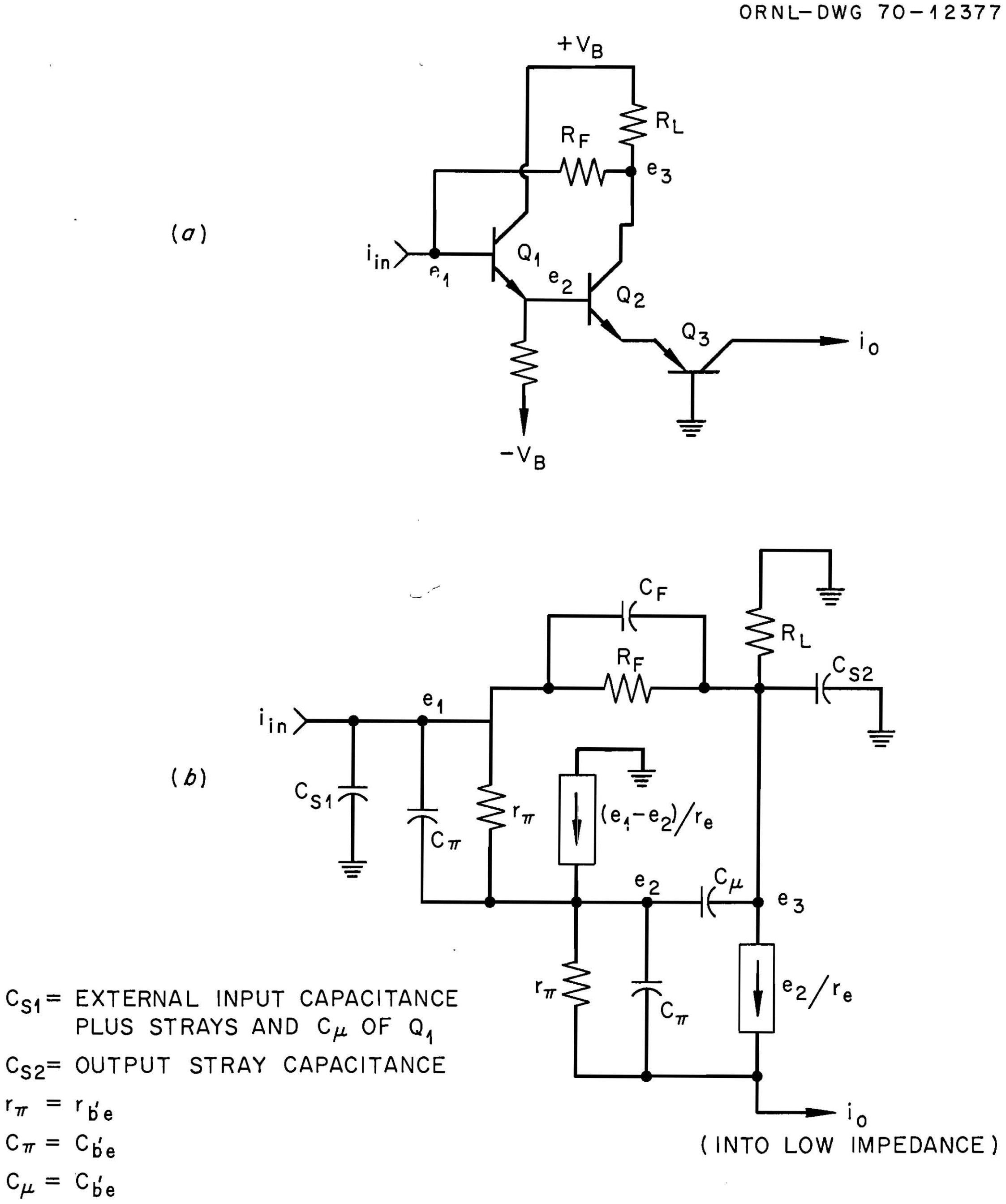

C_{S1} = EXTERNAL INPUT CAPACITANCE PLUS STRAYS AND C_μ OF Q_1

C_{S2} = OUTPUT STRAY CAPACITANCE

$r_\pi = r_{b'e}$

$C_\pi = C_{b'e}$

$C_\mu = C_{b'e}$

Figure 19. (a) Circuit diagram of a high-frequency, two-transistor, shunt-feedback stage with (b) the corresponding equivalent circuit.

impedance of Q_2). Thus, the total input capacitance of the stage is about equal to the collector-base capacitance of Q_1, the output capacitance of a preceding common-base buffer stage, and the input stray capacitance. This total value may be as low as 4×10^{-12} farads. The approximate loop transmission $A\beta$ is

$$A\beta = (A_{b1b2})(A_{b2c2})(A_{c2b1}) \quad , \tag{92}$$

where A_{b1b2} is the voltage gain from the base of Q_1 to the base of Q_2, A_{b2c2} is the voltage gain from the base of Q_2 to the collector of Q_2, and A_{c2b1} is the voltage gain from the collector of Q_2 to the base of Q_1. The value of A_{b1b2} is near unity and the value of A_{b2c2} for R_F much greater than R_L is

$$A_{b2c2} \approx R_L/(r_{e2} + r_{e3}) \quad , \tag{93}$$

where r_{e2} and r_{e3} are respectively the emitter resistance values of Q_2 and Q_3. The high-frequency voltage gain from the collector of Q_2 to the base of Q_1 is

$$A_{c2b1} \approx \frac{1}{1 + j\omega\, R_F\, C_{in}} \quad , \tag{94}$$

if R_F is much less than the input resistance to transistor Q_1.

Equation (92) is given approximately by

$$A\beta \approx \frac{R_L}{(r_{e2} + r_{e3})(1 + j\omega\, R_F\, C_{in})} \quad . \tag{95}$$

For R_L much greater than $(r_{e1} + r_{e2})$, the bandwidth or frequency at which $A\beta$ is unity is approximately

$$f_{-3} \approx \frac{.159}{C_{in}\,(r_{e2} + r_{e1})\,A_o} \quad , \tag{96}$$

where A_o is the mid-frequency current gain R_F/R_L. For a ten milliampere bias current through Q_2 and Q_3, the value of $(r_{e2} + r_{e1})$ is about 6 ohms. For $R_F/R_L = 20$, and $C_{in} = 4 \times 10^{-12}$ farads, the bandwidth is 300 megahertz, and the corresponding phase shift at 100 megahertz is approximately 18 degrees. The current gain of this stage, as was the case for the simpler shunt feedback stage of Fig. 2c, page 10, approaches unity at very large frequencies; thus, the phase shift has a maximum negative value. To obtain a better estimate of the phase-shift characteristics, a more detailed analysis is required.

The approximate hybrid-π equivalent circuit of the shunt-feedback stage of Fig. 19a, page 75, is shown in the b part of this figure. For this equivalent circuit the bias current of Q_2 and Q_3 is assumed to be twice the value of Q_1 in order that $(r_{e2} + r_{e3})$ equal r_{e1}. Also it is assumed that both transistors in the shunt-feedback loop are identical. The nodal equations of this equivalent circuit in matrix form are

$$\begin{vmatrix} (1/r_{in}+C_{in'}s) & -(1/r_\pi+C_\pi s) & -(1/R_F+C_F s) \\ -(1/r_\pi+1/r_e+C_\pi s) & \left[2/r_\pi+1/r_e+(2C_\pi+C_\mu)s\right] & -C_\mu s \\ -(1/R_F+C_F s) & -(-1/r_e+C_\mu s) & (1/R_L+1/R_F+C_o s) \end{vmatrix} \begin{vmatrix} E_1(s) \\ E_2(s) \\ E_3(s) \end{vmatrix} = \begin{vmatrix} I_{in}(s) \\ 0 \\ 0 \end{vmatrix} \qquad (97)$$

where $1/r_{in} = 1/R_F + 1/r_\pi$, $C_o = C_{s2} + C_F + C_\mu$, and $C_{in'} = C_{s1} + C_\pi + C_F$.

Because the expansion, rationalization and approximation process required to obtain a reasonable expression for the system determinant Δ is extremely cumbersome and difficult to document, the details of the process will be omitted. The resulting expression for Δ becomes approximately

$$\begin{aligned}\Delta \approx\ & C_o C_\pi^2 s^3 + \left[C_\pi/R_L + (C_F + C_\mu)/r_e\right] C_\pi s^2 \\ & + \left[2C_\pi/\beta_o r_e R_L + C_\pi/r_e R_F + C_{s1}/r_e R_L + C_F/r_e^2\right] s \\ & + 1/r_e^2 R_f \ , \end{aligned} \tag{98}$$

where β_o is the low-frequency magnitude of h_{fe}. In arriving at this expression the assumptions involved were: $\beta_o >> 1$, $R_L >> r_e$, $R_F >> R_L$ (or $A_o >> 1$), and $\beta_o^2 R_L >> R_F$. Solving Eq. (97) for $E_2(s)$, dividing both sides of the resulting equation by $I_{in}(s)$, and applying the above approximations gives

$$\frac{E_2(s)}{I_{in}(s)} \approx \frac{(1/r_e + C_\pi s)(1/R_L + C_o s)}{\Delta} \quad . \tag{99}$$

The output current i_o is related to the node voltage e_2 by the relationship

$$I_o(s) = E_2(s)(1/r_e + 1/r_\pi + C_\pi s) \approx E_2(s)(1/r_e + C_\pi s) \quad . \tag{100}$$

Substituting Eq. (100) into Eq. (99) gives

$$\frac{I_o(s)}{I_{in}(s)} = \frac{(1/r_e + C_\pi s)(1/r_e + C_\pi s)(1/R_L + C_o s)}{\Delta} \quad . \tag{101}$$

By substituting Eq. (98) into Eq. (101), expanding the numerator of Eq. (101) and factoring out the constant term in the numerator and denominator gives a final expression for the closed-loop current gain.

$$\frac{I_o(s)}{I_{in}(s)} = A_o \left[\frac{\left(\frac{\tau_o}{\omega_T^2}\right) s^3 + \left(\frac{2}{\omega_T^2} + \frac{\tau_o}{\omega_T}\right) s^2 + \left(\frac{2}{\omega_T} + \tau_o\right) s + 1}{\left(\frac{A_o \tau_o}{\omega_T^2}\right) s^3 + \left(\frac{A_o}{\omega_T^2} + \frac{(C_f + C_\mu)\ R_F}{\omega_T}\right) s^2 + \left(\frac{2A_o}{\omega_T \beta_o} + \frac{1}{\omega_T} + A_o r_e C_{s1} + \tau_F\right) s + 1} \right] \cdot \tag{102}$$

where $\omega_T = 1/r_e C_\pi$, $\tau_o = C_o R_L$, $A_o = R_F/R_L$, and $\tau_F = R_F C_F$. If only the first order terms are considered, the dominant term of the pole, $A_o r_e C_{s1}$, yields the same approximate bandwidth predicted by Eq. (96), provided that $(r_{e1} + r_{e2}) = r_e$ and $C_{in} \approx C_{s1}$ of Eq. (102). The denominator of Eq. (102) does not readily factor into discrete poles as does the numerator. Consequently, the phase and log-magnitude frequency response generated by Eq. (102) with $j\omega$ substituted for the Laplace variable s, was calculated by a computer for a frequency range of 50 to 1000 megahertz. The curves of Fig. 20 represent three values of output time constant τ_o. For τ_o very small the response approaches that of a single-pole system. The phase shift is about −16 degrees at 100 megahertz, about the same as was predicted from the initial simplified analysis; and the maximum of approximately −90 degrees occurs near 1000 megahertz. As τ_o is increased, peaking occurs in the 400 megahertz range, causing the magnitude of the phase shift near 100 megahertz to decrease. Excessive peaking should be suppressed to prevent a significant increase in the loop-transmission of the overall preamplifier in the 100 megahertz range.

The phase and magnitude curves were recalculated for variations in C_F. These curves, shown in Fig. 21 indicate how, for a 1000 ohm feedback resistor, extremely small variations of C_F (0.1 pf) can lower the

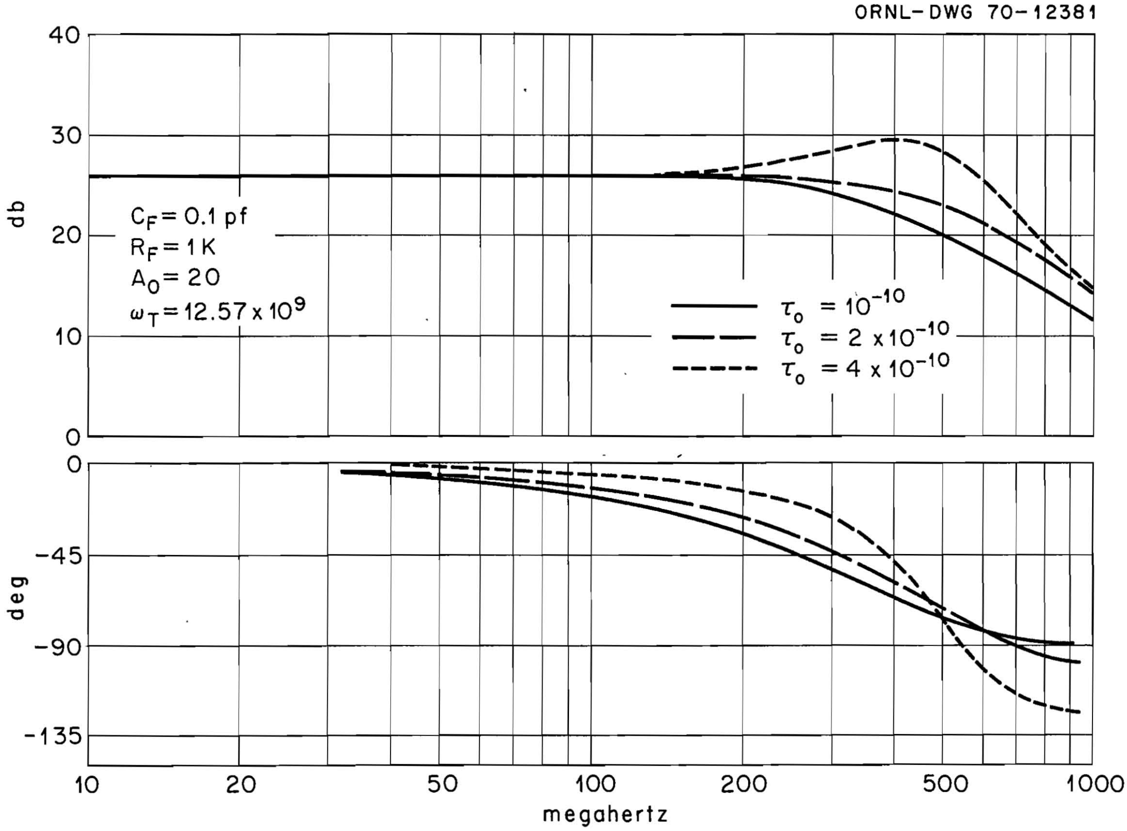

Figure 20. Log magnitude and phase response of the two-transistor, shunt-feedback stage for various values of load time constant τ_0.

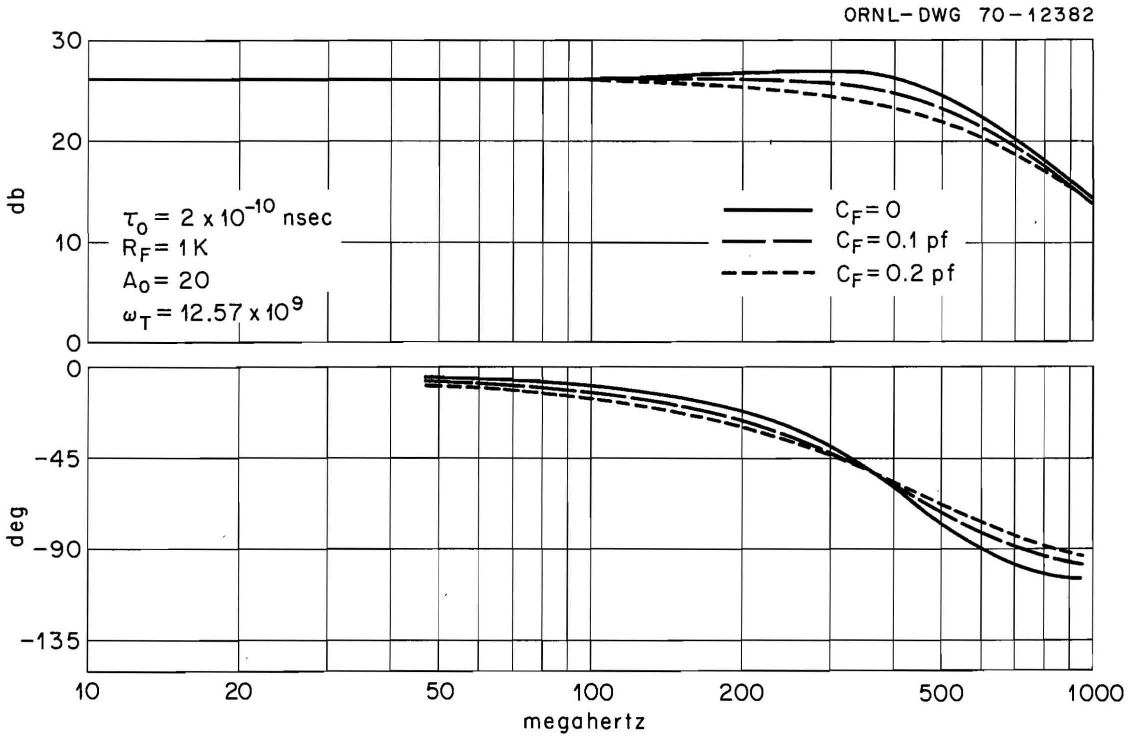

Figure 21. Log-magnitude and phase response of the two-transistor, shunt-feedback stage for various values of feedback time constant τ_f.

bandwidth and increase the magnitude of the phase shift at 100 megahertz. These curves indicate that the 100 megahertz phase shift of this stage for a current gain of twenty is less than that of the other configurations considered for a current gain of ten. A critical parameter is the total input capacitance which must be minimized to achieve maximum bandwidth. To assure minimum input capacitance the use of a preceding, low-output-capacitance, common-base buffer stage is normally required.

To insure that the noise-current contribution of this stage is small compared to that originating in the input FET, it is necessary to derive an expression for the equivalent noise current. The stage is redrawn in Fig. 22 with an equivalent noise-voltage generator $\bar{e}_{nv}$ shown between the emitter of Q_1 and the base of Q_2. This generator is the square root of the sum of the squares of the equivalent noise voltages of Q_1, Q_2, and Q_3.

$$\overline{e_{nv}^2} = \overline{e_{n1}^2} + \overline{e_{n2}^2} + \overline{e_{n3}^2} \quad . \tag{103}$$

With the feedback loop opened between points P and P' and shunting resistors of value R_F placed at the input and output (collector of Q_2) nodes in accordance with open-loop operation, the noise current flowing in R_L due to the indicated noise-voltage generator is approximately $\bar{e}_{nv}/(r_{e2} + r_{e3})$. With the feedback loop closed, the mid-frequency noise current in R_L due to the equivalent noise-voltage generator $\bar{e}_{nv}$ is approximately the open-loop value divided by the mid-frequency loop transmission. From Eq. (95) the mid-frequency loop transmission is $R_L/(r_{e2} + r_{e3})$. Thus the closed-loop noise current in R_L due to the noise voltage generator is $\bar{e}_{nv}/R_L$. The equivalent input noise current is simply this value divided by the closed-loop gain R_F/R_L. Thus,

ORNL-DWG 70-12380

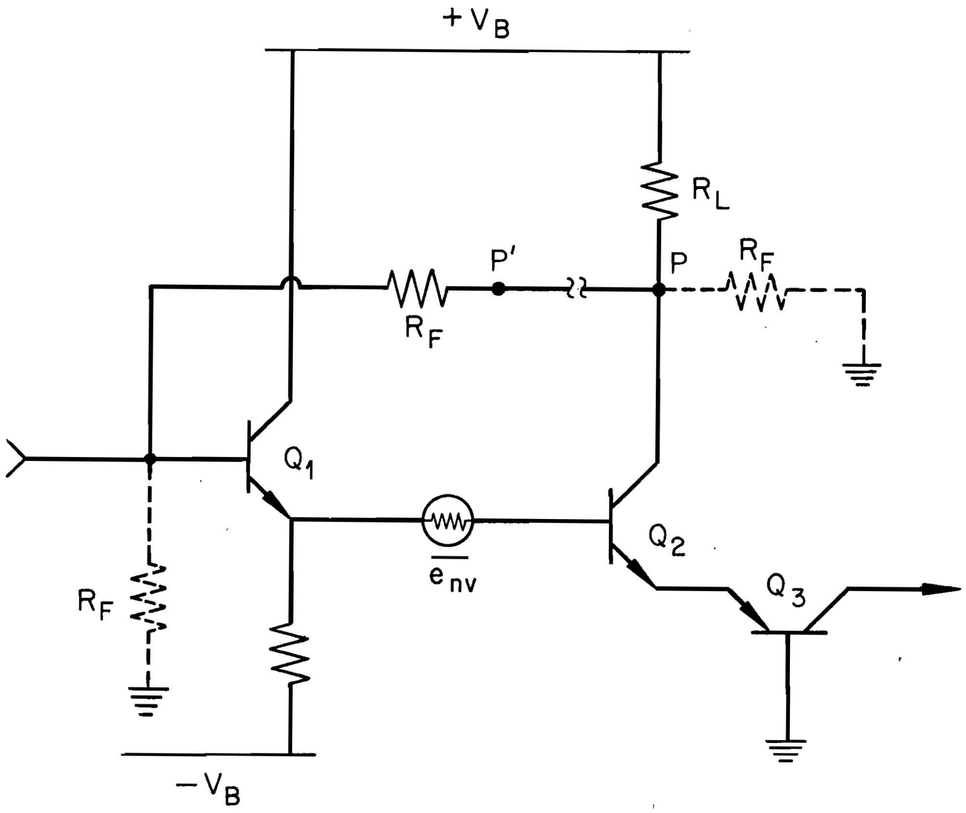

Figure 22. Open-loop circuit diagram of the two-transistor, shunt-feedback stage of Fig. 19a, page 75, with a noise voltage generator added.

$$\bar{i}_{eq1} \approx \bar{e}_{nv}/R_F \qquad \text{amps}/\sqrt{\text{Hz}} \quad . \tag{104}$$

Two other noise sources contribute significantly to the equivalent noise current. One is the thermal noise of the feedback and any input bias resistor. The other is the base-current shot noise of Q_1. The resistor thermal-noise current is expressed by

$$\bar{i}_R = \left[4kT/R_{eq}\right]^{1/2} \qquad \text{amps}/\sqrt{\text{Hz}} \quad , \tag{105}$$

where R_{eq} is R_F in parallel with any bias resistor shunting the input. The shot-noise current associated with the quiescent base current of Q_1 is expressed by

$$\bar{i}_{b1} = \left[2eI_{e1}/\beta_{o1}\right]^{1/2} \qquad \text{amps}/\sqrt{\text{Hz}} \quad , \tag{106}$$

where I_{e1} is the quiescent emitter current and β_{o1} is the low-frequency magnitude of h_{fe}. The total mid-frequency equivalent noise current of the broadband stage under consideration is

$$\bar{i}_{tot} \approx \left[\overline{e^2_{nv}}/R_F^2 + 4\ kT/R_{eq} + 2eI_{e1}/\beta_{o1}\right]^{1/2} . \tag{107}$$

In order to estimate from Eq. (107) the total noise contribution of this shunt-feedback stage, it is necessary to know the equivalent noise voltage of the transistors. The expression of equivalent noise voltage that was derived by Kennedy from the hybrid-π noise model is given by Fq. (2), page 13. In addition, many transistor specification sheets give contours of constant noise figure. For generator resistance values below 50 ohms and for emitter currents below about 5 milliamperes the output noise contributed by the transistor is dominated by the equivalent noise-voltage generator $\bar{e}_n$ of the device. The noise figure is defined by

$$NF = 10 \log \left(\frac{\bar{e}_n + \bar{e}_{th}}{\bar{e}_{th}} \right) , \qquad (108)$$

where $\bar{e}_{th}$ is the thermal noise voltage of the generator resistance. For a Motorola 2N4957 high-frequency, PNP, silicon transistor, a typical noise figure of 3.5 db results for a 2 to 5 milliampere emitter current and a 40-ohm generator resistance. From Eq. (108) the resulting equivalent noise voltage is about 1 nanovolt/$\sqrt{Hz}$. The total equivalent noise current of Eq. (107) can now be found for the desired feedback resistance and emitter bias current.

Output Section

As established in Chapter III, the extent to which the inequality of Eq. (41), page 42, is satisfied determines the degree of mid-frequency preamplifier gain stability to variations in g_m, C_1, A_i, and in the output resistance R_s Fig. 11b, page 40. A large degree of inequality depends on the resistance R_{po} being large. Since this resistance is the parallel combination of the amplifier output resistance R_s and the load resistance R_o, both of these values must be large. The load resistance R_o can be arbitrarily increased so long as the value of feedback resistance R_f is correspondingly increased to maintain the desired feedback ratio. Thus, it is necessary to maximize the value of output resistance R_s to properly satisfy the inequality. For a large value of total input capacitance and a low value of feedback capacitance, the C_1/C_f ratio on the right side of the inequality may be as large as 500. The inequality should be satisfied, if possible, by a factor of 1000. Although the required value of R_{po} depends on the specific values at g_m and A_i used, a value near one megohm may be desired.

The output resistance of transistor Q_3 in Fig. 19a, page 75, is limited to some value less than the normal common-base output resistance because of its relatively low equivalent emitter resistance. As measured at the emitter of Q_2, the mid-frequency equivalent output resistance of the two transistor shunt feedback stage (not considering the shunting input resistance of Q_3) may be found approximately by multiplying the open-loop value by the mid-frequency loop transmission. Multiplication by the loop transmission rather than division is necessary because the feedback mode tends to increase the impedance at this point. The open-loop resistance is essentially the emitter resistance r_{e2} of transistor Q_2, since the base of this transistor is connected to a low resistance source determined by $(r_{e1} + R_f/\beta_{o1})$. More specifically, if

$$r_{e2} \gg \left[r_{b'2} + (r_{e1} + R_f/\beta_{o1})\right] / \beta_{o2} \quad , \tag{109}$$

where $r_{b'2}$ is the base-spreading resistance of transistor Q_2 and β_{o1} and β_{o2} are the small-signal current gains of transistors Q_1 and Q_2 respectively, the open-loop output resistance at the emitter of transistor Q_2 is approximately r_{e2}. Multiplying this resistance by the mid-frequency loop transmission given by the frequency invariant terms of Eq. (95) gives

$$R_{oe2} = \frac{R_L\, r_{e2}}{r_{e2} + r_{e3}} \quad . \tag{110}$$

If transistors Q_2 and Q_3 carry the same bias current, Eq. (110) becomes

$$R_{oe2} = R_L/2 \quad . \tag{111}$$

The load resistor R_L may typically be 100 ohms. Thus, the output resistance R_{oe2} is relatively small.

The output resistance of a common-base stage is inversely proportional to emitter bias current and directly proportional to the external emitter resistance. The expression for the output resistance as a function of the external emitter resistance and the hybrid parameters is found in many transistor texts. Although not commonly published, the hybrid parameters may be found on the specification sheets of some devices.

Because a large external emitter resistance is required, an additional common-base stage following transistor Q_3 (Fig. 19a, page 75) may be needed. The emitter current of the added transistor would have a lower limit determined by bandwidth requirements. Since this stage would add slightly to the phase shift of the overall preamplifier loop transmission, its gain-bandwidth product should be as large as possible.

Low-frequency measurements made of the output resistance of a 2N3933 high-frequency NPN transistor at an emitter current of two milliamperes and an external emitter resistance determined by the collector resistance of another stage indicated a typical value of 5 megohms. At a current of five milliamperes the value decreased to about 0.4 megohms. For a two milliampere bias current and a 100 ohm external emitter resistance, the output resistance was about 0.45 megohms.

A typical circuit diagram of the preamplifier configuration of Fig. 11a, page 40, is shown in Fig. 23. Transistors chosen for Q_6 and Q_7 should have output capacitance values lower than that of C_o to prevent additional high-frequency degradation of the loop transmission. To minimize overloading due to high-count-rate pile up, the base-bias voltages

ORNL-DWG 70-12379

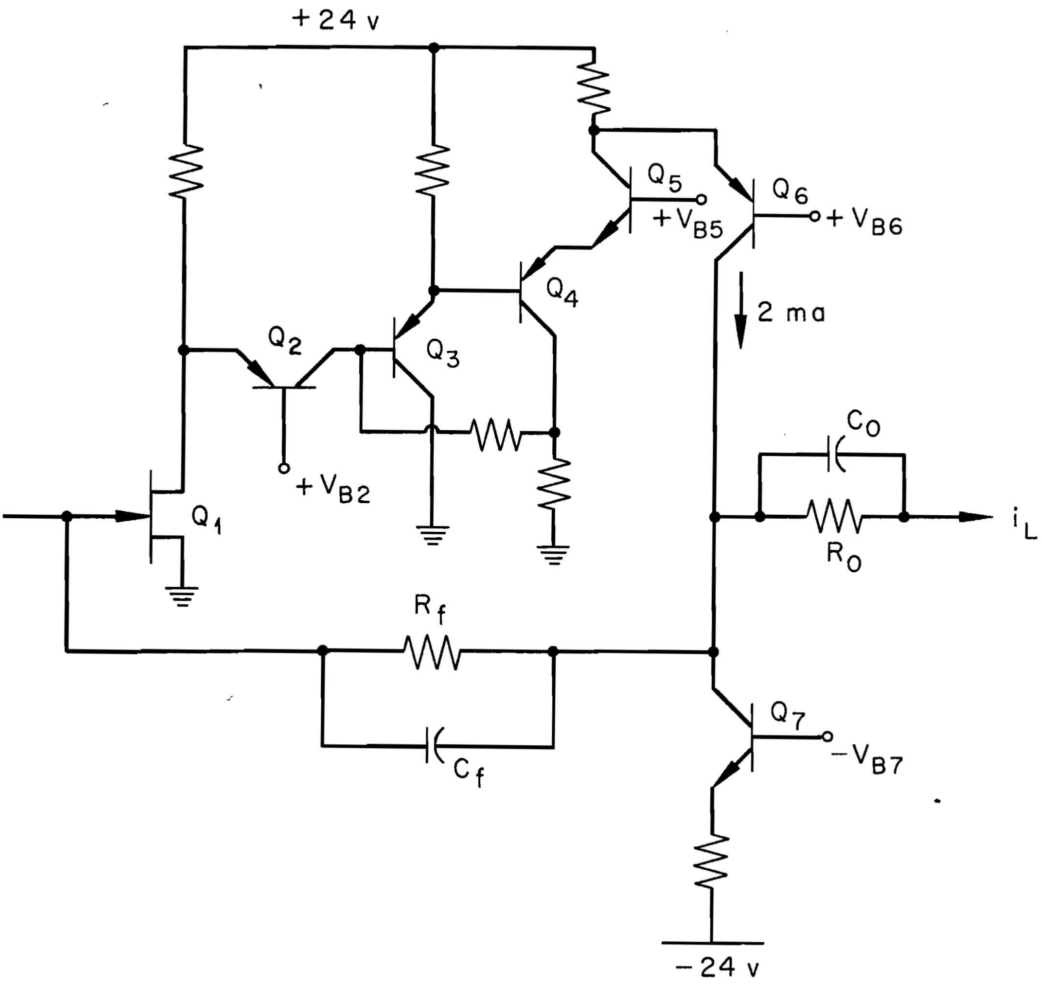

Figure 23. Typical circuit diagram of the preamplifier configuration of Fig. 11a, page 40.

of transistors Q_6 and Q_7 should have as large a magnitude as possible to allow maximum dynamic voltage range at the output node. This stage is primarily designed for small-signal applications. If several stages are cascaded to produce a large current gain, the output-stage configuration has to be designed in accordance with the desired signal current levels.

CHAPTER V

FINAL DESIGN AND EXPERIMENTAL EVALUATION OF THE COMPOSITE CURRENT PREAMPLIFIER

In order to validate the performance criteria developed for the broadband current preamplifier introduced in Chapter III, several units, differing in physical layout, were constructed for testing. The first part of this chapter describes the specific design from which the experimental data documented in this chapter were taken. A measured output noise spectrum is shown for comparison with calculated values. The remaining portion of the chapter describes resolution and timing experiments performed with two lithium drifted germanium detectors having active volumes of 1.7 and 34.1 cubic centimeters. The experiments were performed using a ^{60}Co gamma-ray source.

I. DESIGN OF THE COMPLETE PREAMPLIFIER

Current Gain Selection

In designing a complete current preamplifier consisting of several stages cascaded according to the requirements of Chapter III, it is necessary to first determine the required total current gain. The lower limit of current gain, without signal-to-noise ratio degradation, is established by noise generation in that part of the analyzing system following the preamplifier. For energy measurements the output current of the preamplifier is normally routed to a linear gate or to an integrator. If the choice, for example, is a linear gate having a mid-frequency equivalent noise resistance, R_{nL}, the total current gain is constrained by,

$$A_{i\ tot} \gg \sqrt{\frac{R_{f1}}{R_{nL}}} \quad , \tag{112}$$

where R_{f1} is the feedback resistor of the first preamplifier stage. The degree of inequality determines the percent of the total output noise contributed by the gate at frequencies below the noise-corner frequency. If the total gain $A_{i\ tot}$ is equal to the right side of the inequality, the gate contributes the same output noise power as does the feedback resistor of the first stage, causing the noise corner to increase by $\sqrt{2}$.

Another factor influencing the choice of total current gain is the desired dynamic range over which radiation events are to be timed. If a ten-to-one dynamic energy range is desired and the lower threshold of the leading edge discriminator (LED) is 50 millivolts, for example, the maximum output peak current must produce 500 millivolts across the discriminator input impedance (normally 50 ohms), assuming that the broadband peak noise is below 50 millivolts. The difficulty in satisfying this requirement is not knowing, without some initial experimentation, the peak-current range from the specific detector to be used. The peak detector current depends essentially on the charge collection time and the manner of current pulse formation as well as the radiation energy; consequently, the peak current varies from one detector to the next. The upper limit of the total current gain is determined by the current drive capability of the final stage of the preamplifier.

After brief initial experimentation with two germanium detectors, to be described later, a total current gain of approximately 8000 was selected. In the final design three stages having current gains of forty, twenty and ten were cascaded. Each stage was fabricated separately in a small cast aluminum box and the power supply lines between each stage were filtered with LC attenuation sections. Aluminum boxes were used because of availability, although steel boxes are preferred because of better 60 Hertz shielding properties.

The complete preamplifier layout is shown in Fig. 24. The additional box oriented with its longest dimension perpendicular to the others contains a coupling capacitor, test-pulse injection circuit, and a high-voltage decoupling network for detector bias. If both terminals of the detector are usable, the preamplifier can be connected to the low-voltage output, thus eliminating the need for a coupling capacitor. This is a desired condition since the stray capacitance associated with a coupling capacitor degrades the energy resolution and the additional inductance associated with the longer input signal path may create ringing on the fast-rise-time, output current pulse.

One cannot over emphasize the importance of a proper physical layout. In a broadband amplifier having a large overall current gain and a desired low output noise level, the physical layout may determine success or failure in achieving the desired goals. Special attention should be given to the elimination of ground loops. These extraneous circuit paths may support undesirable feedback currents which may alter the performance in any frequency range.

First-Stage Design

The schematic of the first stage is shown in Fig. 25. This design evolved from the basic configuration of Fig. 11a, page 40. The interstage current gain section A_i is enclosed by dotted lines.

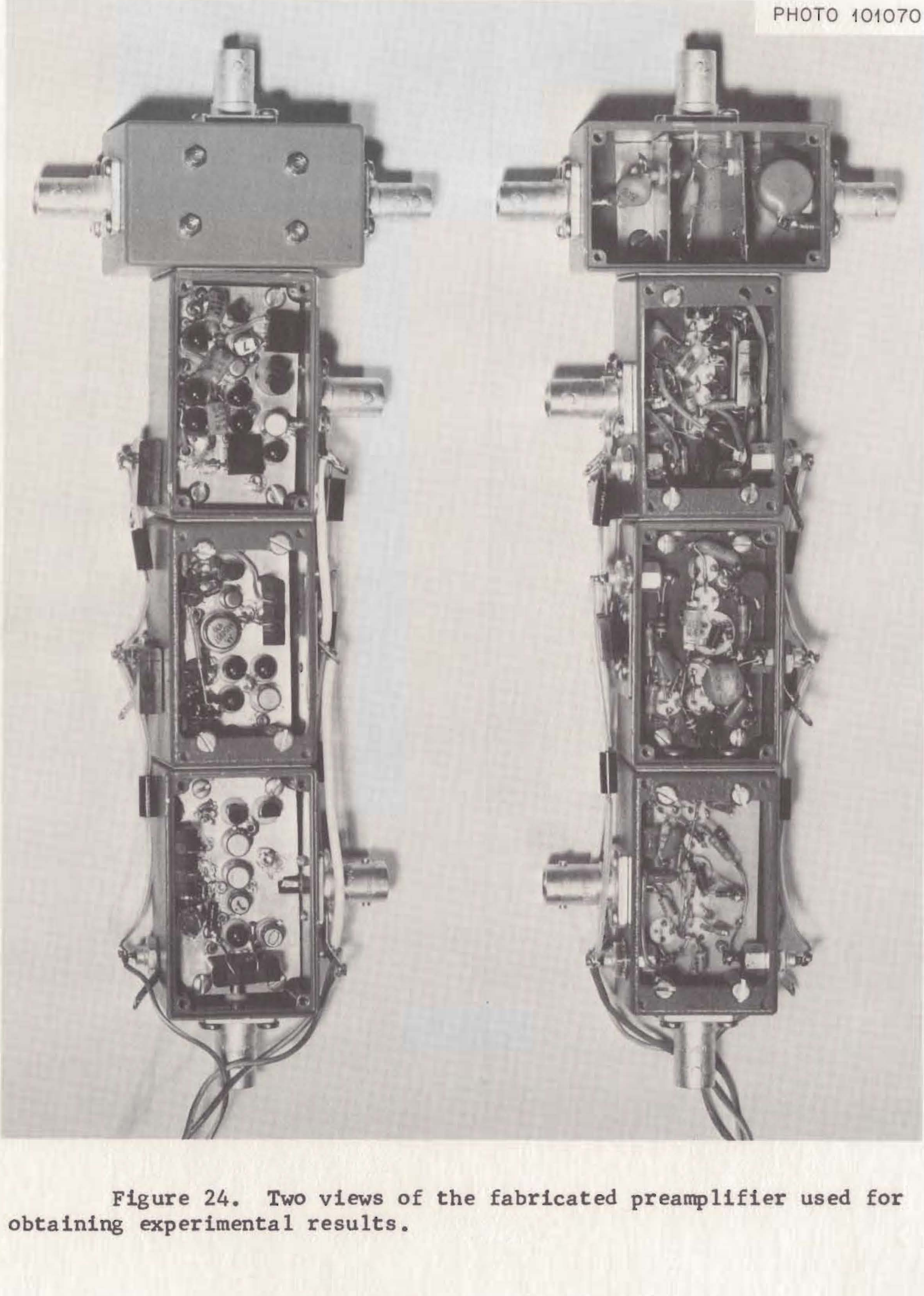

Figure 24. Two views of the fabricated preamplifier used for obtaining experimental results.

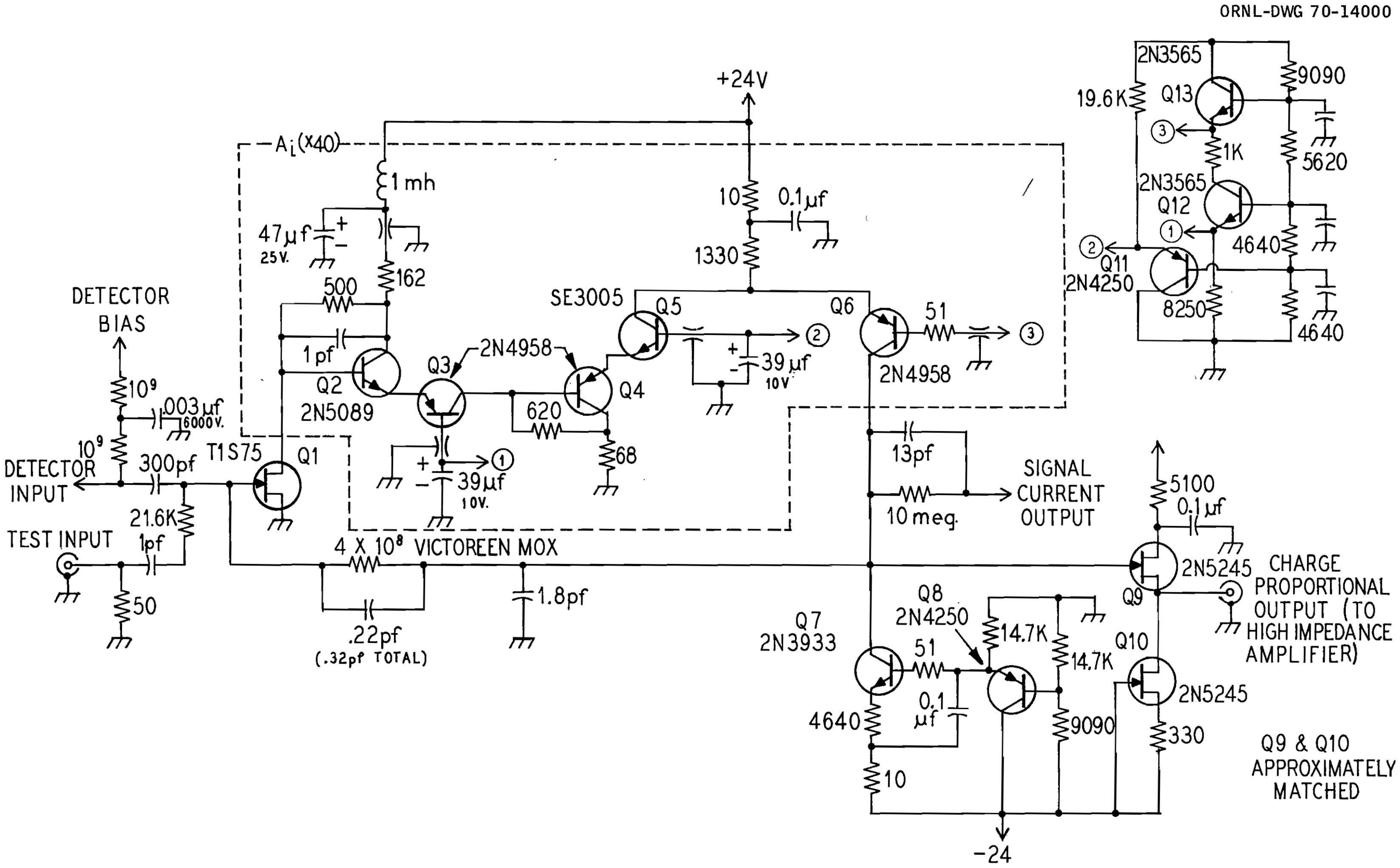

Figure 25. First stage circuit diagram of the preamplifier of Fig. 24.

The closed-loop current gain of this stage is forty. To allow a possible bandwidth given by Eq. (46), page 43, the gain section A_i was also assigned a value of forty. This condition is usually a good starting point in designing a stage. If the resulting bandwidth determined by the ratio of the input FET transconductance to the total input capacitance is too large, excessive overshoot and ringing will occur on the output pulse because of the additional sources of phase shift within the feedback loop discussed in Chapter IV. The desired output pulse response can be obtained by adding an appropriate capacitance to ground at the output node (load end of the feedback resistor), thereby decreasing the loop transmission. Although, for a given bandwidth, there are no specific conditions limiting the gain per stage other than the maximum gain-bandwidth product of the interstage gain section A_i and the delay time through this section, the value of gain should be limited to a value less than about fifty. Proper grounding becomes increasingly difficult for excessively large gain-bandwidth product stages mounted on a common ground-plane board.

The selection of the broadband, current-gain section A_i was based primarily on noise considerations. The modified shunt feedback stage introduced in Chapter IV (Fig. 19a, page 75) requires a very low-capacitance driving source if the maximum bandwidth is to be realized. Therefore, a preceding common-base buffer stage is frequently needed. The common-base buffer stage makes a small but sometimes significant contribution to the mid-frequency equivalent noise current of the broadband gain section. The bandwidth of the single-transistor shunt feedback stage is much less sensitive to additional input capacitance. Thus, for a small value of input-FET gate-to-drain capacitance, a common-base buffer stage is not required. The 2N5089 transistor used for Q_2 has a very low equivalent noise current and an exceptionally low, low-frequency flicker noise component. The gain-bandwidth product of this transistor is about 500 megahertz at a collector current of five milliamperes; thus, to allow adequate bandwidth, only a current gain of four was established for this stage. The second single-transistor, shunt-feedback stage formed by transistor Q_4 was inserted to boost the total current gain of the A_1 section to forty.

The feedback resistor of transistor Q_2 carries the drain current of the input FET thus its value is chosen accordingly. The noise contributed by this resistor can be decreased by increasing its value and inserting a drain-to-power-supply resistor with a large series inductance to furnish the necessary FET bias current.

For high-transconductance input devices, the additional noise contributed by a common-base buffer stage inserted between the input FET and the shunt-feedback stage is probably insignificant. In this case the modified shunt-feedback stage is recommended, even though this design choice was not made for the stage of Fig. 25, page 94.

The choice of an input FET was based on the required transconductance to yield a reasonable bandwidth and noise line width from detectors having capacitance values in the range of from 10^{-11} to 25×10^{-12} farads. The transistor selected was a TIS75 made by Texas Instruments Incorporated. Operating at a drain current of 20 milliamperes this device has a transconductance of typically 20 millimhos. The measured total input capacitance excluding the detector was about 21 picofarads.

Two field-effect transistors, Q_9 and Q_{10}, were added to give a charge proportional output for comparison with the integrated current output. To obtain adequate linearity, the source of Q_9 must drive a large impedance load.

Second-Stage Design

The second stage, shown in Fig. 26, is the same as the abbreviated design of Fig. 23, page 88. The current gain of this stage is twenty. The 4.7×10^6 ohm feedback resistor contributes an output noise power that is equivalent to that contributed by a 7.5×10^9 ohm resistor shunting the input of the first stage. The emitter followers Q_9, Q_{10} and Q_{11} (also used in the first stage) provide low-impedance biasing and excellent power-supply decoupling for the common-base transistors within the amplifier loop. The second stage has no additional features that have not been previously discussed.

Third-Stage Design

The third stage, shown in Fig. 27, was designed to provide a maximum unipolar output current of forty milliamperes and a current gain of ten. Because each of the three stages in the composite preamplifier is inverting, the output signal is positive for a negative detector-current pulse. The total output signal current is divided equally between two identical load impedances to provide both a timing and an energy channel. Each output is thus capable of delivering a positive signal current of twenty milliamperes. Transistors Q_5 and Q_6 carry the total output-signal current and, consequently, must have large gain-bandwidth products at the maximum output signal level. A large gain-bandwidth product, high-current

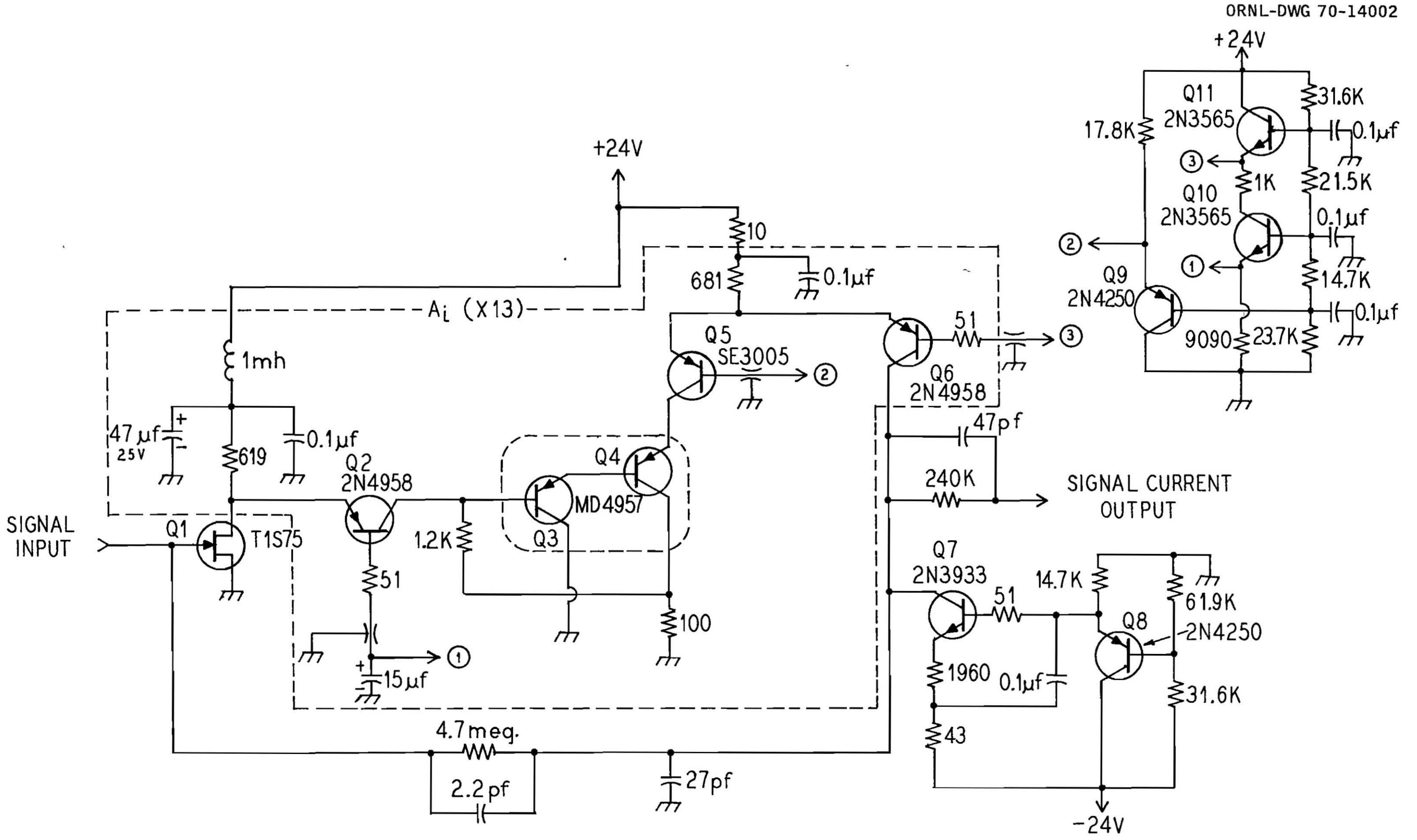

Figure 26. Second stage circuit diagram of the preamplifier of Fig. 24, page 93.

ORNL-DWG 70-14001

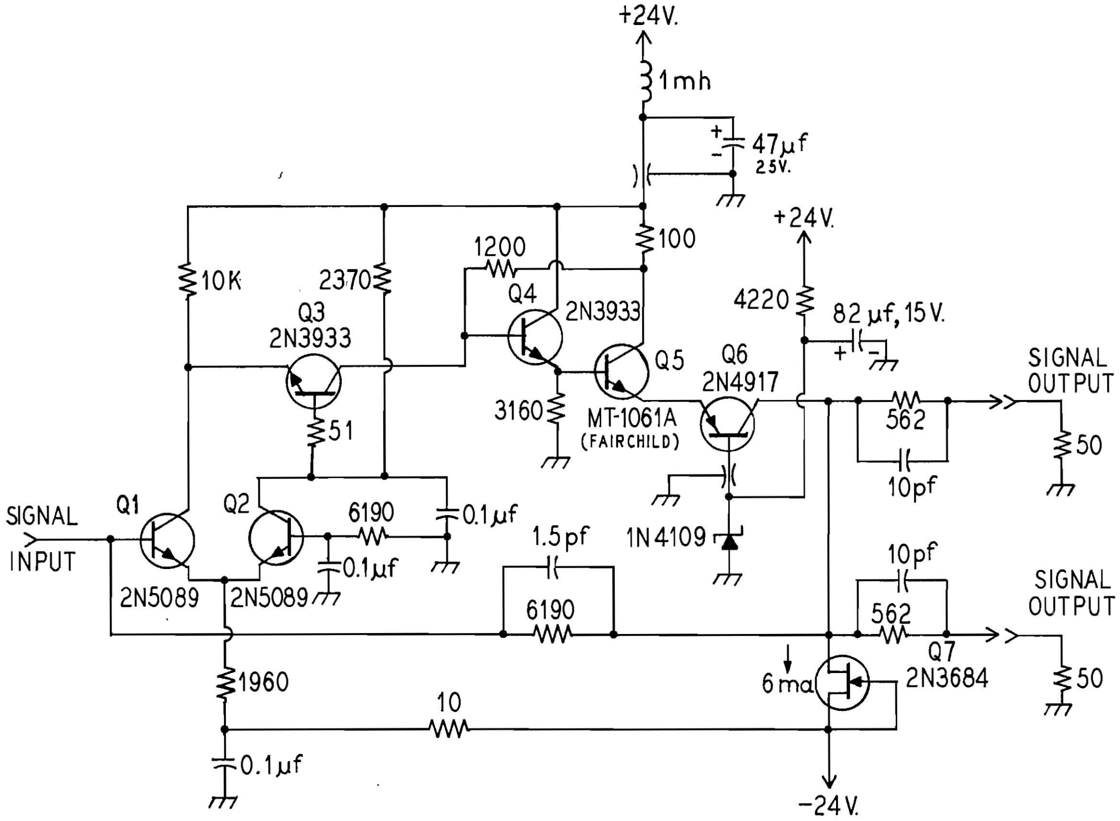

Figure 27. Third stage circuit diagram of the preamplifier of Fig. 24, page 93.

device is especially needed for transistor Q_5 which is within the two-transistor shunt-feedback loop.

The feedback and load resistors were chosen as low as possible to eliminate long time constants in the feedback network. The 6.19×10^3 ohm feedback resistor contributes an output noise current approximately equal to that produced by a parallel 4×10^9 ohm resistor referred to the preamplifier input.

In order to allow an adequate bandwidth, the input device of this stage is required to have a large transconductance. This requirement is based on the 47×10^{-12} farad load capacitor of the second stage that appears essentially as a shunt input capacitor to the third stage. Large h_{FE} bipolar transistors have an adequately low noise-current contribution to justify their use as a third-stage input device. A large transconductance can be obtained by the proper choice of emitter bias current. In this case six milliamperes was chosen giving an effective transconductance of about 0.1 mho for the differential connection. The differential input configuration was used for bias stability and to allow the output quiescent voltage to assume a value very near zero.

The mid-frequency equivalent noise current due to the input transistors is essentially determined by the base-current shot noise of Q_1. Without extensive selection 2N5089 transistors may be found having h_{FE} values in excess of one thousand. For a base current of six microamperes, the shot-noise-current produced is equivalent to the thermal noise current of an 8.64×10^3 ohm resistor. Multiplying this value by the current gain squared of the first two stages results in an equivalent parallel input noise resistance to the first stage of 5.5×10^9 ohms.

Measured Equivalent-Noise-Current Spectrum

The equivalent noise current of the complete three stage preamplifier of Fig. 24, page 93, was obtained by two methods. One method consisted of measuring the narrow-band output noise current and dividing the value obtained by the current gain of the preamplifier at the center frequency of the measuring apparatus. The other method consisted of measuring the narrow-band noise voltage at the charge-proportional output of the first stage (Fig. 25, page 94) and dividing this value by the feedback impedance of the stage calculated at the center frequency of the measuring apparatus. The difference between the two measurements is the noise contributed by the second and third stages. Dividing the narrow-band measurements by the square root of the noise bandwidth of the measuring apparatus gives the unity-bandwidth equivalent noise current (amperes/$\sqrt{\text{Hz}}$) at the frequency of measurement.

For frequencies below 5 x 10^5 Hertz, noise measurements were made with a twin-tee filter amplifier having a Q of ten, feeding a Ballantine model 321 true-RMS VTVM. From 5 x 10^5 Hertz to 10^7 Hertz, noise measurements were made with a Rohde and Schwarz model BN1521 selective microvoltmeter with a constant bandpass of 5 x 10^3 Hertz. The noise measurements made with the selective microvoltmeter were calibrated by comparing the equivalent noise current obtained at 5 x 10^5 Hertz to that obtained with the twin-tee system at the same frequency.

The curves of equivalent noise current derived from the output noise measurements are shown in Fig. 28. For comparison a calculated curve is shown indicating the theoretical contribution of the first-stage feedback resistor and input FET. The noise corner was found from Eq.(84),

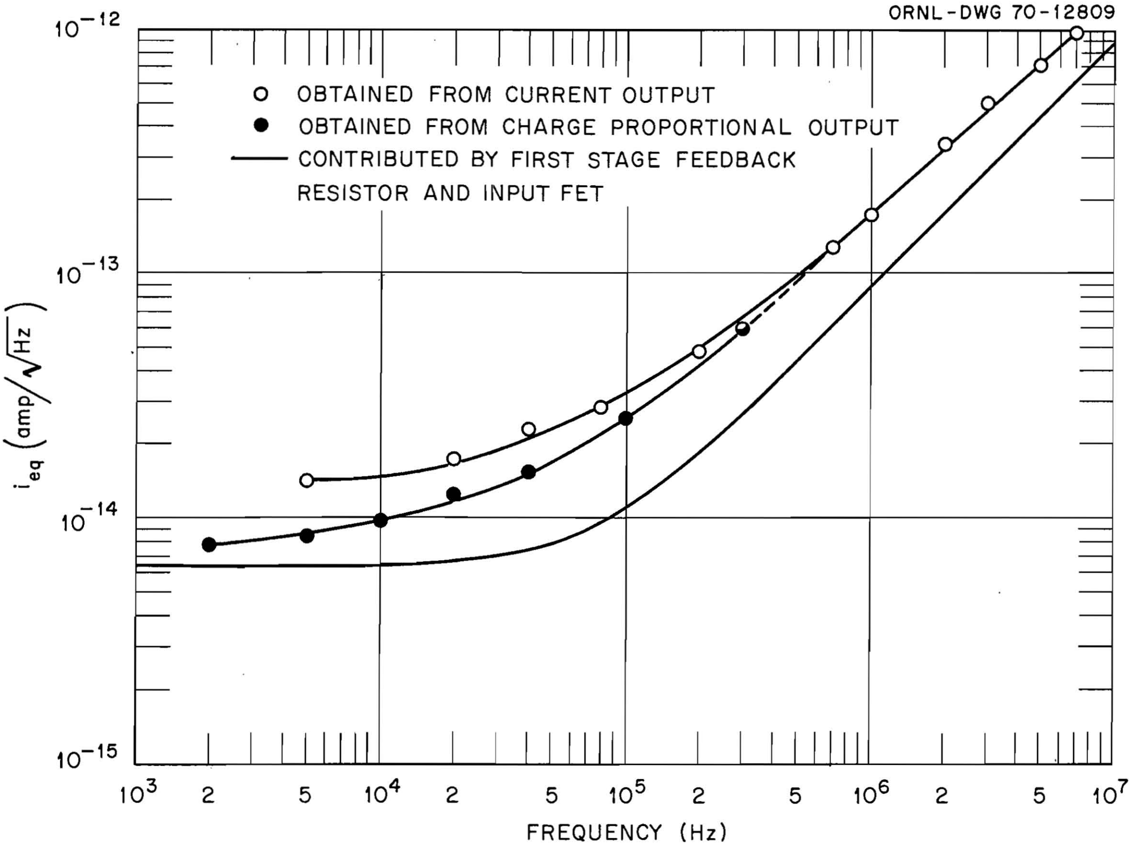

Figure 28. Equivalent noise current spectrum showing a computed curve and two curves resulting from noise measurements from two different outputs.

page 65, with $C_1 = 20 \times 10^{-12}$ farads, $g_m = 16 \times 10^{-3}$ mho, and $R_T = R_f = 4 \times 10^8$ ohms. Nothing was connected to the FFT gate but the feedback resistor and capacitor. The difference between the two measured curves in the low-frequency region indicates the total contribution from the second and third stage feedback resistors, from the first, second, and third stage load resistors, from the base-current shot noise of the third-stage input transistor, and a small contribution from the measuring apparatus. The difference between the calculated curve and the lowest experimentally derived curve is in part due to other noise sources within the feedback loop other than the FET. The approximate factor-of-two difference over most of the frequency range cannot be accounted for. The TIS75 transistor has been reported to exhibit excessively large noise generation. This fact was confirmed for several devices and could possibly be the source of the excess noise measured.

II. EXPERIMENTAL SYSTEM FOR MEASURING NOISE LINE WIDTH

Considerations for Linear Gating

Several applications for linear gating were described in Chapter I. The complexity of an analyzing system involving a time-variant element such as a linear gate is far greater than that required for conventional time-invariant systems. Several papers appearing in recent years have described and analyzed various forms of time variant systems; but, due to the difficulty of implementation and due to the lack of suitable linear gates and other time variant system components, minimal use has been made of the developed technology.

One especially descriptive paper which is applicable to a gated current preamplifier system was written by Blalock and Nowlin.[4] In this paper the authors describe and analyze the noise performance of a system in which an amplified detector current pulse, obtained by differentiating the output signal of a charge-sensitive preamplifier, is gated and shaped by a bipolar filter to give a noise line width equal to that of an ungated system using a unipolar filter of a similar type. Since the output noise power spectrum of the preamplifier developed in this dissertation consists predominately of a white plus an ω^2 component as does the differentiated output noise spectrum of a charge-sensitive preamplifier, the results of the above authors are directly applicable. An important contribution of their paper is the established requirements on the gate width, the relative time orientation of the gate period and amplified detector current pulse, and the following bipolar filter to yield the desired noise line width.

If a noise spectrum consisting of a white plus a band-limited ω^2 component is passed through a linear gate, opened for a time period T_o, and subsequently routed through an appropriate bipolar filter, the noise from the filter observed on an oscilloscope will exhibit at least two quiet spots at which the noise level is significantly lower than it is with the gate open. The zero-crossing time of the filter impulse response must equal the gate width to satisfy the criteria necessary for producing the quiet spots. With this equality, the quiet spots for a symmetrical bipolar filter occur at the filter's impulse response zero crossing and at the point of final base-line return. If the amplified detector current pulse is delayed by $T_o/2$ such that it occurs halfway through the gate period, the resulting output pulse from the filter will peak at the observed noise quiet spot. This condition is illustrated in Fig. 29. In order to make use of the authors' definitions, the time axis is shifted to allow the detector current pulse to occur at zero. The signal-to-noise ratio for a pulse peak occurring at the noise quiet spot is the same as obtained from a unipolar filter fed from an ungated preamplifier system.

The triangular pulse shaping described in the paper yields a very good signal-to-noise ratio but requires relatively elaborate instrumentation. Also, for shaped pulses of short duration, the exact peak of the triangular pulse is difficult for the pulse-height analyzer to accurately detect. Consequently, to allow a simpler experimental set-up while providing a reasonably small noise line width to allow a comparison between gated and ungated noise performance, another type of bipolar filter was chosen.

A direct method of integrating the amplified and gated detector current pulse for energy analysis is shown in Fig. 30a and c. For a large-output-impedance gate indicated in Fig. 30a, the output current signal may simply be integrated by a parallel RC network having a time constant many times larger than the duration of the detector current pulse. Final filtering may be accomplished simply by removing the resistor R and extracting a current through a series inductance-resistance branch as shown in Fig. 30b. The resulting impulse response of the filter is

$$h(t) = \frac{1}{\beta}\left(e^{-\alpha t} \sin \beta t\right), \tag{113}$$

where

$$\beta = \left[1/LC - r^2/4L^2\right]^{1/2} , \tag{114}$$

and

$$\alpha = r/2L \quad . \tag{115}$$

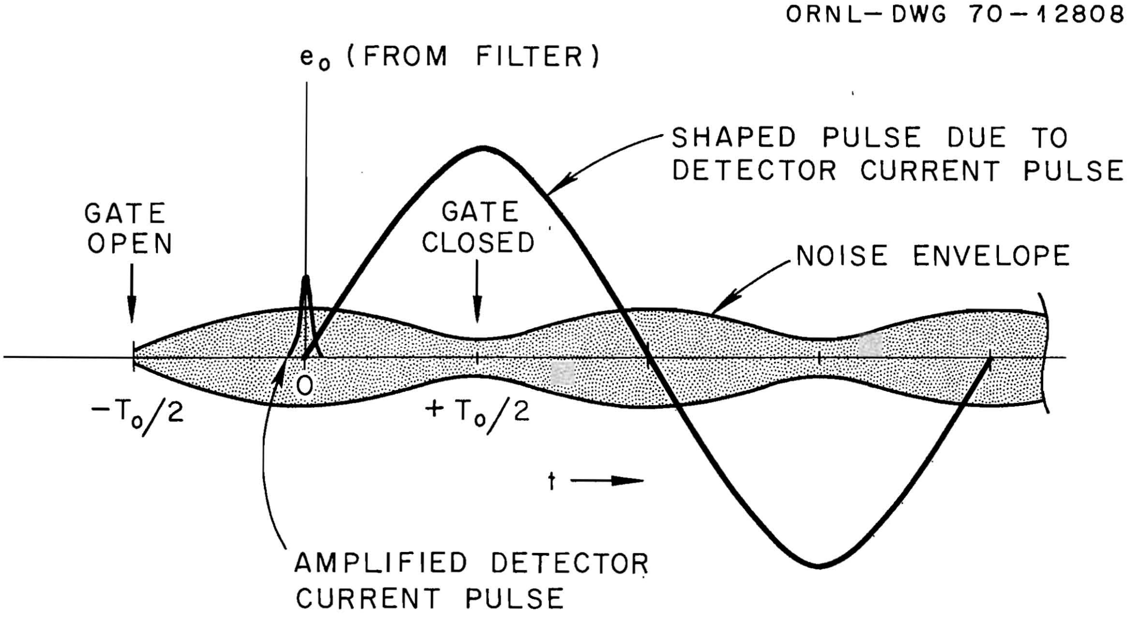

Figure 29. Illustration of the time orientation of the gate period and the amplified detector current pulse for realization of the optimum signal-to-noise ratio from a symetrical bipolar filter.

ORNL-DWG 70-12807

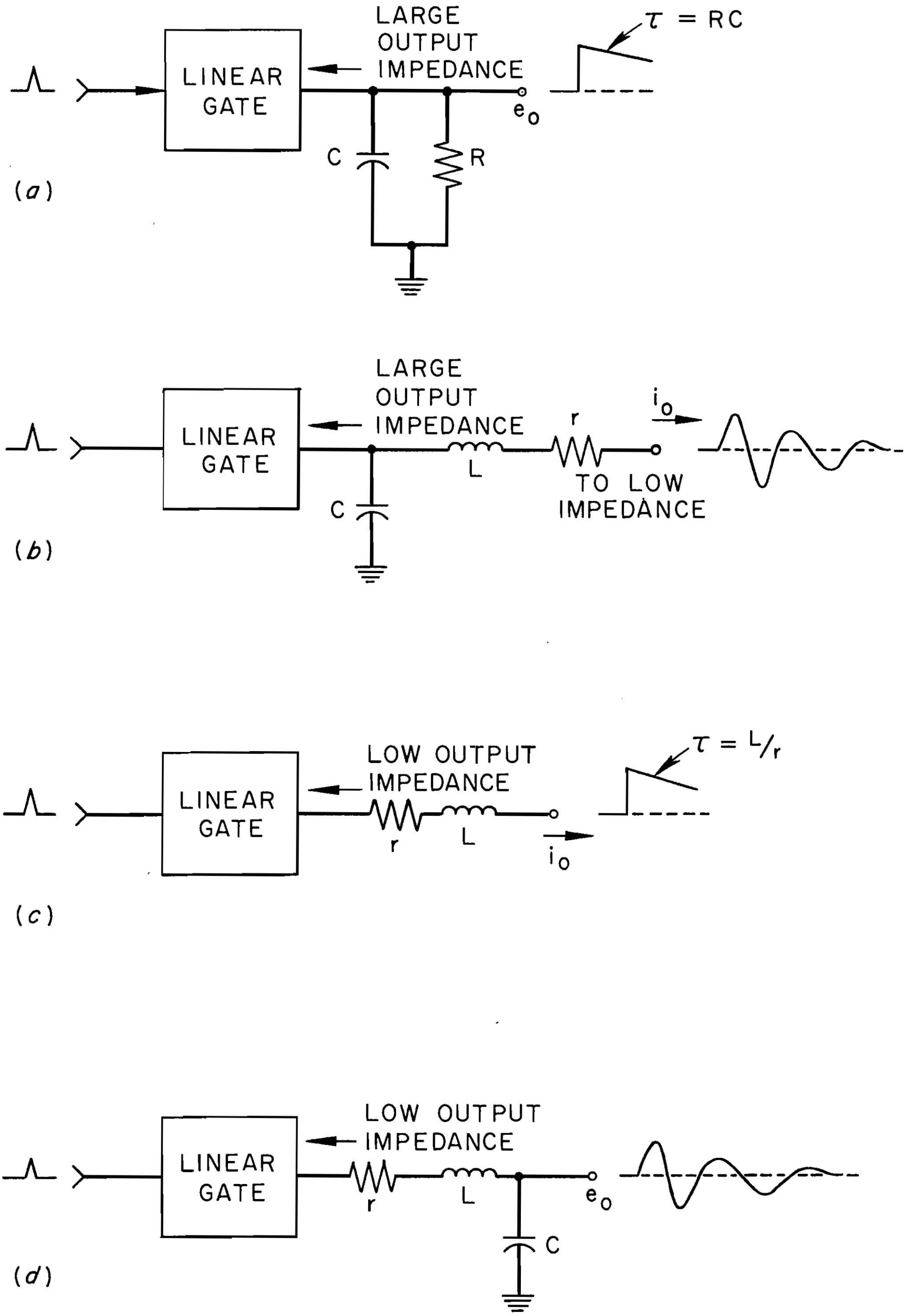

Figure 30. Illustration of pulse integration and RLC shaping from linear gates having either high or low output impedances.

The above three equations describe a damped sinusoid. The peaks of the response are proportional to the total charge in the current pulse. For fairly large damping and typical zero-crossing times, the ringing decays rapidly enough so that most pulse-height analyzers process only the first peak. The extended ringing is, however, undesirable for high-count-rate conditions. For low-output-impedance gates integration of the gated current pulse can most simply be accomplished by an inductor as shown in Fig. 30c. The simple modification of Fig. 30d allows final filtering and creates the same impulse response as described by Eqs. (113), (114), and (115).

By following the guidelines established by Blalock and Nowlin, the cusp factor for the simple RLC filter of Fig. 30b and d operating from a gated noise spectrum can be derived. The procedure is given in Appendix B. From the analysis the cusp factor, defined as the noise-to-signal ratio of the RLC filter to the noise-to-signal ratio of the optimum filter (cusp), is given by

$$\text{C.F.} = \left[Q_o \sinh \frac{\pi}{2Q_o}\right]^{1/2} , \tag{116}$$

where

$$Q_o = \omega_o L/r ,$$

and

$$\omega_o = 1/LC .$$

The result of Eq. (116) is based on the LC resonant frequency ω_o being equal to the preamplifier noise-corner frequency and the gate width being equal to the width of a single lobe of the pulse from the filter

$$T_c = \frac{1}{2\,f_o} , \tag{117}$$

where f_o is $\omega_o/2\pi$. Although not realizable, the cusp factor limit as Q_o approaches infinity is a case of interest. As the value of $1/Q_o$ becomes very small, the value of the hyperbolic sine of Eq. (116) is asymptotic to the value of its argument; consequently, as Q_o approaches infinity the hyperbolic sine may be replaced by its argument. Thus, Eq. (116) reduces to

$$\lim_{Q_o \to \infty} \text{C.F.} = \sqrt{\frac{\pi}{2}} \approx 1.25 \quad . \tag{118}$$

The cusp factor as a function of Q_o is illustrated in Fig. 31. Above a Q_o value of about three, small improvement is gained by making Q_o larger.

System Description

A block diagram of the experimental system used to obtain noise-line-width measurements is shown in Fig. 32. The detector used in the experiments was a lithium drifted germanium detector, normally denoted Ge(Li), of planar construction having an active volume of 1.7 cubic centimeters. The detector capacitance is 9×10^{-12} farads at an operating potential of 1500 volts. With the three-stage preamplifier of Fig. 24, page 93, connected to the detector, three noise-line-width measurements were made.

The first measurement was obtained by analyzing the charge-proportional output from the first stage. This channel is similar to the normal charge-sensitive preamplifier analyzing system. A Tennelec TC-200 main amplifier having RC-RC shaping was used. Since only a 400-channel analyzer was available, a Tennelec TC-250 bias amplifier was incorporated to allow the two ^{60}Co peaks to span the 400-channel range. By this method a calibration of about 0.5 kev per channel was obtained.

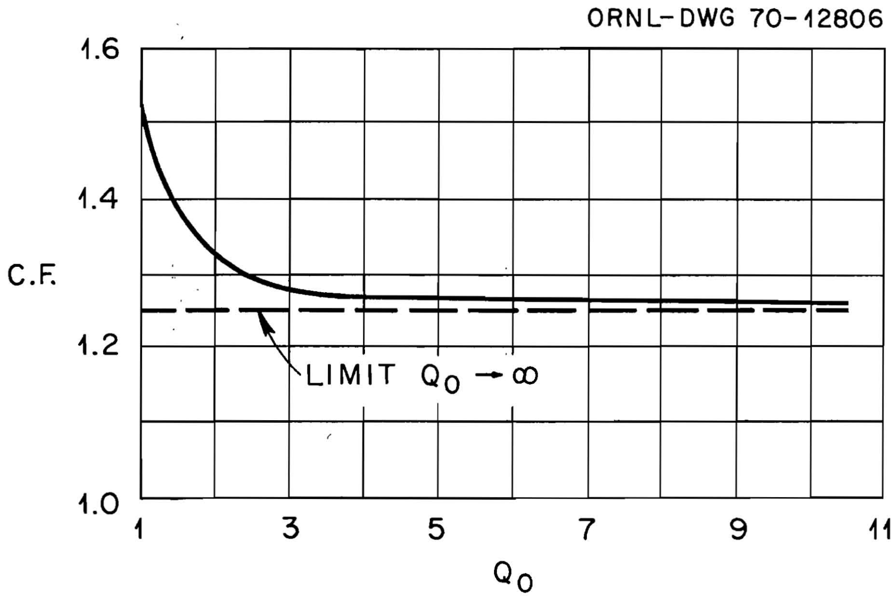

Figure 31. Variation of the cusp factor as a function of Q_o for the RLC filter.

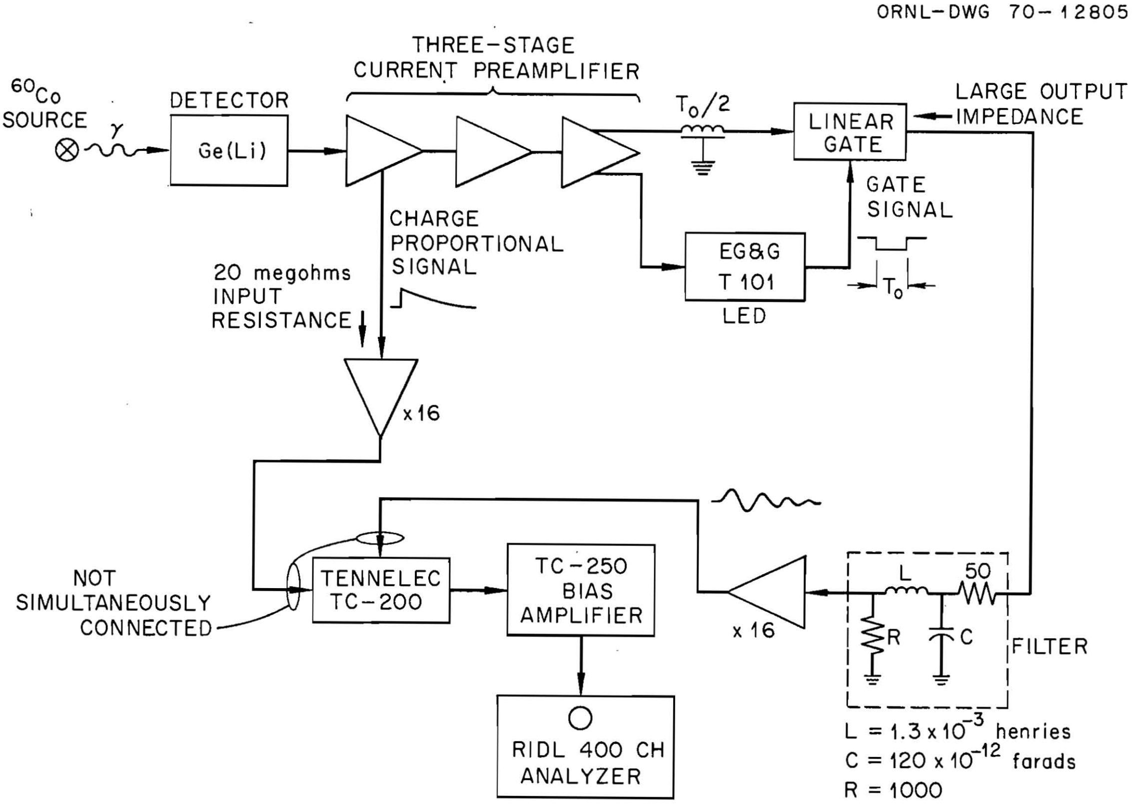

Figure 32. Experimental system for noise line width measurements.

The second noise-line-width measurement was made by operating the linear gate normally open, replacing the RLC filter with an integrating RC network as shown in Fig. 30a, page 107, and using the RC-RC shaped main amplifier in the manner used for the first measurement. This second measurement allows the resolution of the amplified and integrated current pulse to be compared to the resolution obtained from the charge-proportional output.

The third noise-line-width measurement was designed to check the theoretical noise performance of the gated system. One output current signal from the preamplifier was delayed by $T_o/2$ and routed to the gate input. The other preamplifier current output operated a leading-edge discriminator which provided a gate signal of width T_o. Thus, in accordance with the theoretical gating requirements, the amplified, detector-current pulse was centered within the gate-open period. The pulse from the gate was shaped by the RLC filter discussed, passed through a broadband amplifier and through the first two sections of the TC-200 main amplifier with the RC filtering switched out.

The gate used was a slight modification of that described by Smith[24] The linear signal path through the gate consists of a bipolar-transistor, common-base bridge configuration. This circuit is inadequate in three respects. First, the pedestal stability without considerable care in component selection and matching is inadequate to allow use of a gate open time long enough for the optimum filter. For gate widths several microseconds long, very small pedestal drifts can create signficant output area variations. Secondly, over a large dynamic current range, the linearity of the gate limits that of the system. The linearity of the gate used was slightly greater than one percent over a sixteen milliampere current range. The third disadvantage to the gate design is the required large bias currents which create large shot-noise currents in the bridge transistors. Large gate noise requires a larger preamplifier current gain and, subsequently, a larger preamplifier output-signal current range. The gate has good switching-time and rise-time capabilities. With all parameters considered this gate design has more to offer than many others. Like most linear circuits the best gate design for a given application involves several design trade-offs.

Experimental Results

The noise line width measured from the charge-proportional output and from the integrated current output was obtained at several values of equal RC-RC filter time constants. Because, for large gate open times, the drift in the gate pedestal caused fluctuations in the amplitude of the filtered output pulse, the noise line width of the gated system was only obtained for a filter center frequency of 4×10^5 Hertz. The noise-corner frequency of the preamplifier as illustrated in Fig. 29, page 106, is less than 10^5 Hertz. Thus, the need for a more stable gate design is apparent. The results of the noise line width measurements are tabulated in Table I.

The RLC filter used had a value of Q_o near three. From Fig. 31, page 110, the corresponding cusp factor for this value is about 1.27 compared to 1.36 for the unipolar RC-RC filter. Comparing the noise-line width from the 4×10^5 Hertz RLC filter with gating to that from the 0.4 μs RC-RC filter (also having a 4×10^5 Hertz center frequency) without gating shows the validity of the calculated cusp factor for the gated

TABLE I

MEASUREMENTS OF NOISE LINE WIDTH FOR THREE OUTPUT MODES AND FOUR VALUES OF FILTER TIME CONSTANT

RC-RC Time Constant (μs)	Charge Proportional Output (kev fwhm)	Integrated Current Output (kev fwhm)	Gated Current Output (kev fwhm)
0.4	2.49	2.76	2.7 (RLC filter)
0.8	2.26	2.54	-
1.6	2.04	2.35	-
3.2	1.98	2.37	-

system. The reason that these two noise-line-width measurements do not differ by the ratio of the cusp factors of the filters may be due to the fact that the center frequencies are not optimum. The minimum gated noise line width is dependent on proper adjust of the linear delay between the preamplifier and gate and the proper adjustment of the gate width.

The data of Table I is based on pulser resolution. Although in actual experiments the noise line width due to both the detector and the preamplifier is of primary interest, observing the noise line width due only to the preamplifier for the three different methods used to obtain an energy proportional output allows a more precise comparison.

As stated previously the resolution experiments were not intended to indicate optimum noise performance but were primarily performed to evaluate the system for comparison with expected results. The total parallel input noise resistance of the first preamplifier stage excluding the input FET is calculated to be about 1.4×10^8 ohms. This number includes the feedback and detector bias resistor and the equivalent noise resistance associated with a detector leakage current of about 0.2×10^{-9} amperes. The total input capacitance at the FET gate was about 30×10^{-12} farads, and the input device transconductance was about 16×10^{-3} mhos. From Eq. (84), page 65, the noise-corner frequency is about 81×10^3 Hertz. Inserting this quantity into Eq. (83), page 64, gives a theoretical noise line width of 1.32 kev FWHM. This number should compare reasonably well with the resolution measured for the 1.6 and 3.2 μs RC-RC filter time constants operating from the charge-proportional output. However, measured numbers are approximately fifty percent higher. Noise sources within the feedback loop following the input FET were not considered in the calculated noise line width. Added contributions from these other sources, however, should not account for a fifty percent increase. The equivalent noise current spectrum of Fig. 28, page 102, shows the same trend. As mentioned, the excess noise is probably due to the TIS75 transistor. Specific selection of input devices or the choice of a different type would eliminate most of the excess noise. The difference in the noise line width between the charge-proportional output and the ungated current output indicates that the noise contribution from the second and third stages of the total preamplifier plus that contributed by the linear gate.

III. TIMING EXPERIMENTS

Detectors Used

In order to evaluate the timing capabilities of the preamplifier, timing experiments were performed with two Ge(Li) detector configurations. One detector was the 1.7 cubic centimeter planar type that was used for the energy experiments. The other detector was a true coaxial configuration having an active volume of 34.1 cubic centimeters and a capacitance of about 23×10^{-12} farads at 2800 volts. The resolution specified for this detector was 2.3 kev FWHM. As mentioned in the previous section, the capacitance for the planar detector is 9×10^{-12} farads. The problems associated with determining the exact time at which a radiation event occurs within a semiconductor detector are too involved to be discussed in this dissertation. A treatment of the subject is found in a review paper by Quaranta et al.[7]

System Configuration

The block diagram of the system that was used for the timing experiments is shown in Fig. 33. The basic purpose of the system was to detect the coincident radiation from a ^{60}Co gamma-ray source with two separate timing channels. One serving as a standard with a known capability of measuring the radiation occurrence time and the other consisting of the semiconductor detector and current preamplifier under test. The standard timing channel consisted of an RCA 8575 photomultiplier tube operating from a one-inch diameter, one-inch thick Naton 136 plastic scintillator. The base used for the tube was an ORTEC model 270 incorporating constant-fraction-of-pulse-height triggering. The measured time resolution for this channel was about 400×10^{-12} seconds over a 100 to 1 range of radiation energies.

From the opposing channel under test both timing and energy information were taken. A timing pulse was obtained from one preamplifier output by means of an ORTEC 453 constant-fraction-of-pulse-height discriminator.[5] A conventional leading edge discriminator followed this to provide additional fan-out for oscilloscope triggering and the analyzer gate generator. The output of the 453 discriminator and the timing pulse from the standard channel operated a time-to-amplitude converter (TAC). Fluctuations in the pulse amplitude from the TAC indicate variations in radiation event detection time in one channel relative to the other. To determine the energy range over which events were being timed in the channel under test, the second preamplifier current output was routed through the open gate (to obtain an impedance transformation) to an integrating network and then to the TC-200 main amplifier using RC-RC

ORNL–DWG 70–12804

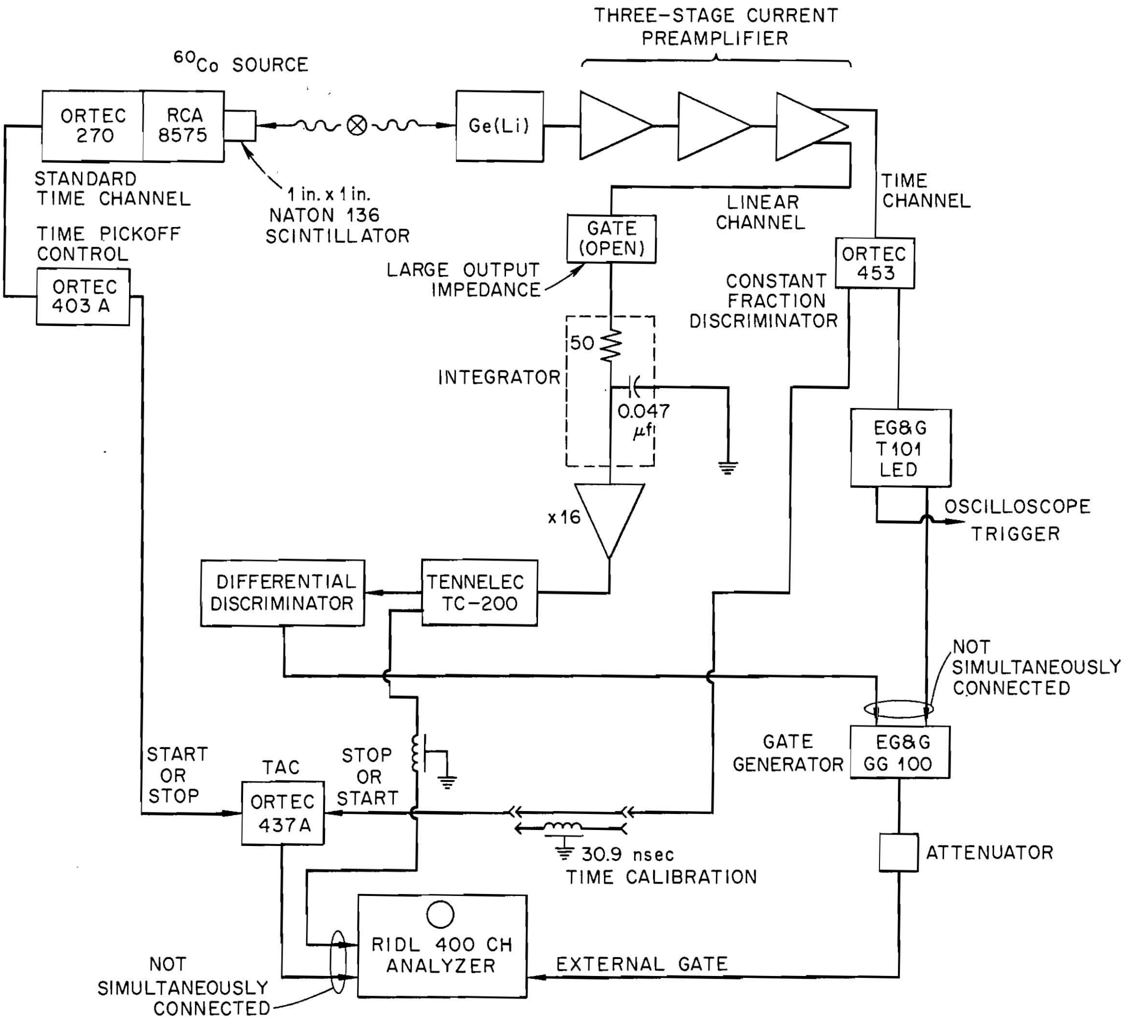

Figure 33. Experimental system for time resolution measurements.

shaping. The dynamic range was determined by analyzing the output of the main amplifier, with the analyzer externally gated from the regenerated 453 discriminator output signal. For narrow-dynamic-range timing measurements, the main amplifier output was routed to a differential discriminator which was adjusted to detect the desired energy window. Logic pulses from this discriminator, resulting from linear input pulses falling within the preset discriminator window, were used to generate an analyzer gate signal. With the analyzer operating in the external-gate mode, only coincident events of the desired energy range were timed.

Timing Measurements

With the 9 x 10^{-12} farad, 1.7 cc planar detector connected to the preamplifier, the ten-to-ninety percent rise time was slightly less than 10^{-8} seconds. At the expense of slightly larger broadband noise the rise-time could be reduced to 7 x 10^{-9} seconds. Typical waveforms of the amplified detector current pulses are shown in Fig. 34a.

After several initial time resolution trials, the ORTEC 453 constant-fraction-of-pulse-height discriminator was operated at a trigger fraction of 0.4 although the setting did not seem critical. The front-panel delay cable required to establish optimum triggering was determined, by experimentation, to be about two feet of RG 58/U. The walk adjustment was set to give a visual monitor pulse array with the majority of the full range of waveforms crossing as near zero volts as possible. The threshold dial was set by the energy channel to allow the maximum dynamic range without excessive triggering due to noise. A typical counting rate from this discriminator was 30,000 counts per second.

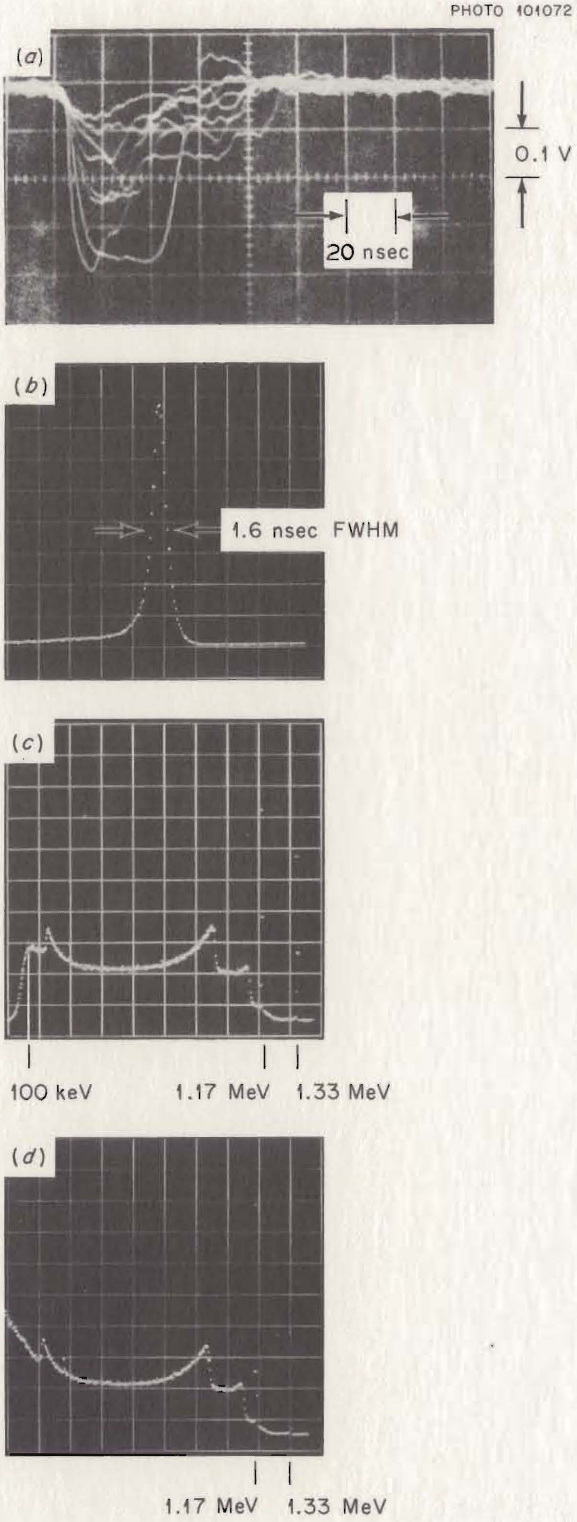

Figure 34. Experimental results from the 1.7 cc. Ge(Li) planar detector showing (a) current waveforms (b) wide-dynamic-range time run with (c) the corresponding ^{60}Co energy spectrum to indicate the dynamic range and (d) a normal internally-gated analyzer spectrum for comparison.

The time distribution for a typical wide-dynamic-range timing run is shown in Fig. 34b. The photomultiplier tube in the standard channel was operating over a 100 to 1 energy range at a counting rate of about 20,000 counts per second. The time values indicated include contributions from this channel. The spectrum of Fig. 34c, obtained from the linear channel with the analyzer gated indirectly from the 453 discriminator (Fig. 33, page 118), indicates the energy range over which the timing was performed. The spectrum of Fig. 34d, obtained with the analyzer internally gated, is shown for comparison; although, the energy calibration of the display is not quite the same.

A narrow-dynamic-range time resolution run was performed with the analyzer externally gated only for pulses in the linear channel corresponding to the two ^{60}Co gamma-ray peaks. The measured time resolution was 0.9×10^{-9} seconds FWHM.

The timing experiments were repeated with the 34.1 cc coaxial detector. All factors were the same as for the planar detector except the adjustment of the 453 constant-fraction-of-pulse-height discriminator. Due to the larger capacitance, the ten-to-ninety percent rise time was increased to about 15×10^{-9} seconds. Consequently, a delay cable consisting of four feet of RG 58/U was needed for optimum performance from the 453 discriminator. Timing accuracy from this detector could have been improved by decreasing the rise time. However, because suitable input devices were not available the preamplifier was maintained in the state used for the smaller detector.

Displayed analyzer data for timing experiments using the coaxial detector are shown in Fig. 35. A wide-dynamic-range timing run is

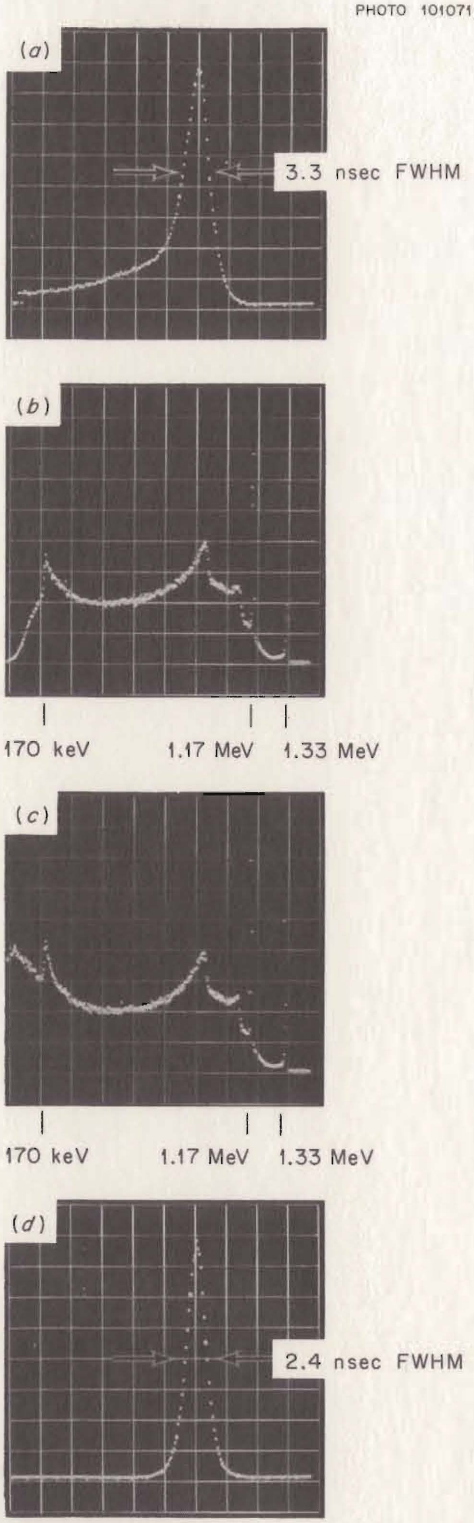

Figure 35. Experimental results from the 34.1 cc. Ge(Li) coaxial detector showing (a) a wide-dynamic-range time run with (b) the corresponding ^{60}Co energy spectrum to indicate the dynamic range and (c) a normal internally-gated analyzer spectrum for comparison. A time run involving only the two ^{60}Co gamma-ray peaks is shown in (d).

indicated in Fig. 35a with the corresponding energy spectrum of Fig. 35b obtained with the analyzer externally gated by the 453 discriminator (Fig. 33, page 118). The spectrum of Fig. 35c was obtained with the analyzer internally gated for comparison. The timing run displayed in Fig. 35d corresponds to a dynamic range including only the two ^{60}Co gamma-ray peaks.

The experimental timing results are best summarized by Fig. 34, page 120, and Fig. 35. The results of the noise line width measurements appear in Table I, page 114.

CHAPTER VI

CONCLUSIONS

I. GENERAL SUMMARY

The primary objective of this thesis was to develop a current preamplifier having sufficient bandwidth and linearity to amplify the current pulses from nuclear radiation detectors for both energy and timing information. A design goal was to achieve an energy resolution comparable to that obtained with present charge-sensitive preamplifier configurations. Low-noise amplification of the detector current signal prior to integration yields greater flexibility in signal processing. This advantage is especially of interest where linear gating prior to signal integration is desired.

In Chapter I various applications of detector current amplification were discussed. In addition, several techniques and amplifier configurations presently used for the purpose were delineated.

The limitaions, primarily with respect to noise performance, of a basic operational-amplifier, shunt-feedback amplifier stage having either bipolar or field-effect input transistors was discussed in Chapter II. The low- and mid-frequency equivalent noise current obtainable from the FET input was found to be considerably lower for the same amplifier because of the base-current shot noise generated in the bipolar transistor. The lower limit to the mid-frequency equivalent noise current of the FET input configuration was shown to be imposed by the thermal noise of the feedback resistor having an upper value limited by bandwidth requirements.

The result of the investigation of this chapter was that for a minimum low- to mid-frequency signal-to-noise ratio from the FET input, shunt-feedback configuration, the required value of feedback resistance inherently causes signal integration, resulting in the charge-sensitive configuration. Thus, at this point, the differentiated charge-sensitive configuration was found to have superior noise performance to the other current-amplifying configurations described.

In the first part of Chapter III criteria were established for differentiating the output pulse of a charge-sensitive preamplifier without appreciably affecting the signal-to-noise ratio. Subsequently, a new FET-input, shunt-feedback configuration having a constant current gain equal to the ratio of RC feedback impedance to RC load impedance was described. The bandwidth is a function of this ratio and is independent of the value of feedback resistance; consequently, feedback resistance values typical of those used in conventional charge-sensitive preamplifiers may be employed. The general configuration is shown in Fig. 11a, page 40. Equations were developed to predict critical impedance and transfer parameters and performance criteria. For conditions specified in Chapter III the bandwidth is given approximately by

$$f_{-3} \approx \frac{g_m}{2\pi C_1} \quad , \tag{46}$$

and the input impedance approximately by

$$Z_{in}(j\omega) \approx \frac{1}{g_m(1 + j\omega C_1/g_m)} \quad . \tag{51}$$

The equivalent-noise-current squared is constrained by the ratio of the total input capacitance squared to the transconductance of the input FET.

After the preamplifier output noise passes through an integrating network, the resulting noise level is the same as that for a charge-sensitive preamplifier having the same gain and input device. Requirements were derived for cascading stages to achieve large current gains. Because stages can be directly cascaded to achieve large current gains of large bandwidths, a complete current preamplifier having the noise performance of a conventional charge-sensitive preamplifier can be realized with relative ease.

In Chapter IV the circuit realization of the basic preamplifier configuration described in Chapter III was considered, including the requirements on the input device to achieve the desired bandwidth and noise line width and the development of a broadband current gain stage required for the current gain section A_i of Fig. 11a, page 40. An abbreviated circuit design is presented in Fig. 23, page 88.

Considerations for choosing the total preamplifier current gain and the complete design and evaluation of a three-stage current preamplifier having a current gain of 8000 and a ten-to-ninety percent rise time of 7×10^{-9} seconds were described in Chapter V. Criteria developed by Blalock and Nowlin[4] for linear gating of the amplified detector current pulse were presented. Based on these criteria, the gated cusp factor for an easily realized RLC filter for use in a gated energy analyzing system was derived. Experiments were performed with an energy analyzing system to confirm the noise performance predicted in Chapters III and IV. For the integrated output current signal shaped by an RC-RC filter, a noise line width of 2.35 kev FWHM (RC = 1.6 μs) was measured (Table I, page 114). The system was not optimized for minimum noise line width.

Timing experiments described in Chapter V were performed by measuring the relative occurrence time of the coincident radiation from a ^{60}Co source with two separate timing channels, one a standard channel using a photomultiplier tube with a plastic scintillator and the other a test channel using a Ge(Li) semiconductor detector. Two Ge(Li) detectors were used. One was a planar configuration having an active volume of 1.7 cubic centimeters, and the other was a true coaxial configuration having an active volume of 34.1 cubic centimeters. The timing uncertainty measured from the planar detector was 1.6×10^{-9} seconds FWHM for a dynamic energy range of 13.3 to 1. The timing uncertainty measured from the coaxial detector was 3.3×10^{-9} seconds FWHM for a dynamic range of 7.8 to 1.

II. AREAS FOR FURTHER STUDY

The task of optimizing the noise perfromance of the new current-preamplifier configuration is the same as that required for the conventional charge-sensitive preamplifier. Specific selection and cooling of the input device could greatly reduce the system noise line width.

Continued effort is needed in the area of gated filters. Based on the work of Nowlin,[25] practical lumped element bipolar filters can probably be realized to give a substantial improvement in gated signal-to-noise ratios over those of the simple RLC filter considered in Chapter V. Further work is also needed in the general area of gated filters. The remaining obstacle to the acceptance of gated systems is the lack of linear gates having adequate bandwidth and linearity for precision energy measurements.

Another area for further study is the investigation of count-rate performance. This area was not experimentally investigated but is one of foremost importance to many experimenters.

Further improvements are possible in the physical layout of the preamplifier. With the proper layout the system bandwidth could probably be extended beyond 70×10^6 Hertz. The increased bandwidth capability is desirable for some timing applications.

LIST OF REFERENCES

LIST OF REFERENCES

1. F. S. Goulding, "Preamplifiers," Proceedings of the Semiconductor Nuclear-Particle Detector and Circuit Conference, National Academy of Sciences Publication 1593, Washington, D.C. 1969, pp. 381-392.

2. Emanuel Elad, "FET Preamplifiers for Semiconductor Radiation Detectors," Proceedings of the Ispra Nuclear Electronics Symposium, Ispra, Italy, May 6-9, 1969, pp. 21-34.

3. F. Plasil, R. L. Ferguson, and H. W. Schmitt, to be published.

4. T. V. Blalock and C. H. Nowlin, "Time Variant Filters for Generating Bipolar Pulses with Signal-to-Noise Ratios of Unipolar Pulses in Nuclear Pulse Amplifiers," The Review of Scientific Instruments 40(8), pp. 1093-1100 (1969).

5. ORTEC Application Note AN31, "Timing with Ge(Li) Detectors," 1970.

6. J. K. Millard and T. V. Blalock, "A Low-Noise Wide-Band Current Preamplifier for Use with Semiconductor Detectors," Proceedings of the Semiconductor Nuclear-Particle Detector and Circuits Conference, National Academy of Sciences Publication 1593, Washington, D. C., 1969, pp. 476-483.

7. A. Alberigi Quaranta, M. Martini, and G. Ottaviani, "The Pulse Shape and the Timing Problem in Solid State Detectors," IEEE Transactions on Nuclear Science NS-16(2), pp. 35-61 (1969).

8. I. S. Sherman and R. G. Roddick, "Low Noise Preamplifier for Simultaneous High Resolution Energy and Time Measurement with Semiconductor Detectors," IEEE Transactions on Nuclear Science NS-17(1), pp. 252-259 (1970).

9. E. J. Kennedy, "A Study of Theoretical and Practical Limitations of Low-Current Amplification by Transistorized Current-Feedback DC Electrometers," Ph.D. Dissertation, The University of Tennessee, Knoxville, Tennessee, 1967.

10. T. V. Blalock, "Optimization of Semiconductor Preamplifiers for Use with Semiconductor Radiation Detectors," Ph.D. Dissertation, The University of Tennessee, Knoxville, Tennessee, 1965.

11. F. S. Goulding, J. Walton, and D. F. Malone, "An Opto-Electronic Feedback Preamplifier for High-Resolution Nuclear Spectroscopy," Nuclear Instruments and Methods 71(3), pp. 273-279 (1969).

12. V. Radeka, "Charge Amplification Without Charge Leak Resistor," IEEE Transactions on Nuclear Science NS-17(3), pp. 433-439 (1970).

13. C. H. Nowlin and J. L. Blankenship, "Elimination of Undesirable Undershoot in the Operation and Testing of Nuclear Pulse Amplifiers," Review of Scientific Instruments 36(12), pp. 1830-1839 (1965).

14. A. van der Ziel, "Thermal Noise in Field-Effect Transistors," Proceedings of the IRE 50(8), pp. 1808-1812 (1962).

15. A. van der Ziel, "Gate Noise in Field-Effect Transistors at Moderately High Frequencies," Proceedings of the IEEE 51(3), pp. 461-467 (1963).

16. F. M. Klaassen and J. Prins, "Noise of Field-Effect Transistors at Very High Frequencies," IEEE Transactions on Electron Devices ED-16(11), pp. 952-957 (1969).

17. A. van der Ziel, "Carrier Density Fluctuation Noise in Field-Effect Transistors," Proceedings of the IEEE 51(11), pp. 1670-1671 (1963).

18. C. T. Sah, "Theory of Low-Frequency Generation Noise in Junction-Gate Field-Effect Transistors," Proceedings of the IEEE 52(7), pp. 795-814 (1964).

19. E. Fairstein and J. Hahn, "Nuclear Pulse Amplifiers - Fundamentals and Design Practice," Nucleonics 23(11), pp. 50-55 (1965).

20. T. V. Blalock, "Wide-Band Low-Noise Charge Sensitive Preamplifier," IEEE Transactions on Nulcear Science NS-13(3), pp. 457-467 (1966).

21. C. J. Rush, "New Technique for Designing Fast Rise Transistor Pulse Amplifiers," Review of Scientific Instruments 35(2), pp. 149-156 (1964).

22. F. M. Cherry and D. E. Hooper, "The Design of Wide-Band Transistor Feedback Amplifiers," Proceedings of the I.E.E. 110(2), pp. 375-389 (1963).

23. J. K. Millard, "New Shunt-Series Nanosecond Pulse Amplifier," Review of Scientific Instruments 38(2), pp. 169-175 (1967).

24. B. Smith, "A Linear Gate with High Precision," Nuclear Instruments and Methods 55(1), pp. 138-140 (1967).

25. C. H. Nowlin, "Pulse Shaping for Nuclear Pulse Amplifiers," IEEE Transactions on Nuclear Science NS-17(1), pp. 226-241 (1970).

APPENDIXES

APPENDIX A

For a negative feedback amplifier having a single pole response, the loop transmission $A\beta$ has a lagging phase shift equal to or near ninety degrees at that frequency for which the magnitude of $A\beta$ equals unity. This frequency is normally defined as the system bandwidth. If other sources of phase shift are inserted within the feedback loop without appreciably affecting the magnitude of $A\beta$, the closed-loop frequency response will begin to peak near the bandwidth frequency ω_B as the value of additional phase shift is increased. To estimate the additional phase shift that may be tolerated at ω_B without producing excessive overshoot, the general form of a single-pole, closed-loop transfer function may be modified by inserting a phase factor $e^{-j\omega\tau}$ in $A\beta$, where τ represents an inserted time delay. The general expression for the loop transmission having a single-pole response with the inserted phase term is

$$A\beta = \frac{K' e^{-j\omega\tau}}{1 + j\omega/\omega_o} , \qquad (119)$$

where ω_o is the angular frequency associated with the open-loop pole. The closed-loop transfer function becomes

$$A_{CL} = \frac{\dfrac{K}{1 + j\omega/\omega_o}}{1 + \dfrac{K' e^{-j\omega\tau}}{1 + j\omega/\omega_o}} . \qquad (120)$$

Substituting the trigonometric form of the phase term and simplifying yields

$$A_{CL} = \frac{K}{(1 + K' \cos\omega\tau) + j(\omega/\omega_o - K' \sin\omega\tau)} . \qquad (121)$$

For small values of $\omega\tau$ and large values of K' the real part of the denominator becomes approximately $K'\cos\omega\tau$. To find the overshoot produced for various τ it is necessary to observe the behavior of the magnitude of A_{CL} as a function of frequency. The magnitude of the denominator becomes

$$|D| = \left[K'^2 + (\omega/\omega_o)^2 - 2K'(\omega/\omega_o)\sin\omega\tau\right]^{1/2} \quad . \tag{122}$$

The closed-loop bandwidth ω_B obtained for the system without the delay factor is, from Eq. (120), given by

$$\omega_B = K'\omega_o \quad . \tag{123}$$

Substituting this equation into Eq. (122) with $1/\omega_o$ factored out gives

$$|D| = \frac{1}{\omega_o}\left[\omega_B^2 + \omega^2 - 2\omega_B\omega\sin\omega\tau\right]^{1/2} \quad . \tag{124}$$

Normalizing the frequency with respect to ω_B results in

$$|D| = K'\left[1 + \frac{\omega^2}{\omega_B^2} - 2\frac{\omega}{\omega_B}\sin\left(\frac{\omega}{\omega_B}\right)(\tau\omega_B)\right]^{1/2} \quad . \tag{125}$$

Since $|A_{CL}| = \frac{K}{|D|}$, (126)

a plot of $|D|$ as a function of frequency for various values of $\tau\omega_B$ represents the reciprocal behavior of A_{CL}. A plot showing the normalized magnitudes of both the denominator and its reciprocal is represented in Fig. 36. From this plot 0.6 radians or 35 degrees seems to be about the maximum value of $\tau\omega_B$ without excessive overshoot. Thus, the maximum allowable loop-transmission phase shift including that due to the dominant pole is about −125 degrees.

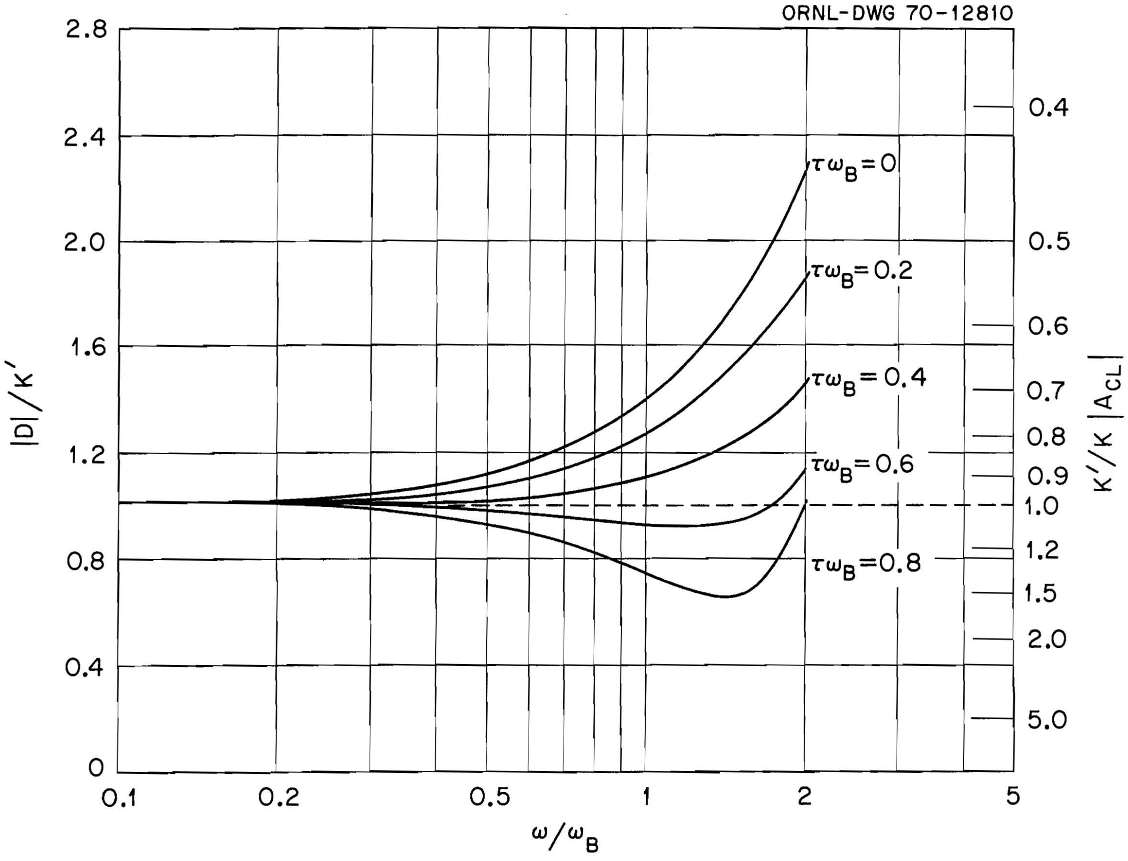

Figure 36. Magnitude response of a single-pole, closed-loop amplifier stage as an added phase shift is increased.

APPENDIX B

The evaluation of the cusp factor for the RLC filter operating from a gated noise spectrum requires first an expression for the output noise from the filter. This expression may be found from Eq. (38) of Ref. 4. The third term of this equation must vanish at a time $T_o/2$ (Fig. 29, page 106) if the switching noise is to be minimum at the time of measurement. This requires

$$h\ (t - T_o/2) = h\ (t + T_o/2) = 0 \tag{127}$$

when t equals $T_o/2$. The time T_o is equivalent to τ in the reference. The impulse response of the RLC filter [Eq. (113), page 105] vanishes when the sine term vanishes, thus Eq. (127) is satisfied when

$$\sin \beta(0) = \sin \beta(T_o) = 0. \tag{128}$$

Since $\sin \beta(0)$ is identically zero, it is only necessary to show that $\sin \beta(T_o)$ is zero. The requirement that the time from pulse initiation to zero crossing be equal to the gate width T_o automatically defines β as

$$\beta = \pi/T_o \quad . \tag{129}$$

Thus

$$\sin \beta T_o = \sin \pi = 0 \quad . \tag{130}$$

Consequently, the impulse response indeed vanishes at $T_o/2$, and the noise quiet spots in time do occur at the peak of the pulse that is initiated at t equal zero.

The first term of Eq. (38), Ref. 4, due to the white noise at t equal $T_o/2$, can be integrated by parts to give

$$\frac{K^2\omega_n^2}{\beta^2}\int_0^{\pi/\beta}\left(e^{-2\alpha t}\sin^2\beta t\right)dt = \left[\frac{K^2\omega_n^2}{4\alpha(\alpha^2+\beta^2)}\right](1 - e^{-2\pi\alpha/\beta}) \ . \qquad (131)$$

The second term due to the ω^2 portion of the input noise spectrum , can be integrated by parts in general form. This process yields

$$K^2\int_0^{\pi/\beta}\left[h(t)h''(t)\right]dt = K^2\left\{h'(t)h(t)\Big|_0^{\pi/\beta} - \int_0^{\pi/\beta}\left[h'(t)^{\ 2}\right]dt\right\} . \qquad (132)$$

The term h'(t)h(t) vanishes when evaluated between the limits of zero and π/β. The remaining term yields three integrals.

$$\begin{aligned} K^2\int_0^{\pi/\beta}\left[h'(t)\right]^2 dt = {} & K^2\int_0^{\pi/\beta}(e^{-2\alpha t}\cos^2\beta t)\, dt \\ & - \frac{2K^2\alpha}{\beta}\int_0^{\pi/\beta}(e^{-2\alpha t}\sin\beta t\cos\beta t)dt \\ & + \frac{K^2\alpha^2}{\beta^2}\int_0^{\pi/\beta}(e^{-2\alpha t}\sin^2\beta t)\, dt. \end{aligned} \qquad (133)$$

The third term of this equation is the same as α^2/ω_n^2 times the left side of Eq. (131). Integration by parts yields a solution to the first term of Fq. (133) as

$$\begin{aligned} K^2\int_0^{\pi/\beta}(e^{-2\alpha t}\cos^2\beta t)dt = {} & \frac{K^2\alpha}{2(\alpha^2+\beta^2)}(1 - e^{-2\pi\alpha/\beta}) \\ & + \frac{\beta^2K^2}{4\alpha(\alpha^2+\beta^2)}(1 - e^{-2\pi\alpha/\beta}) \ . \end{aligned} \qquad (134)$$

Similarly, the second term becomes

$$\frac{2K^2\alpha}{\beta}\int_0^{\pi/\beta}(e^{-2\alpha t}\sin\beta t\cos\beta t)\,dt = \frac{\alpha K^2}{2(\alpha^2+\beta^2)}(1 - e^{-2\pi\alpha/\beta}). \tag{135}$$

The output-noise squared equals the sum of the right side of Eqs. (131), (134), and (135) plus the value of the third term of Eq. (133) which was stated to be α^2/ω_n^2 times the expression in Eq. (131). The sum is

$$\sigma_{gh}^2 = K^2\left[\frac{\omega_n^2}{4\alpha(\alpha^2+\beta^2)}(1 - e^{-2\pi\alpha/\beta}) + \frac{\alpha}{2(\alpha^2+\beta^2)}(1 - e^{-2\pi\alpha/\beta}) + \frac{\beta^2}{4\alpha(\alpha^2+\beta^2)}(1 - e^{-2\pi\alpha/\beta}) - \frac{\alpha}{2(\alpha^2+\beta^2)}(1 - e^{-2\pi\alpha/\beta}) + \frac{\alpha}{4(\alpha^2+\beta^2)}(1 - e^{-2\pi\alpha/\beta})\right]. \tag{136}$$

Simplifying yields

$$\sigma_{gh}^2 = \frac{K^2}{4\alpha}(1 - e^{-2\pi\alpha/\beta})\left(\frac{\omega_n^2}{\alpha^2+\beta^2} + 1\right). \tag{137}$$

Since the measurement is made at t equal $T_o/2$ or $\pi/2\beta$ [Eq. (129)], the impulse response peak at this time is

$$h_p = \frac{1}{\beta}e^{-\alpha\pi/2\beta}. \tag{138}$$

Dividing Eq. (137) by Eq. (138) gives the noise-to-signal ratio as

$$R_{N/S} = \frac{K\beta e^{\alpha\pi/2\beta}}{2\sqrt{\alpha}}\left[(1 - e^{-2\pi\alpha/\beta})\left(\frac{\omega_n^2}{\alpha^2+\beta^2} + 1\right)\right]^{1/2}. \tag{139}$$

By definition

$$Q_o = \omega_o L/r \quad , \tag{140}$$

and

$$\omega_o = \sqrt{1/LC} \quad . \tag{141}$$

From Eqs. (114) and (115), page 105,

$$\beta = \frac{\omega_o}{2Q_o} \left[4Q_o^2 - 1 \right]^{1/2} \quad , \tag{142}$$

and

$$\alpha = \frac{\omega_o}{2Q_o} \quad . \tag{143}$$

Thus,

$$\frac{\alpha}{\beta} = \left[4Q_o^2 - 1 \right]^{-1/2} \quad , \tag{144}$$

and

$$\frac{\beta}{\sqrt{\alpha}} = \left[\frac{\omega_o}{2Q_o} \quad (4Q_o^2 - 1) \right]^{1/2} \quad . \tag{145}$$

Applying Eqs. (142), (143), (144), and (145) to Eq. (139) yields

$$R_{N/S} = \frac{K\ e^{\pi/4Q_o}}{2} \left[2\ \omega_o Q_o \left(\frac{\omega_n^2}{\omega_n^2} + 1 \right) (1 - e^{-\pi/Q_o}) \right]^{1/2} \quad . \tag{146}$$

This equation may be revised as

$$R_{N/S} = K/2 \left[2\omega_o \left(\frac{\omega_n^2}{\omega_o^2} + 1 \right) \right]^{1/2} \left[Q_o \ (e^{\pi/2Q_o} - e^{-\pi/2Q_o}) \right]^{1/2} \tag{147}$$

If the LC resonant frequency ω_o equals the noise-corner frequency ω_n, Eq. (147) can be simplified to

$$R_{N/S}\big|_c = K \left[2\omega_n\ Q_o\ \sinh \left(\frac{\pi}{2Q_o} \right) \right]^{1/2} \quad . \tag{148}$$

The noise-to-signal ratio for the cusp is

$$R_{N/S}\Big|_c = K\ (2\omega_n)^{1/2} \quad . \tag{149}$$

Thus, the cusp factor defined as the ratio of Eq. (148) to Eq. (149), becomes

$$\text{C.F.} = \left[Q_o \ \sinh \frac{\pi}{2Q_o}\right]^{1/2} \quad . \tag{150}$$

VITA

Joe Kenneth Millard was born in Athens, Tennessee, on March 14, 1940. He attended elementary schools in Blount County and was graduated from Maryville High School in 1958. In June 1963, he received the B.S. degree in electrical engineering from the University of Tennessee. While working on the B.S. degree, he was a member of the Cooperative Engineering Scholarship Program doing his field work at the Martin Marietta Corporation in Orlando, Florida. He was also a member of Eta Kappa Nu and a student member of the Institute of Electrical and Electronic Engineers.

In August 1964, he received the M.S. degree in electrical engineering from the University of Tennessee. Since August 1964 he has been employed by the Oak Ridge National Laboratory. During this time he has been working toward the Ph.D. degree in electrical engineering at the University of Tennessee.